



Faculty of Science and Technology
MESA⁺ Research Institute
Inorganic Materials Science Group
Master thesis

University of Twente



Synthesis and characterisation of templated mesoporous silica membranes



Alisia M. Peters

University of Twente

P.O. Box 217

7500 AE Enschede

The Netherlands

Internet: <http://www.ims.tnw.utwente.nl>

April 2003- January 2004

Summary

A conventional (mesoporous) membrane has the disadvantage that the separating layer has a wide pore size distribution and high tortuosity. These properties affect the permeability and selectivity negatively. A method to control the pore size and tortuosity of the top-layer is using template-directed systems (for example the cubic MCM-48). To find out more about these systems, the objectives of this research project are to find a suitable synthesis for MCM-48 silica membranes supported on conventional macroporous α -alumina supports and to characterise the silica layer. To try to understand more in a shorter time frame, also powders and wafers are produced and characterised.

Two synthesis routes (Honma and McCool) with surfactant templates were reproduced. The main properties studied during this project are the mesoporosity of the silica layer, the structure of the layer and the permeability and selectivity. The mesoporosity was determined with nitrogen adsorption/desorption and permporometry. The structure was examined by XRD, optical microscopy, SEM, TEM and gas permeation. To understand the performance of the membranes, liquid permeation with four organic solvents and POM retention were measured.

The objectives of this research project have been reached. Silica membranes with a MCM-48 structured top layer have been synthesised with the Honma sol. The silica could not be coated on α -alumina directly and was therefore coated on γ -alumina, which gave excellent results. XRD patterns and TEM pictures reveal a well-ordered cubic structure with an orientation perpendicular to the surface. Permporometry measurements show that the membranes are mesoporous with a pore diameter of 2-4.2 nm. The McCool synthesis seemed to be very promising at first. The powders have high BET surface areas, mesoporous adsorption/desorption isotherms and the XRD plots show a MCM-48 structure. The characterisation of the silica layers on wafers and membranes, however, did not result in the same conclusions. The permporometry measurements determine that the pore sizes (3.5-4.2 nm) are in the desirable mesoporous range, but there is no MCM-48 structure visible in the XRD plots. Although no structure is seen, the McCool membranes are effective in retention measurements with POM in toluene. The retention of POM is more than 97.1%, which is very good.

The final conclusion is that using the Honma synthesis seems to be the best route to produce templated MCM-48 membranes, whereas the McCool synthesis route should be taken to find out more details about the silica powders.

Preface

This report is the result of ten months of research in the Inorganic Materials Science group of the faculty of Science and Technology. The past five and a half years at this university have been very pleasant for me and this final project has been a crown on the job. It was hard work sometimes, but the wonderful group members made life fun!

I would like to thank Sankho (my direct supervisor) in particular for all the insight and encouraging words he provided during this period of time. Also the rest of my graduation committee (André, Barbara, Louis and Dave) have been very helpful in discussing my results for which I am very grateful. Of course I could not have done this without the people who have helped me explaining the practical work and helping me with experiments. I would especially like to thank Mieke, Wika and Cindy for their time and also Herman, Vilmos and Louise thanks for the (many) good results! Finally, also Paul and my parents and brother have been of great help during the last five and a half years. Thanks for all the patience and the cheering up during the mental breakdowns. To all the other people who have helped me with their time and listening ears: Thanks!

Table of contents

1. Introduction	9
2. General theory	11
2.1. Sol-gel technology	11
2.1.1. Hydrolysis and condensation	12
2.1.2. Gelation	13
2.1.3. Ageing	14
2.1.4. Drying	14
2.1.5. Densification	15
2.2. Template-directed synthesis	15
2.3. Templated silica structures	17
2.3.1. History	17
2.3.2. Structure	18
2.3.3. Mechanism	19
3. Methods and materials	21
3.1. Support preparation	21
3.2. Membrane preparation	21
3.2.1. First membrane synthesis	21
3.2.2. Different synthesis approaches	23
3.3. Powder preparation	24
3.4. Materials	24
4. Powders	27
4.1. Theory	27
4.1.1. Nitrogen adsorption/desorption	27
4.1.2. TGA	29
4.1.3. XRD	29
4.2. Experimental	31
4.3. Results	32
4.3.1. Nitrogen adsorption/desorption	32
4.3.2. TGA	33
4.3.3. XRD	34
5. Wafers	35
5.1. Experimental	35
5.2. Results	35
5.2.1. XRD	35
6. Membranes	37
6.1. Theory	37
6.1.1. Permporometry	37
6.1.2. SEM	38
6.1.3. EDX	39
6.1.4. TEM	40
6.1.5. Liquid permeation and retention	41
6.1.6. Gas permeation	42

6.2. Experimental	43
6.3. Results	43
6.3.1. Permporometry	43
6.3.2. Optical microscopy	45
6.3.3. XRD	46
6.3.4. SEM and EDX	46
6.3.5. TEM	47
6.3.6. Liquid permeation and retention	49
6.3.7. Gas permeation	49
6.3.8. Rhodamine colouring	50
7. Discussion	51
7.1. Honma sol	51
7.2. McCool sol	52
7.3. General remarks	54
8. Conclusions and recommendations	55
8.1. Conclusions	55
8.2. Recommendations	55
9. Literature	58
10. List of symbols	60
10.1. Latin symbols	60
10.2. Greek symbols	61
Appendix A: adsorption/desorption isotherms	63
A.1 Honma powders	63
A.2 McCool powders	66
Appendix B: X-ray diffraction plots	71
B.1 Powders	71
B.2 Wafers	74
B.1 Membranes	77
Appendix C: pore size distributions	79
Appendix D: liquid permeation and retention graphs	85
D.1 Liquid permeation	85
D.2 Retention	86

1. Introduction

Membranes play a central role in our daily lives. Not only biological membranes in nature, also synthetic membranes have become increasingly important. The use of membranes for micro- and ultrafiltration in the world is estimated to be 200,000 m² [1]. This membrane material can be either polymeric or ceramic. The portion of ceramic membranes is only 10%, but this young field is expanding rapidly. Ceramic membranes have many advantages over organic membranes. They are stable at high temperatures and under most chemical environments. Also, these membranes are mechanically much stronger and have longer lifetimes because of the possibility of rigorous and repetitive cleaning operations. The main disadvantage is the higher costs.

Conventional inorganic membranes for liquid separation processes are in general made by sol-gel processing of inorganic precursors [1]. In general, an inorganic membrane is a combination of a macroporous support, a mesoporous layer and if necessary a microporous top-layer (figure 1.1).

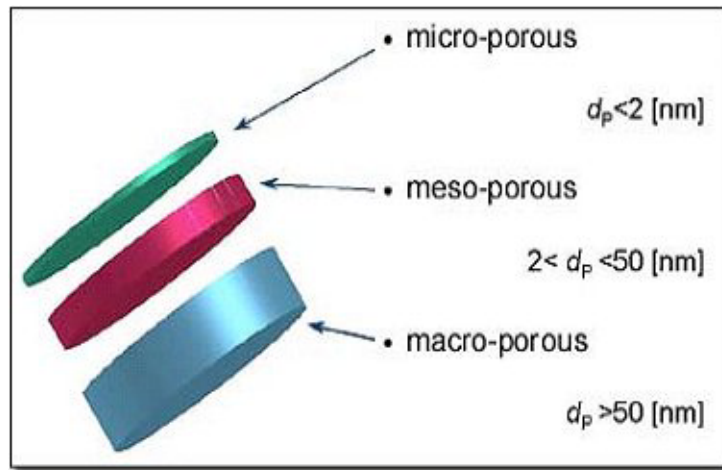


Figure 1.1: Build up of conventional inorganic membrane

A conventional (mesoporous) membrane such as γ -alumina has the disadvantage that the separating layer has a wide pore size distribution and high tortuosity. These properties affect the permeability and selectivity negatively. A method to control the pore size and tortuosity of the top-layer is using template-directed systems. A well-known example of a template-directed inorganic material is mesostructured silica [2-6]. Template-directed silica is synthesised using arrays of self-assembled surfactant molecules as structure directing templates, around which the inorganic precursor is polymerised. Depending upon surfactant concentration and processing conditions, the final pore structure of silica will exhibit hexagonal (MCM-41), cubic (MCM-48) or lamellar (MCM-50) symmetry. Due to the 3D pore structure, MCM-48 is the most desirable structure for a membrane layer. Chapter 2 will go into detail and give the theoretical background of the sol-gel technology and template-directed synthesis.

The objectives of this research project are to find a suitable synthesis for MCM-48 silica membranes supported on conventional macroporous α -alumina supports and to characterise the silica layer. The most important factors to retrieve from characterisation measurements are the mesoporosity of the silica layer, the structure of the pores in the silica and the performance of the membrane in liquid permeation processes. A membrane with a well-defined structure

and a high mesoporosity will lead to better permeation and retention results. The membranes could for instance be used to filter out the homogeneous catalyst POM from an organic effluent stream. Chapter 3 describes the synthesis routes that were explored to create MCM-48 powders, wafers and membranes. It also lists the chemicals that were used during synthesis and characterisation.

Chapter 4 explains the techniques that were used to characterise the silica powders and covers the results obtained from these experiments. Powder preparation is relatively fast and its characterisation gives a lot of information about the material properties. Nitrogen adsorption/desorption measurements were performed to retrieve information about the mesoporosity in the powders. To determine the structure of the silica powder, low angle X-ray diffraction was performed. The calcination temperature was based on thermal gravimetric analysis results.

Chapters 5 and 6 have the same outline for the description of the experiments on wafers and membranes respectively. The only experiments done on wafers were X-ray diffraction measurements to detect the structure of the silica layer. The membranes were investigated intensively:

- the mesoporosity was examined by permoporometry and gas permeation measurements
- structural measurements including X-ray diffraction, optical microscopy, scanning electron microscopy, and transmission electron microscopy
- liquid permeation and retention measurements were performed to test the permeability of the membrane

Chapter 7 discusses the results from chapters 4 to 6 and chapter 8 gives final conclusions and recommendations for future work.

Additional information, such as adsorption/desorption isotherms, X-ray diffraction plots, pore size distributions and liquid permeation results, can be found in the appendices A-D.

2. General theory

In this chapter, several topics are discussed to provide important background information for this research project. First, the basic principles of the sol-gel technology are explained. After that, the differences between conventional sol-gel synthesis and template-directed synthesis are explained and more specific comments on templated silica structures are given.

2.1 Sol-gel technology

The sol-gel technique is well-known in inorganic materials science. It is based on the generation of colloidal suspensions (“sols”), which are converted to viscous gels and then to solid material [7]. The steps in the silicon alkoxide sol-gel process are:

Hydrolysis: $\text{Si(OR)}_4 + n\text{H}_2\text{O} \rightarrow \text{Si(OR)}_{4-n}(\text{OH})_n + n\text{ROH}$

Condensation: $(\text{OR})_3\text{SiOH} + \text{HOSi(OR)}'_3 \rightarrow (\text{OR})_3\text{Si-O-Si(OR)}'_3 + \text{H}_2\text{O}$ or
 $(\text{OR})_3\text{SiOR} + \text{HOSi(OR)}'_3 \rightarrow (\text{OR})_3\text{Si-O-Si(OR)}'_3 + \text{ROH}$

Gelation: Formation of a “spanning cluster” across the vessel, giving a network with high viscosity, which entraps the remaining solution.

Ageing: A range of processes, including formation of further cross-links, associated shrinkage of the gel as covalent links replace non-bonded contacts, Oswald ripening and structural evolution with changes in pore sizes and pore wall strengths.

Drying: The loss of water, alcohol and other volatile components. This first happens via syneresis (expulsion of the liquid as the gel shrinks) and then via evaporation of liquid from within the pore structure with associated development of capillary stress, which frequently leads to cracking. It does also include supercritical drying, in which capillary stress is avoided by the use of supercritical fluids (e.g. CO_2) in conditions where there are no liquid/vapour interfaces.

Densification: Thermal treatment leading to collapse of the open structure and formation of a dense ceramic.

Sol-gel synthesis knows many advantages, such as low temperatures during all procedures (except for the densification), mild chemical conditions and control over pore size, porosity and pore wall chemistry. Despite these advantages, sol-gel syntheses are not without limitations. The precursors are often expensive and sensitive to moisture. The process is also time-consuming, particularly where careful ageing and drying are required. Finally the problems of structural change on densification and of shrinkage and stress cracking on drying require careful attention [7].

2.1.1 Hydrolysis and condensation

The first step in sol-gel chemistry is the hydrolysis, which can occur by acid or base-catalysed processes, as shown in figure 2.1 for a silicon alkoxide.

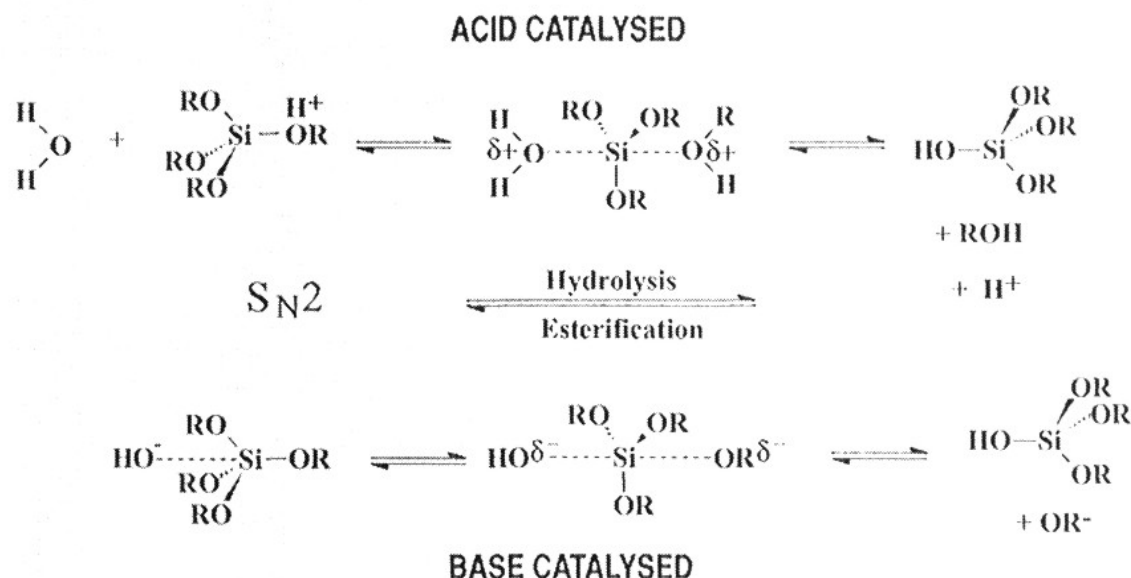


Figure 2.1: Hydrolysis mechanisms [7]

When the rates of hydrolysis of different silicon alkoxides are compared, it is found that the steric bulk of the alkoxy group exerts a large influence. Larger alkoxy groups lead to more steric hindrance and overcrowding of the transition state, thus leading to slower reactions. Therefore, tetramethylorthosilicate (TMOS) hydrolyses faster than tetraethylorthosilicate (TEOS). This is emphasized by the rate constants given in table 2.1.

Table 2.1: Hydrolysis rate constants of different silica sources

Si(OR)₄; R =	Hydrolysis rate constant / 10⁻² l*mol⁻¹*s⁻¹*[H⁺]⁻¹
C ₂ H ₅ -	5.1
C ₄ H ₉ -	1.9
C ₆ H ₁₃ -	0.83
(CH ₃) ₂ CH(CH ₂) ₃ CH(CH ₃)CH ₂ -	0.30

In addition to the above-mentioned steric effects of the substituents, the hydrophobic or hydrophilic character of the precursor must also be taken into account. Because of the hydrophobic nature of the ethoxy groups, TEOS and water are immiscible in all proportions and it is necessary to add a co-solvent to achieve miscibility and hydrolysis. Figure 2.2 shows the phase diagram for TEOS / ethanol / water.

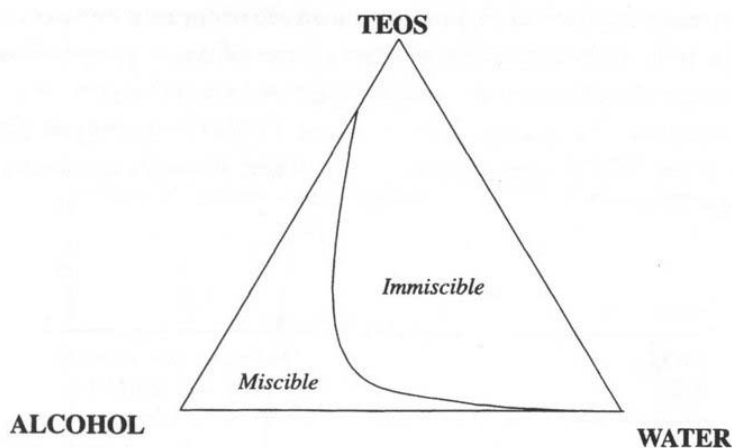


Figure 2.2: The phase diagram of TEOS / ethanol / water

The choice of co-solvent is important, since the use of a different alcohol from the alcohol generated by hydrolysis of the alkoxide can lead to trans-esterification and affect the whole hydrolysis and condensation reaction sequence. The co-solvent may influence the drying process as well.

The second step in sol-gel chemistry is the condensation of either water or alcohol. As with initial hydrolysis, condensation reactions may be acid or base catalysed. Figure 2.3 shows the condensation mechanism. In this reaction the silica polymerises and forms a network.

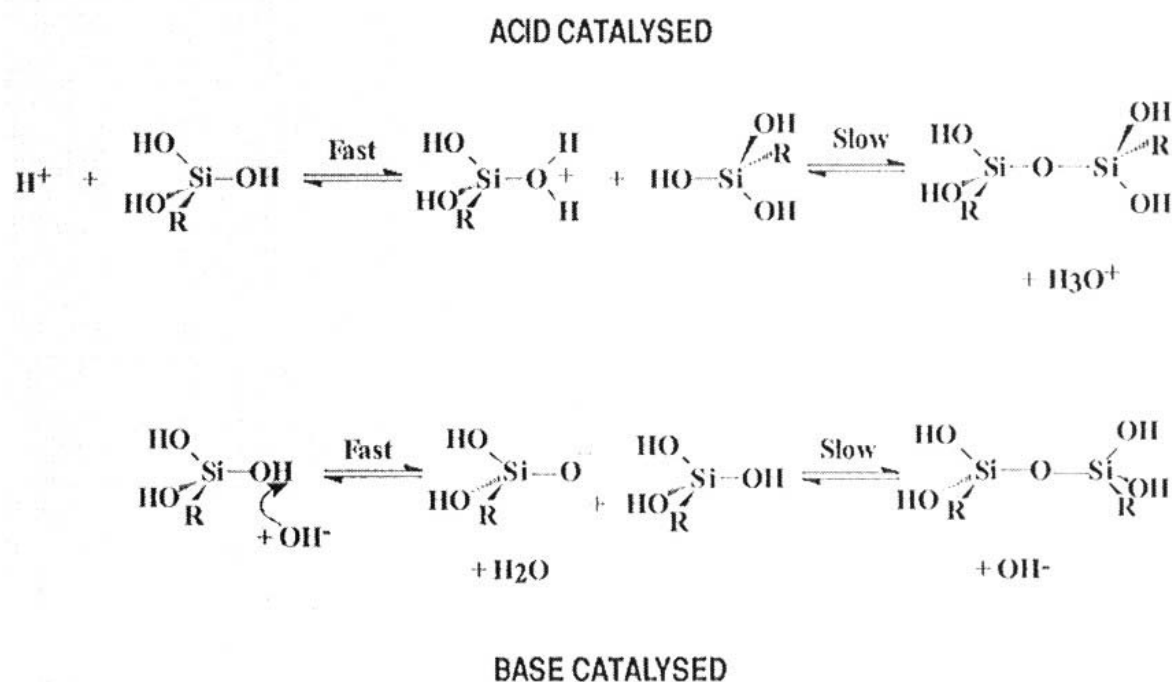


Figure 2.3: Condensation mechanisms

2.1.2 Gelation

After these chemical reactions, gelation takes place. Gelation occurs when links form between silica sol particles, produced by hydrolysis and condensation, to such extent that a giant spanning cluster reaches across the containing vessel. At this point, although the mixture has a

high viscosity, many sol particles are still present as such, entrapped in the spanning cluster. This initial gel has a high viscosity but low elasticity. There is no exothermic or endothermic, nor any discrete chemical change at the gel point, only the sudden viscosity increase. Following gelation, further cross-linking and chemical inclusion of isolated sol particles into the spanning cluster continues, leading to an increase in the elasticity of the sample.

2.1.3 Ageing

Understanding of gelation is important in applications requiring processing of either fluid (e.g. spin- or dip-coating) or self-supporting (e.g. casting) precursors. However, the continuing chemical and physical changes during ageing are of even more importance. NMR studies of gelled samples show a continuing gradual increase in the number of Q^3 and Q^4 Si species (i.e. Si attached via 4 oxygen links to three and four other silicon atoms) [7]. This is due to cross-linking via trans-pore condensation reactions of pore surface hydroxy groups. It can continue for months at room temperature, the rate depending on pH, temperature and gel composition. The net effect of these processes is a stiffening and shrinkage of the gel.

Another process associated with ageing is often referred to as coarsening or ripening. In this process, material dissolves from the surface of large particles and deposits on the initially narrow “necks” which join particles to each other. See figure 2.4.

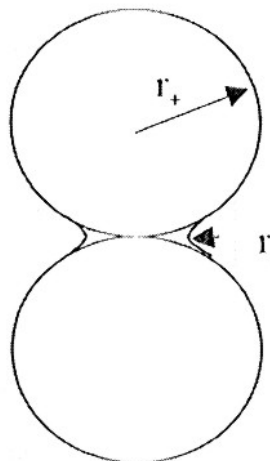


Figure 2.4: Radii of curvature of particles and “necks”

Ageing is often seen as a significant disadvantage, but considering the following points, the significance of ageing will become clear:

- Ageing usually improves the properties of the material.
- The ageing process can be controlled by varying the pH, temperature, pressure, ageing liquid medium and initial precursor mixture composition. It may thus be used to provide a range of material properties.

2.1.4 Drying

After the ageing of the gel, it must be dried to stop the structure from altering. The process of drying is based on evaporation by a sweeping gas [8]. There are four main stages in the drying of a gelled sample:

- The constant rate period

Initially a gel will shrink by an amount equal to the volume of water or other liquid, which has evaporated. This phase can only occur in gels which are still very flexible and compliant, and therefore able to adjust to the reduced volume.

- The critical point

As the gel dries and shrinks, additional cross-linking leads to a more compact structure and therefore increased stiffness. At the critical point, the gel becomes sufficiently stiff to resist further shrinkage as liquid continues to evaporate. At this point the liquid begins to recede into the porous structure of the gel. Due to its surface tension and the small size of the gel pores, very large pressures are generated across the curved interfaces of the liquid menisci in the pores. Unless the gel has been very carefully prepared to have optimum cross-linking, as well as been very carefully aged, it will crack due to this capillary stress.

- First falling-rate period

Due to the hydrophilic nature of the pore walls and capillary forces, a thin liquid film remains on the pore walls as the bulk of the liquid recedes into the capillary pores. Flow to the surface of this film followed by evaporation, as well as direct evaporation from the filled pore region, leads to further drying. Cracking may occur at any stage of this phase of drying.

- Second falling-rate period

As the meniscus recedes from the surface, it becomes increasingly difficult to maintain the liquid film on the pore wall, due to evaporation. In the beginning of the second falling-period this film is broken and further liquid transport from the filled portion of the pore must involve a vaporisation step before the liquid reaches the surface.

Various methods to avoid cracking during the drying procedure are [8]:

- Supercritical drying
- Freeze-drying
- Drying control chemical additives (DCCAs)
- Ageing

2.1.5 Densification

Although there are many applications of silica gels prepared and dried at or near room temperature, heat treatment is necessary for the production of dense glasses and ceramics from gels. From the discussions so far it is clear that, by control of the hydrolysis, condensation, ageing and drying stages, materials with a wide range of pore sizes, pore wall characteristics and general microstructure can be prepared. The detailed effects of heat treatment therefore depend on the particular characteristics of the material at the end of the low-temperature drying process. The general aspects of heat treatment are the process of particles growing together and neck-forming followed by the forming of an intersecting network of pores and particles.

2.2 *Template-directed synthesis*

When organic molecules other than solvents are added to a sol, they become entrapped upon gelation and will be retained in the xerogel (figure 2.5, xeric means dry) [7]. This procedure can be used to control the structure of the gel. The organic molecules mould the inorganic phase and after ageing and drying the gel and subsequent removal of the template the organic molecule will leave a precise imprint.

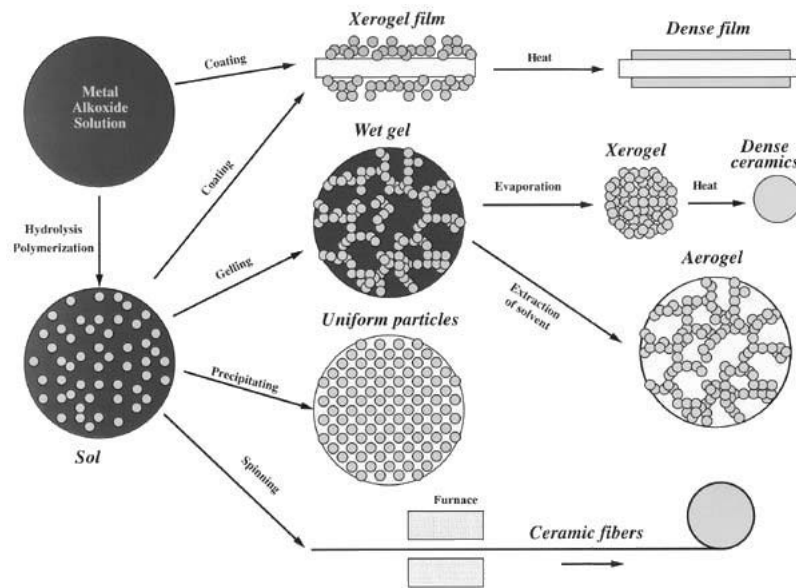


Figure 2.5: Flowchart sol-gel process [9]

The basics of organic templating are shown in figure 2.6. The silica source will polymerise around the organic template, which is burned out in an oven after the polymerisation has been completed. This leaves a pore with a similar structure as the template structure.

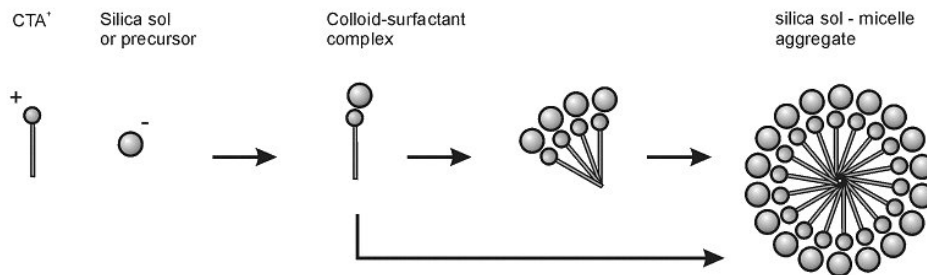


Figure 2.6: Schematic organic templating approach [10].

The properties of the silica structure and pore dimensions are governed by the type of organic template (also called surfactant) and process conditions. The length of the surfactant is the easiest factor to influence the pore size (every additional C adds 2.25 Å to the diameter of the pore), but also addition of extra organic compounds, the choice of solvent and the template removal method are influencing factors. The electrical charge of the surfactant and the formation mechanism of the silica structure determine the thickness of the walls. [11]

The template is based on a micelle ordering. A typical phase diagram is shown in figure 2.7. When the surfactant concentration is increased to a point beyond the first critical micelle concentration (CMC 1), the loose molecules form micelles. The lowest temperature at which micelles can form is called the Krafft temperature, which depends on the solubility of the surfactant [12]. After passing another CMC, the micelles gather together in rods. Further increase will lead to three structures: hexagonal, cubic or lamellar. As can be seen in the same figure, but more clearly in figure 2.8, the hexagonal and lamellar structures can only have transport when oriented in the right direction. However, recent publications [13-15] have shown that the hexagonal structure tends to orientate its pores parallel to the surface (and therefore per-

pendicular to the transporting direction). The cubic structure has the advantage that the orientation at the surface does not matter. Transport is possible in all directions, because of the connected pores of the 3D structure.

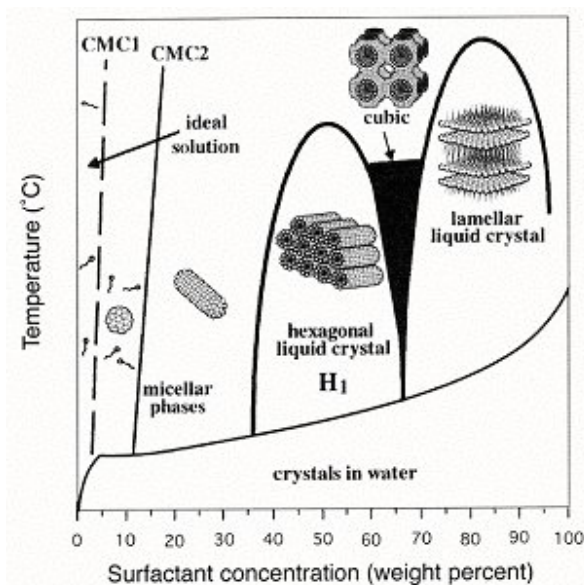


Figure 2.7: Phase diagram of the silica-surfactant system

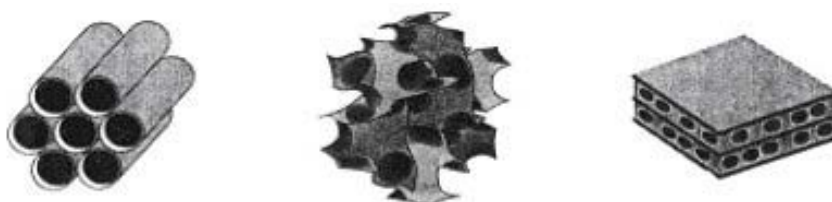


Figure 2.8: Hexagonal, cubic and lamellar templated silica structures

2.3 Templated silica structures

2.3.1 History

In 1992, J. S. Beck et al. [2] discovered a new kind of mesoporous silica powder synthesis. The mesoporous molecular sieves were designated as M41S. One member, MCM-41, exhibits a hexagonal arrangement of uniform mesopores. Well-defined pores (minimal radius \approx maximal radius) in the range of 15 to over 100 Å and ordering of the pores are very useful in membrane research. Other members of this family are the cubic (MCM-48) and lamellar (MCM-50) phases. [16] These researchers found that relative concentrations of the chemicals present in the synthesis solutions were of great importance for the final pore structures. They also showed that the pore diameter of MCM-41 increases as the chain length of the surfactant increases.

The MCM-48 structure was barely mentioned in the first reports on M41S powders [2, 3]. An accurate synthesis procedure was not published until approximately one year later [4]. The main difference in the synthesis of MCM-48 compared to that of MCM-41 is the surfactant to silica ratio in the synthesis solutions [5]. Huo et al. [6] have systematically investigated different surfactants in order to obtain a reliable synthesis of cubic materials.

The first synthesis of a mesoporous silica film with hexagonal pore ordering was reported by Yang et al. [13]. They grew thin films with thicknesses ranging from 0.2 to 1.0 μm on a cleaved mica substrate. The pores were parallel to the mica surface though. Aksay et al. [17] showed that mesostructured silica films can be grown at substrates ranging from hydrophilic mica to hydrophobic graphite. The substrate-surfactant interactions were found to influence the pore structure. Furthermore, films have been grown at the water-air surface [18, 19]. These films can easily be isolated since they do not interact with any substrate. Mesoporous films have also been prepared by utilizing deposition on a polyethylene substrate [20], a dip-coating method [21] and a pulsed laser method [22].

A major disadvantage of the films discussed so far is that the pores are aligned parallel to the substrate or interface that they were grown on. In potential applications such as membranes and sensors for large molecules, the pores must be perpendicular to the solid substrate or interface. One possible way to deal with this problem is to synthesize three-dimensional mesoporous films. Tolbert et al. [23] grew this type of (cubic) film both on mica substrate and at the water-air interface.

Generally, MCM-48 type materials have been obtained using high surfactant to silica ratios (from 0.65 to 1.5) [24]. It is also believed that the presence of polar organic additives in the synthesis gel is mandatory for the formation of the cubic structure [6]. In most of the reported synthesis of MCM-48 materials, tetraethylorthosilicate (TEOS) has been used as silica source. Upon hydrolysis, TEOS yields to the formation of ethanol (see hydrolysis and condensation equations), which induces the formation of the cubic structure. It has also been reported that the use of gemini surfactants (which contain two polar head-groups separated by a variable length methylene chain) induce the formation of the cubic structure [25].

2.3.2 Structure

Studies show [26] that MCM-48 is much better organized (on a 100 \AA length scale) and much more homogeneous than the product of a typical MCM-41 synthesis. At the short-range scale, 1 to 10 \AA , MCM-48 (like MCM-41) is an amorphous hydroxylated silicate [27]. Very little is understood about its structure. The Q^4 ($\text{Si}[\text{OSi}]_4$) to Q^3 ($\text{Si}[\text{OSi}]_3\text{OH}$) ratio is usually 2:1, but the wall-thickness in MCM-48 is undetermined. It is also somewhat unclear if the wall is uniform or if there are some microporous pores in the walls.

The structure of MCM-48 on the 100 \AA length scale (medium range) has been shown to be such that the mid-plane of the wall lies on the minimal surface known as the gyroid surface [27]. Such a surface is as concave as it is convex, except at the flat points [16]. Figure 2.9 shows a schematic image of the crystallographic unit cell [28]. The structure consists of two interpenetrating three-dimensionally continuous networks. The networks are composed of cylinder-like connectors aligned along (110) directions joining in threes at nodes. There are 16 triple junction nodes per unit cell.

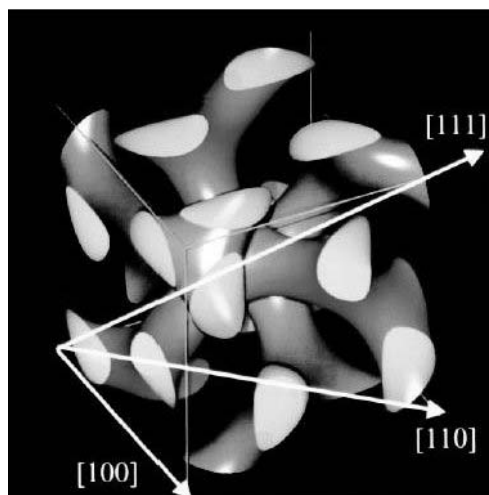


Figure 2.9: Schematic of the crystallographic unit cell of the double gyroid morphology.

At the 1- μm level MCM-48 forms particles that, when observed by very high resolution scanning electron microscopy, exhibit facets. The particles are not usually monodisperse, but range in sizes between 0.1 and 1 μm . The regular morphological nature of the particles, which tends to a truncated octahedral, is a result of the excellent organization of the wall structure in MCM-48 right across the particulates [27].

2.3.3 Mechanism

There is a remarkable similarity between the M41S materials and lyotropic liquid crystalline phases [16]. This, and the fact that the pore sizes are tuneable from 15 to 100 \AA , led to the suggestion of the liquid crystal templating (LCT) formation mechanism [2, 3, 29]. Two possible pathways were proposed [2]. One in which the liquid crystal phase is intact before the silicate species are added and another one in which the addition of the silicate somehow affects the assembly of surfactants into ordered arrays. See figure 2.10. In either case a liquid crystal template is implicated [30].

The formation of different phases (hexagonal, cubic or lamellar) by changing the surfactant to silicate ratio also supports the liquid crystal templating mechanism, since this variation in reactant composition changes both the surfactant concentration and the ionic strength, either of which can induce liquid crystal phase changes [2].

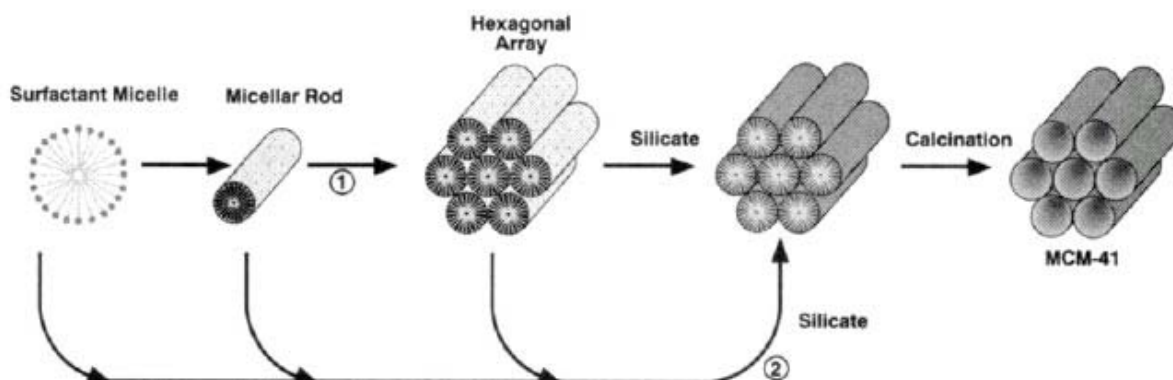


Figure 2.10: Possible mechanistic pathways for the formation of MCM-41: (1) liquid crystal phase initiated and (2) silicate anion initiated

However, the first pathway does not seem very likely [16, 5], since the amount of surfactant in the synthesis solutions is less than what is needed to form liquid crystalline phases in pure water. Several other and more sophisticated formation models have been proposed later on. Common for these is the consideration that surfactants in solution conduct the ordering of the materials, but the type of interactions between the surfactants and inorganic species are viewed differently.

The most extensive studies on the formation mechanisms of mesoporous structures have been done by Stucky and co-workers [4, 6, 25, 31-33]. They have developed a cooperative model that describes the formation of surfactant-inorganic materials.

The formation mechanism proposed by Stucky [4] can be summarized in three steps:

- 1) Net ionic exchange of monoanions (OH^- , Cl^- , Br^-) by polycharged anionic inorganic species.
- 2) Organization of new liquid crystalline-like array. This process in particular has been studied by Stucky et al. [33], who decoupled the surfactant self-assembling process and the polymerisation effects.
- 3) Condensation of the organic phase.

3. Methods and materials

In this chapter the details of the experimental synthesis are given. The recipe for the first set of experiments is taken from an article by Honma et al. [34]. The templated silica system is described with good results and the recipe is easy to follow. Further research was done on the basis of articles by Kim [35] and McCool [36]. The preparation methods of the sol, powder and membrane are given, as well as the choices that were made during the project.

3.1 Support preparation

The flat membrane supports on which the silica layers are coated are made of α -alumina (AKP-30). To prepare 9 supports, 160 g of AKP-30 is added to 160 g of 0.02 M HNO_3 in a beaker. The suspension is ultrasonically treated for 15 minutes and filtered through a metal filter with 200 μm pores. After the filtering, the suspension is poured into the moulds. The moulds are placed on a vacuum bench and the pump is allowed to drain off the water for three hours. The supports are dried overnight and sintered at 1100°C for 1 hour with a heating/cooling rate of 2°C/min. The supports are cut to fit a diameter of 39 mm and thickness of 2 mm. The result is a flat α -alumina support with a pore diameter of 80 nm and a porosity of 35%.

Some supports needed a γ -alumina coating. The dip sol is prepared by mixing 30 ml of boehmite sol with 20 ml of PVA (polyvinyl alcohol) solution, which is made with 150 g of 0.05 M HNO_3 added to 4.5 g of PVA (MW=72000 g/mol) and stirred for 2 hours at 80°C. The supports were dip-coated into the γ -sol with turning speed 10 (approx. 23.9 cm s^{-1}) and dip-coating speed 0.2 (approx. 1.1 cm s^{-1}). To calcine the membrane, the oven settings for this system were set at 800°C or 900°C / $\uparrow\downarrow$ 1°C/min / 180 min. This procedure was done only once, because the results from permoporometry measurements indicate a defect free layer. The result is a flat γ -alumina support with a pore diameter of 3-4 nm and a layer thickness of 1.5 μm .

3.2 Membrane preparation

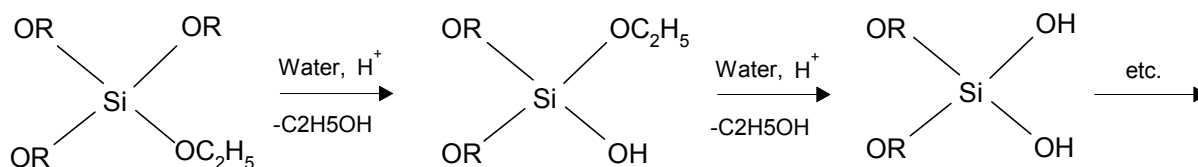
3.2.1 First membrane synthesis

For the preparation of a templated membrane, a sol has to be made from a silica source and a surfactant via the sol-gel technique. As described in paragraph 2.2, its structure can be very different depending on the silica:surfactant ratio. To prepare a sol with a cubic structure, a specific CTAB: SiO_2 (cetyltrimethylammonium bromide, figure 3.3 (left)) molar ratio was used, which lies between the amounts for a hexagonal (< 0.12) and a lamellar structure (> 0.14) [37]. The synthesis recipe that has been followed originally in this research is described by I. Honma et al. [34]. The membranes that were produced in the article showed well-formed, reproducible templated silica layers.

First, 8.0 ml of silica source TEOS (tetraethoxyorthosilicate, figure 3.3 (right)) is measured in a 10 ml cylinder. All liquids, except the small amount of HCl, can be measured in this cylinder. Together with 17.47 ml of the solvent 1-propanol it is stirred at 600 rpm in a 100 ml flask for 5 minutes. The TEOS was then hydrolysed by an HCl solution in water (0.33 ml HCl in 2

ml water) and stirred for 60 minutes. Co-solvent 2-butanol (8.75 ml) was added and stirring was continued for another 30 minutes. The reactions that are taking place are (figure 3.1):

Hydrolysis:



Condensation:

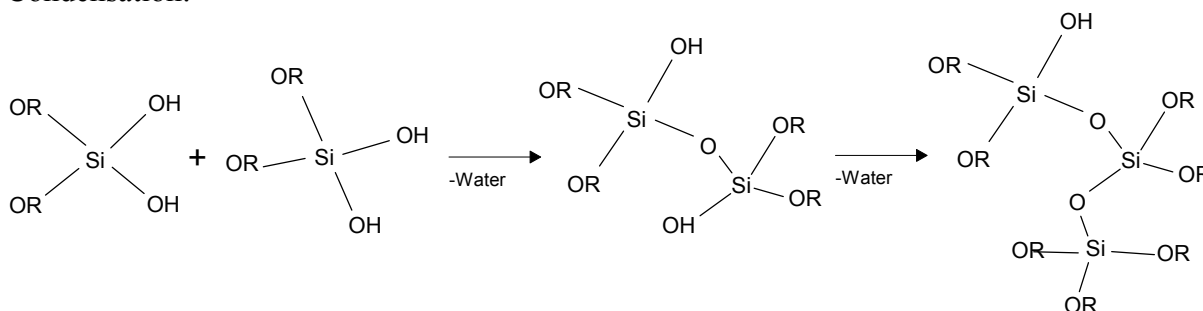


Figure 3.1: Hydrolysis and condensation reactions

The last step is to prepare a solution of 1.75 g of CTAB (weighed off in a petri dish on an analytical scale) dissolved in 4.43 ml of Q2 water. This surfactant solution is prepared separately and then poured into the silica solution. Again, stirring for a period of 60 minutes is necessary. The sol has to be aged in a fridge for at least one night to form its silica structure. The longer the ageing time, the more developed the structure gets.

Alumina supports were dip-coated into the sol (turning speed 10 (approx. 23.9 cm s^{-1}) and dip-coating speed 0.2 (approx. 1.1 cm s^{-1}), see figure 3.2). To burn out the surfactant and calcine the membrane, the oven settings for this system were set at $450^\circ\text{C} / \uparrow\downarrow 0.2^\circ\text{C}/\text{min} / 180 \text{ min}$. The whole procedure was repeated once more to create a thicker and crack-free layer onto the support.

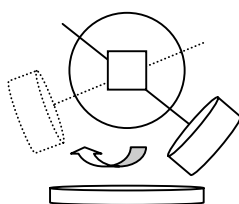


Figure 3.2: Dip-coating set-up

During dip-coating of the support in the surfactant silica sol, preferential evaporation of ethanol concentrates the sol to non-volatile surfactant and silica species [38]. The progressively increasing surfactant concentration drives self-assembly of silica/surfactant micelles and their further organization into liquid crystalline mesophases. This results in rapid formation of highly ordered mesostructured silica films with controlled pore structure (e.g. hexagonal or cubic), depending on the choice of surfactant and initial ethanol/silica/surfactant molar ratio in the starting sol.

3.2.2 Different synthesis approaches

Because the first synthesis did not result in a silica layer on the α -alumina membrane (paragraph 6.3), a different approach was tested. This technique is described by Y.-S. Kim and S.-M. Yang [35]. The pores are filled with a polymer solution, which closes the pores before dip-coating with silica. A solution of 10 wt% PVA is made by dissolving 10 g of PVA (MW=13000-23000 g/mol) in water and stirring it for 2 hours at 80°C.

The supports were dip-coated with the PVA solution to fill the pores (turning speed 10 (approx. 23.9 cm s^{-1}) and dip-coating speed 0.1 (approx. 0.6 cm s^{-1})). After drying overnight, the supports were dip-coated with the Honma silica sol. To burn out the PVA and calcine the membrane, the oven settings for this system were set at 550°C / $\uparrow\downarrow 1^\circ\text{C}/\text{min}$ / 180 min. The whole procedure was repeated once more to create a thicker layer onto the support. The PVA-synthesis route unfortunately resulted in a loose layer of silica on top of the alumina support (paragraph 6.3), which could not be used.

After being confronted with these results, the decision was made to look into completely different syntheses. Up till now, four types of MCM-48 syntheses have been described in literature:

- via quaternary ammonium surfactants like CTAB and CTAC [34, 36, 39-44]
- with gemini surfactants (one tail, two heads) [23]
- or DDAB surfactants (one head, two tails) [45]
- using non-ionic polymer chains as structure directing agents [46-49]

Gemini and DDAB surfactants are not common commercial products yet and therefore experimenting with this synthesis method was not pursued. Using polymers will create a too large pore size. There are many articles that describe successful syntheses while using quaternary ammonium surfactants. As these procedures are easy to follow without the need of special (expensive) chemicals, a similar synthesis procedure to Honma was followed, described by B.A. McCool et al. [36].

First, 22.3 ml of silica source TEOS (tetraethoxyorthosilicate) is measured in a 25 ml cylinder and poured into a 200 ml flask. 17.5 ml of the solvent ethanol is stirred in at 600 rpm. The TEOS is then hydrolysed by an HCl solution in water (5 μl HCl in 1.8 ml water) and refluxed at 60°C for 60 minutes. After cooling to room temperature, more ethanol (99.1 ml) and aqueous HCl (395 μl in 7.2 ml water) is added. Finally 5.102 g CTAB is weighed off in a petri dish on an analytical scale and mixed into the solution. The article describes that the sol has to be aged in a fridge for at least a week before coating to form its silica structure.

The supports were dip-coated (turning speed 10 (approx. 23.9 cm s^{-1}) and dip-coating speed 0.2 (approx. 1.1 cm s^{-1})). To burn out the surfactant and calcine the membrane, the oven settings for this system were set at 450°C / $\uparrow\downarrow 0.2^\circ\text{C}/\text{min}$ / 180 min. The whole procedure was repeated once more to create a thicker and crack-free layer onto the support.

3.3 Powder preparation

After one or more days of ageing, a sol can be dried in a glass petri dish under air or nitrogen. The gas has a low velocity and is flowing parallel over the surface for 8 hours or more. Ethanol will be evaporated after a few hours and a glassy material is left in the dish. At first the powders were calcined at 400°C (↑↓ 0.2°C/min / 180 min), but the powders were brown from organic residue when they came out of the oven. According to TGA measurements, the powder needed to be heated up to at least 550°C. This is also according to [12] the temperature to eliminate the surfactant CTAB.

3.4 Materials

The details of the chemicals that were used for these syntheses and the permoporometry and liquid permeation measurements are given in table 3.1. Figure 3.3 shows the structural formulas of CTAB and TEOS. The structure of the sandwiched POM ($\{[\text{Zn}(\text{H}_2\text{O})]_2\text{ZnW}(\text{ZnW}_9\text{O}_{34})_2\}^{\text{q-}}$, polyoxomethalate) catalyst used in the retention measurements is given in figure 3.4. The catalyst was provided by DSM dissolved in water and toluene. It is a Keggin structure with Na^+ counter ions in water and a quaternary ammonium counter ion in toluene. Its size is in the order of 1.5 nm.

Table 3.1: Chemicals

Chemical	Supplier	Cas-number	Purity [%]
AKP-30	Sumitomo Chemical Company	1344-28-1	99.5
2-butanol (C ₄ H ₁₀ O)	Merck	78-92-2	99
CTAB (C ₁₉ H ₄₂ BrN)	Aldrich	57-09-0	-
CTAC (C ₁₉ H ₄₂ ClN)	Acros	112-02-7	99
Cylcohexane (C ₆ H ₁₂)	Merck	110-82-7	99.5
Ethanol (C ₂ H ₆ O)	Merck	64-17-5	99
HCl (1N)	Merck	7647-01-0	37
Hexane (C ₆ H ₁₄)	Lamers & Pleuger	110-54-3	technisch
HNO ₃ (0.02 M)	Merck	7697-37-2	65
HNO ₃ (0.05 M)	Merck	7697-37-2	65
1-propanol (C ₃ H ₈ O)	Acros	71-23-8	> 99
PVA (72000 g/mol)	Fluka	9002-89-5	> 98
PVA (13000-23000 g/mol)	Aldrich	9002-89-5	> 98
TEOS	Aldrich	76-10-4	> 98
Toluene (C ₇ H ₆)	H. Assink	108-88-3	technisch

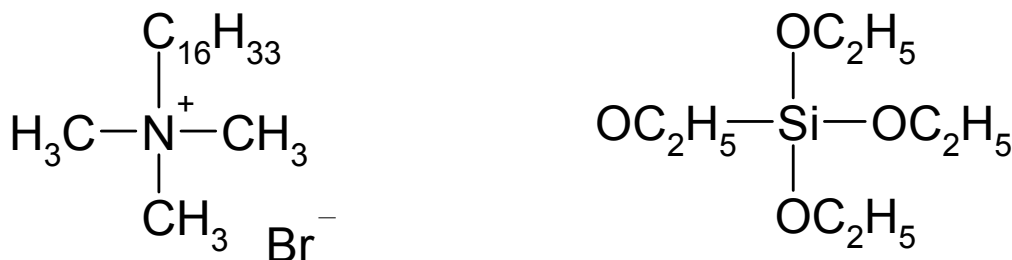


Figure 3.3: Cetyltrimethylammonium bromide (left) and tetraethoxyorthosilicate (right) structure

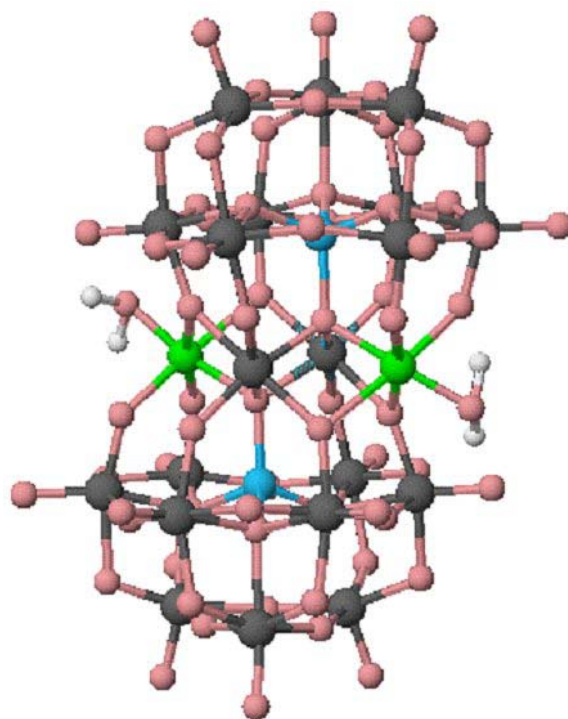


Figure 3.4: POM catalyst structure $\{[Zn(H_2O)]_2ZnW(ZnW_9O_{34})_2\}^{9-}$

4. Powders

Although the final goal is to make and characterise templated silica membranes, producing powders could be a quick way to see what is actually going on in the sol. The sols were dried at different ageing times to see if the structure of the sol developed over time. In the theoretical paragraphs of this chapter and the following ones, the techniques that are used for the characterisation of the materials are discussed. The powders were characterised by nitrogen adsorption/desorption, TGA and XRD. In the experimental part, more details are given on which powders were produced and characterised. Finally the results of the characterisations are described.

4.1 Theory

4.1.1 Nitrogen adsorption/desorption

Adsorption techniques are used to determine the porosity and specific surface area of materials. The most common adsorbate is probably N₂ at its boiling point (77.4 K). Different models for calculating the pore size distribution have been developed. Langmuir described a monolayer adsorption method using the following assumptions [7, 50]:

- The surface of the adsorbent is flat
- All adsorption sites are energetically equivalent
- The adsorbed gas molecules do not mutually interact
- The adsorbed molecules have a fixed position on the surface

In practice, however, these assumptions are seldomly met: surfaces are never flat and adsorption sites are not energetically equivalent and adsorbed gas molecules do have mutual interactions.

Brunauer, Emmett and Teller developed a more practical method, which still uses the above-mentioned suppositions, but allowed for the adsorption of multilayers. In this model the assumption is made that adsorption forces are short-range forces, i.e. that the heat of adsorption of the first layer is higher than that of following layers. In these other layers the heat of adsorption is assumed to be equal to the latent heat of condensation of the adsorbed gas.

The BET equation reads:

$$\left(\frac{p}{p^0 - p} \right) = \frac{1}{v_m C} + \frac{(C-1) \left(\frac{p}{p^0} \right)}{v_m C} \quad 4.1$$

p/p^0 = relative pressure [-]

p^0 = vapour pressure above a multilayer of adsorbate [Pa]

v = volume of gas adsorbed [m³/g STP]

v_m = volume of gas adsorbed in the monolayer [m³/g STP]

$C = e^{(Q-L)/R}$ [-]

Q = heat of adsorption of the first layer [J/molK]

L = latent heat of condensation of the gas [J/molK]

R = gas constant [J/molK]

The BET surface area (S_{BET}) can be calculated (see equation 4.2) if v_m is known. This value can be obtained through a plot of the volume of gas adsorbed versus the relative pressure (p/p^0), whereby v_m is calculated from the intercept of the first part of the isotherm.

$$S_{\text{BET}} = \frac{N_{\text{av}} O_m v_m}{RT_0} \quad 4.2$$

S_{BET} = BET surface area [m^2/kg]
 N_{av} = constant of Avogadro [$1/\text{mol}$]
 O_m = area of 1 mol N_2 [m^2]
 T_0 = room temperature [K]

The obtained isotherms generally can be grouped in 5 classes, the characteristic features of which are shown in figure 4.1. Isotherm type I is typical for adsorption in microporous materials where the BET equation is not valid. Type II isotherms are characteristic for non-porous materials and types III and V are obtained for very weak adsorption interactions of which the fundamentals are not very well understood.

For mesoporous materials, generally isotherms of type IV are obtained. At low relative pressures the adsorption only occurs as a thin layer on the walls (monolayer coverage). Depending on the pore size, a sharp increase is seen at relative pressures from 0.25 to 0.5. This corresponds to capillary condensation of the gas in the mesopores. The sharpness of the increase reflects the uniformity of the pore sizes and the height indicates the pore volume. A hysteresis effect is often observed for N_2 adsorption-desorption isotherms when the pore diameter is larger than approximately 40 Å. [16]

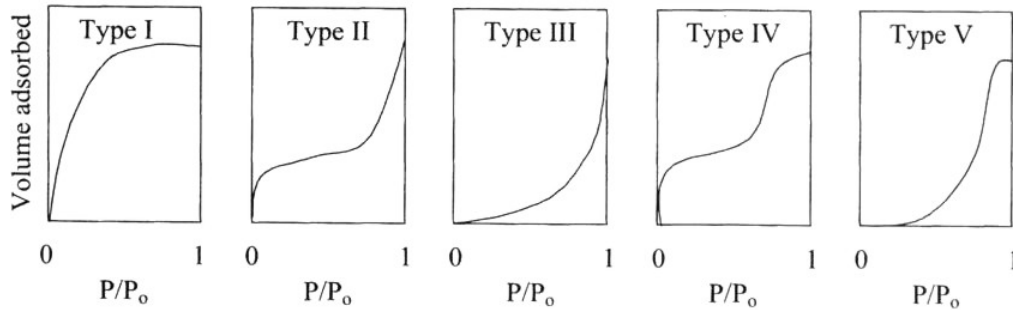


Figure 4.1: Characteristic shapes of the five classes of BET adsorption isotherms

This is explained by the Kelvin equation, which states that the vapour pressure of curved surfaces differs from that of planar surfaces [7]. As a consequence, the rate of desorption in pores can differ from the rate of adsorption, depending on the size and shape of the curve. This means that the shape of the isotherms can be related to the pore size distribution in the material. By applying the Kelvin equation (4.3) in an appropriate form a gradual desorption experiment can be used to obtain a pore volume distribution in the form of a plot of $\Delta V^0/\Delta \bar{r}$ as a function of the average pore radius \bar{r} .

$$\frac{p}{p_0} = \exp\left(\frac{-2\sigma v_m}{RT r_k}\right) \quad 4.3$$

$$r_p = r_k + t \quad 4.4$$

σ = surface tension [N/m]
 r_k = Kelvin radius [m]
 r_p = pore radius [m]
 t = t-layer (monolayer of N_2 adsorbed at very low concentrations) [m]

The total porosity can be calculated from equation 4.5 [60].

$$\varepsilon = \frac{V_p}{V_p + \frac{1}{\rho}} \times 100\% \quad 4.5$$

ε = porosity [%]
 V_p = pore volume [cm^3/g]
 ρ = density solid phase [g/cm^3]

4.1.2 TGA

For Thermal Gravimetric Analysis (TGA) material is suspended from a balance and the weight loss is monitored during controlled heating or cooling or under isothermal conditions. The components are determined by a mass spectrometer.

4.1.3 XRD

In X-Ray Diffraction (XRD) a beam of X-rays, with wavelength $\lambda \sim 0.5 - 2 \text{ \AA}$, is incident on a surface and is diffracted by the crystalline phases in the specimen according to Bragg's law (equation 4.6, figure 4.2). The intensity of the diffracted X-rays is measured as a function of the diffraction angle 2θ and the specimen's orientation [51].

$$\lambda = 2d \sin \theta \quad 4.6$$

λ = wavelength [m]
 d = spacing between atomic planes in crystalline phase [m]
 θ = angle [$^\circ$]

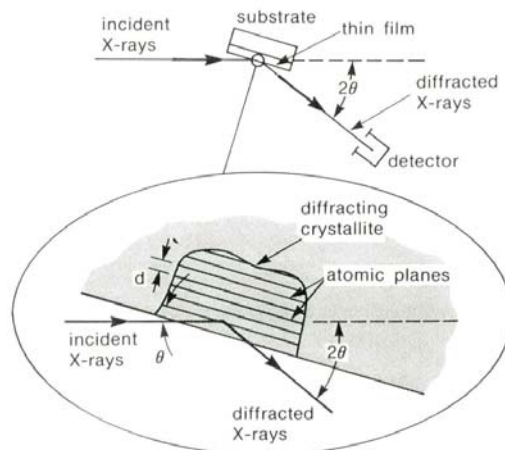


Figure 4.2: Basic features of a typical XRD experiment

XRD provides direct information of the pore architecture of the materials (e.g. geometry, lattice constants, orientation, defects [52]). For mesoporous materials, the diffraction patterns only have reflection peaks in the low-angle range, meaning 2θ less than 10° [16]. No reflections are seen at higher angles. It has therefore been concluded that the pore walls mainly are amorphous. The ordering lies in the pore structure and the low-angle diffraction peaks can be indexed according to different lattices. In literature many examples of the MCM-41 to 50 spectra are given, but not most of them are not very clear. Typical powder spectra, which show all important peaks, are given in figure 4.3 [2, 53].

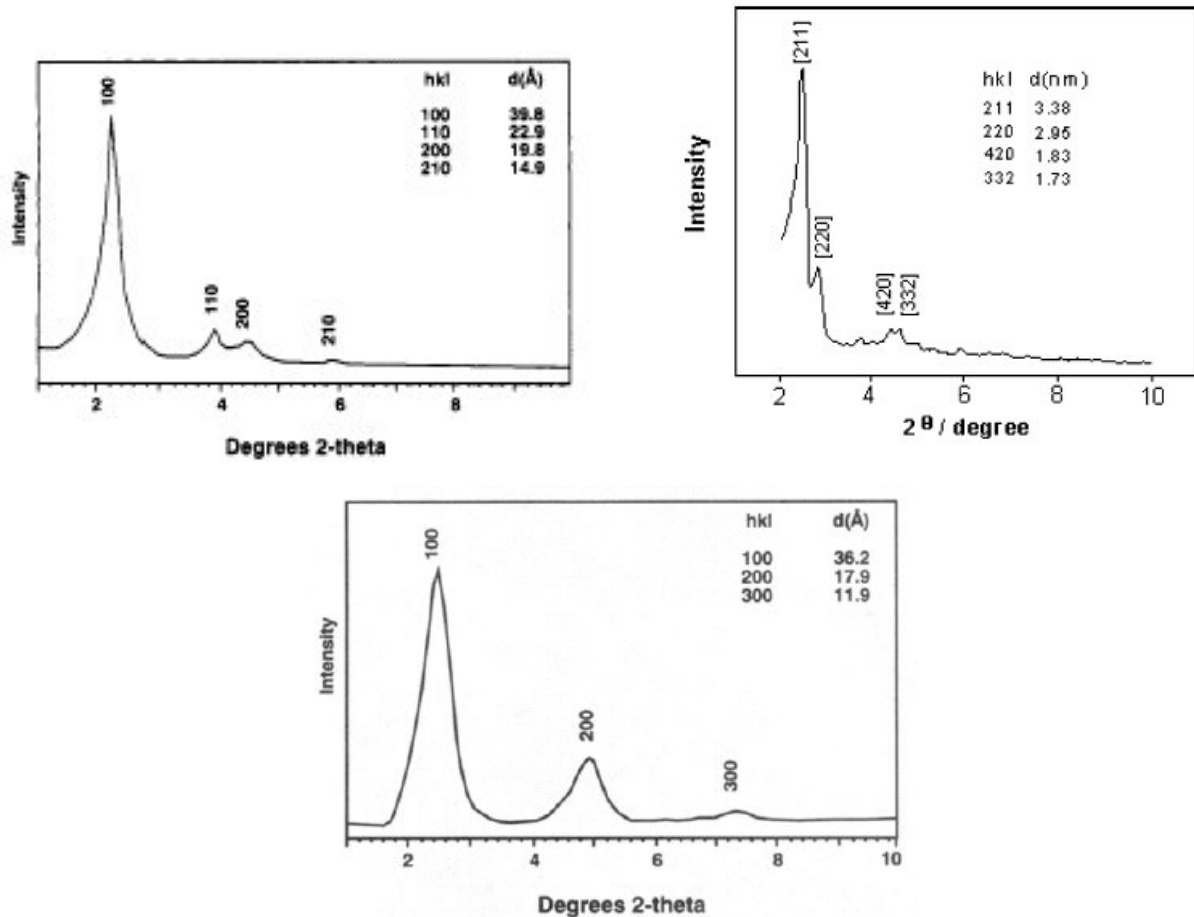


Figure 4.3: XRD powder spectra of the MCM-41 (top, l), MCM-48 (top, r) and MCM-50 (bottom) structure

Typical for the cubic structure are the shoulder around 3° and the two peaks close together around 4.5° . The MCM-41 spectrum does not have a shoulder and has three broader peaks. Equation 4.7 gives the formula to match the peaks with the cubic structure. When the plot matches the structure, all peak-assignments will result in one lattice parameter.

$$\frac{1}{d^2} = \frac{1}{a^2} \left(\frac{1}{h^2} + \frac{1}{k^2} + \frac{1}{l^2} \right) \quad 4.7$$

a = lattice parameter [m]
h, k, l = Miller indices [-]

4.2 Experimental

To produce templated silica powders, all syntheses described in chapter 3 were used. The powders produced via the first synthesis procedure (the Honma synthesis in paragraph 3.2.1) were dried under a constant nitrogen stream after allowing them to age in the fridge for various times (one to eight days). The original article mentions nothing about the ageing time and other references also give very little or inconsistent information. One article [39] specifically states that ageing the sol for 24 hours gives no organization. Only after 7 days the sol has reached the best structure. Figures 4.4 a and b [24] also show a dynamic system. Dependent on the calcining temperature, the MCM-48 mesophase only appears between a few hours and 7 days.

The Honma synthesis is originally carried out with CTAC (cetyltrimethylammonium chloride) instead of CTAB. To determine if there is any difference in the results, also powders with CTAC were made.

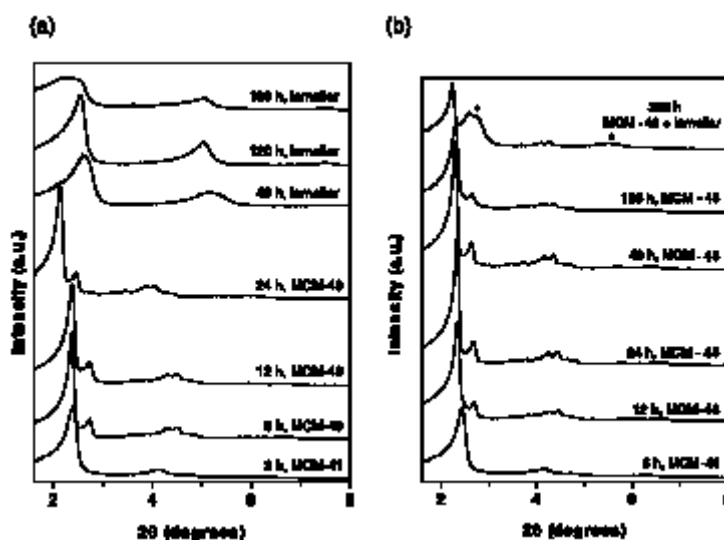


Figure 4.4: XRD patterns of the different mesophases obtained after different crystallisation times at 150°C (a) and 135°C (b) from gels having the following molar composition: $\text{SiO}_2:0.30\text{CTAOH}:39\text{H}_2\text{O}$. The figure in the reference is of poor quality. Figure (a) contains patterns after 3 hours until 100 hours, starting at the bottom with MCM-41, then three MCM-48 structures and finally three lamellar patterns. Figure (b) contains patterns after 6 hours until 300 hours, starting at the bottom with MCM-41, then four MCM-48 structures and finally a MCM-48 + lamellar pattern.

The second series of powders, which is produced via the synthesis described by B.A. McCool et al. (3.2.2), differs in procedure and in added solvent from the Honma synthesis. The sol is ethanol-based and is refluxed for 1 h at 60°C before adding the CTAB. Furthermore, the article states clearly that the ageing time should be one week. Only then will the structure form. To verify this and to measure any differences in pore sizes and structure in time, powders were dried under air after ageing times ranging from 7 to 36 days.

All powders have been characterised by nitrogen adsorption/desorption (Micrometitics type ASAP 2400). The adsorption measurements are performed with nitrogen at 77K and with a minimum surface area of 10 m². The results of the BET surface measurement contain an error of 3 to 5%. For the TGA (Mettler) measurements only two Honma sols with CTAB have been used (uncalcined or calcined at 400°C). The measurements were performed with 36 to 44

grams of silica powder. Both Honma (prepared with CTAB) and McCool powders have also been measured with XRD (PANalytical X'Pert-APD, CuK α radiation ($\lambda = 1.54 \text{ \AA}$), 40 kV, 50 mA) at low angles (usually 0 to 10 $^\circ$).

4.3 Results

4.3.1 Nitrogen adsorption/desorption

All nitrogen adsorption and desorption measurements on the calcined powders produced via the Honma synthesis show that there is no mesoporous ordering in the powders (appendix A, paragraph A.1). The isotherms are more like type I isotherms for microporous systems instead of the type IV (figure 4.1) that was expected. The adsorption isotherms for the powders made with CTAC are not mesoporous either. Table 4.1 shows BET surface areas and pore diameters, which have been calculated from the adsorption data. The BET surface area is high, which points towards a very open structure. Judging from the curve of the isotherms and the pore diameters, however, all pores are micropores and not many changes during the ageing process are observed, even after long-term ageing.

Table 4.1: Adsorption/desorption data Honma powders

Surfactant	Ageing time	Isotherm	BET surface area [m ² /g]	Pore diameter [nm]
CTAB	1 day	Microporous	1032	1.79
CTAB	2 days	Microporous	916	1.35
CTAB	24 days	Microporous	971	1.36
CTAC	1 day	Microporous	1077	1.75
CTAC	3 days	Microporous	1125	1.70
CTAC	6 days	Microporous	1037	1.80

The nitrogen adsorption and desorption isotherms of the powders produced via the McCool synthesis show a microporous isotherm after 7 days of ageing (figure A.7). From this result one could conclude that after one week of ageing the MCM-48 structure has not formed yet. After 10 to 14 days, the measurements result in mesoporous isotherms (figures A.8-A.12). If powder and membrane layers would be comparable, the advice would be to coat the supports after 10 days of ageing or longer. However, except from the fact that the drying mechanism is completely different, the powders that were retrieved after 21 days of ageing gave an unexpected result (figure A.13). The isotherms were again of the microporous type. After ageing for 28 and 36 days (figures A.14 and A.15), the isotherms showed a mesoporous curve again. These results conclude that the structure of the sol is constantly changing. Table 4.2 shows that in time not only the shape of the curve changes, but also the values for surface area, pore diameter and (mesoporous) porosity. These values have been calculated with equations 4.1 to 4.5. The density of silica was taken as 2.2 g/cm³. For the mesoporous isotherms, the mesoporous porosity has been calculated by comparing the mesoporous section of the curve with the total porosity. The values in table 4.2 are given as the real percentage of the membrane that has mesopores. For example (10 days): when 51.6% of the adsorbed volume is mesoporous (160 cm³/g of the total 310 cm³/g) and the total porosity is 52.8%, the mesoporosity is 27.3%.

When comparing the data retrieved from the mesoporous curves, there is not much variance in the data for the BET surface area (747-854 m²/g), the pore diameter (2.34-2.56 nm) and the mesoporous porosity (21.3-27.3 %). When the 7 and 21-day powders are included, the differ-

ence is clearly visible. These both powders have higher surface areas, smaller pore diameters and a lower porosity.

Table 4.2: Adsorption/desorption data McCool powders

Ageing time	Isotherm	BET surface area [m ² /g]	Pore diameter [nm]	Total porosity [%]	Mesoporous porosity [%]
7 days	Microporous	1038	1.68	33.9	-
10 days	Mesoporous	747	2.56	52.8	27.3
11 days	Mesoporous	764	2.47	52.6	25.4
12 days	Mesoporous	783	2.37	52.2	25.2
13 days	Mesoporous	804	2.42	53.3	25.8
14 days	Mesoporous	795	2.51	53.9	26.5
21 days	Microporous	995	1.86	43.6	-
28 days	Mesoporous	848	2.36	49.2	21.3
36 days	Mesoporous	854	2.34	48.8	23.3

4.3.2 TGA

Judging from the brown colour of the first few Honma powders that were calcined, not all carbon was removed at 400°C. TGA measurements were performed on these powders to determine to which calcining temperature the powder should be heated so that all unwanted compounds could be removed. First, an uncalcined powder was heated up in air to 800°C with a rate of 5°C/min. The weight loss curve is given in figure 4.5. At 400°C the weight loss is still not complete. There is still a considerable loss between 400 and 550°C. Calcining powders at 550°C was set as the standard.

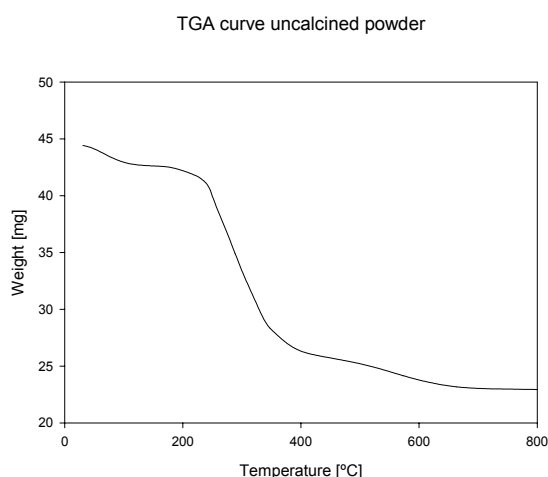


Figure 4.5: Weight loss curve for uncalcined Honma powder after ageing for 1 day

Also, a calcined brown powder was measured with a combined set-up of TGA and a mass spectrometer (800°C / 1°C/min) to measure which compounds are released at what temperature. Figure 4.6 (l) shows the same trend from 400 to 800°C as in the measurement of the uncalcined powder. The weight loss from 25 to 400°C already took place in the oven during the first calcining sequence. As can be seen from figure 4.6 (r), the components that are released are CO and H₂O (Ar and O₂ are from the carrier gases). This confirms the suspicion that the carbon caused the brown colour.

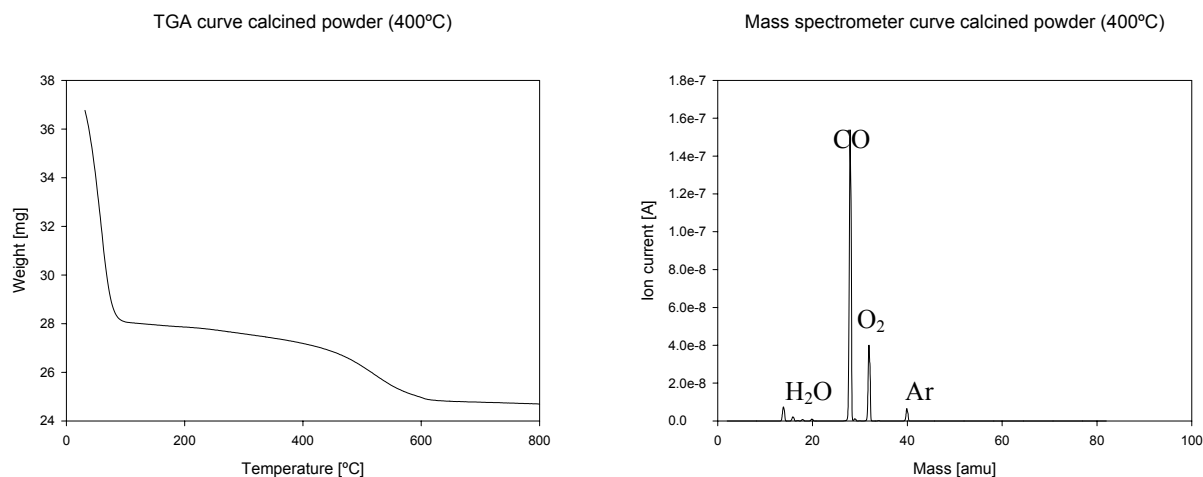


Figure 4.6: (l) Weight loss curve for calcined Honma powder after ageing for 2 days; (r) mass spectrometer results for same powder

4.3.3 XRD

The low angle X-ray diffraction measurements that were done on the Honma powders show no sign of ordering. Also no peaks at higher angles appeared. One of the thoughts after analysing the adsorption/desorption data was that the powder could have a zeolite structure. If a zeolite had formed, sharp peaks would have appeared in the higher angle region. This is however also not the case.

Also, low angle X-ray diffraction measurements were done on the McCool powders that were aged for 7, 10, 14, 21 and 28 days. The XRD plots are given in appendix B, paragraph B.1. The powders that were formed after 7, 21 and 28 days resemble the cubic plot in literature (figure 4.3) the most. At 7 days, the plot shows a clear [211] peak at 2.81° with a [220] shoulder at 3.09° (also see table 4.3). The d-spacings (respectively 3.14 nm and 2.91 nm) also match the values in literature. Two more important peaks ([420] and [332]) are situated at 5.05 and 5.63 nm with d-spacings of respectively 1.75 nm and 1.57 nm. When calculated with the formula for the cubic structure (equation 4.7), the average lattice parameter of this powder is approximately 7.82 nm.

Table 4.3: XRD data on 7 day McCool powder

2 θ angle [°]	d-spacing [Å]	h	k	l	Lattice parameter [nm]
2.2134	39.88	2	0	0	7.98
2.8101	31.41	2	1	1	7.69
3.0291	29.14	2	2	0	8.24
5.0517	17.48	4	2	0	7.82
5.6302	15.68	3	3	2	7.36

After ageing for 21 or 28 days, the MCM-48 characteristic shoulder peak is still clearly visible, but the plots lack the distinctive [420] and [322] peaks. They are hidden under a broad bump. Especially when the slow scan in figure B.5 is viewed, it is clear that no distinction can be made. The [211] and [220] peaks are situated around the same angles as in the 7-day figure.

Figures B.2 and B.3 show no real MCM-48 characteristics. These plots could also belong to a weakly defined hexagonal (MCM-41) structure. Literature references for these structures can be found in articles [48, 54, 55].

5. Wafers

The wafers were only investigated by XRD. The theory of XRD has already been explained in paragraph 4.1.3 and therefore only the experimental conditions and the results will be presented.

5.1 Experimental

The preparation of the wafers is similar to the membrane preparation described in paragraph 3.2. To compare the Honma and the McCool synthesis routes, four wafers were initially produced (table 5.1, wafers 1-4), two with each sol. The silicon wafers are spin-coated with the sol at a spinning rate of 4000 rpm for 30 seconds. Also the drying procedure of the spin-coating process is similar to the drying during and after dip-coating. In both cases thin layers will be formed. The difference, however, is that wafers have a smooth dense surface and the surface of the membrane supports is very rough and porous.

One wafer of each sol was measured uncalcined and the others were calcined first. In a later stage, uncalcined wafer 3 has been calcined at a maximum temperature of 450°C and calcined wafer 4 has been calcined at 550°C (temperature of powder calcination). All wafers have been measured with XRD (PANalytical X'Pert-MPD, CuK α radiation ($\lambda = 1.54 \text{ \AA}$), 40 kV, 50 mA) at low angles (0 to 10°).

Table 5.1: Description of the wafers

Wafer	Sol	Calcination temperature
1	Honma, CTAB	uncalcined
2	Honma, CTAB	450°C
3	McCool	uncalcined
3+	McCool	450°C
4	McCool	450°C
4+	McCool	550°C

5.2 Results

5.2.1 XRD

Appendix B (paragraph B.2) gives the XRD plots of all wafers. Wafer 1 and 2 were produced with the Honma sol and have a similar structure to the McCool powders after 10 or 14 days of ageing. Before calcining two broad peaks are visible, which disappear after calcination at 450°C. It is an unknown structure or perhaps a pattern of two or more combined phases.

Wafers 3 and 4 (McCool synthesis) show clearer peaks. As can be seen from the calculations in table 5.2, the uncalcined wafer 3 contains a layer (which is lamellar or has hexagonal structure with pores parallel to the surface) has an average lattice parameter of 7.06 nm. The calcined wafer (number 4) gives a structure that cannot be defined. Also calcining at higher temperatures (wafer 4+) does not alter the structure. There is a difference with wafer 3+. The uncalcined wafer 3 (with a lamellar kind of structure) was calcined after 46 days and shows more of a cubic structure than the other wafers. The additional information that wafers 4 and 4+ give is that the uncalcined wafer does not have a lamellar structure, but probably a flat lying hexagonal structure. Otherwise, the lamellas would have collapsed during calcination and no structure would have been seen.

Table 5.2: XRD data on wafers 3 and 4

Wafer	2 θ angle [$^{\circ}$]	d-spacing [\AA]	h	k	l	Lattice parameter [nm]
3	1.2737	69.30	1	0	0	6.93
	2.4943	35.39	2	0	0	7.08
	3.7415	23.60	3	0	0	7.08
	4.9693	17.77	4	0	0	7.11
	7.4540	11.85	6	0	0	7.11
4	3.3200	26.59	?	?	?	?
	3.6231	24.37	?	?	?	?
	4.6114	19.15	?	?	?	?
	4.8617	18.16	?	?	?	?

6. Membranes

This chapter describes the characterisation of the different membranes. Both sols were used to prepare the membranes. The characterisation techniques that were used (permporometry, electron microscopy, permeation and retention) are first described theoretically after which the results are described per technique.

6.1 Theory

To reveal the structure of the membranes many different techniques were used. They can be split up into structural measurements like permporometry, microscopy (optical, SEM and EDX, TEM) and XRD and performance measurements like liquid permeation, retention and gas permeation measurements.

6.1.1 Permporometry

Permporometry is used to measure the size distribution of active pores with radii of 1 to 50 nm in a membrane [56]. It is based on the controlled blocking of pores by capillary condensation of a vapour phase and the simultaneous measurement of the diffusional flux of a non-condensable gas through the open pores.

The membrane is clamped between two flowing gas streams [57]. The permeate side of the membrane is swept by a single inert gas (e.g. N_2). The feed side of the membrane is swept by a mixture of the inert gas, a condensable vapour and a probe gas that is quantitatively measurable in trace levels (e.g. O_2). The partial pressure of the condensable vapour is raised and lowered to close or open pores of different sizes (typically 1-2.5 nm). Once the pores are filled with liquid and the partial pressure is lowered, the pores open (largest first) and gas is transported through the membrane. The amount of O_2 that diffuses into the permeate-side stream will increase in proportion to the number and size of open pores. The whole desorption process is visualised in figure 6.1.

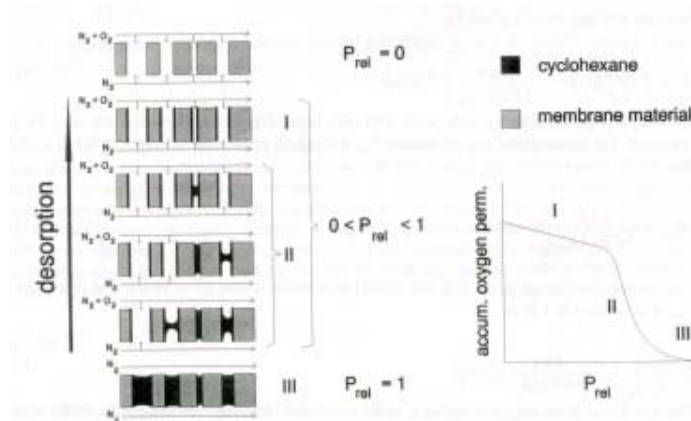


Figure 6.1: Scheme of the desorption step in the permporometry process

The theoretical equations are already explained in paragraph 4.1.1. Permporometry also uses the Kelvin equation (4.3). The uncertainty in the pore size results (approx. 0.5 nm) can result from membrane swelling, non-cylindrical pores and experimental measuring uncertainties.

6.1.2 SEM

In figure 6.2 a typical Scanning Electron Microscope (SEM) is shown [52]. A SEM gives a very detailed picture (nanometer scale) of a surface by emitting and detecting electrons. The cathode (tungsten or LaB_6) emits electrons thermionically, which are then drawn to the anode. Two successive condenser lenses focus the electrons into a beam with a very fine spot size ($\sim 50\text{\AA}$). Pairs of scanning coils, which are located at the objective lens, deflect the beam either linearly or in raster fashion over a rectangular area of the sample surface.

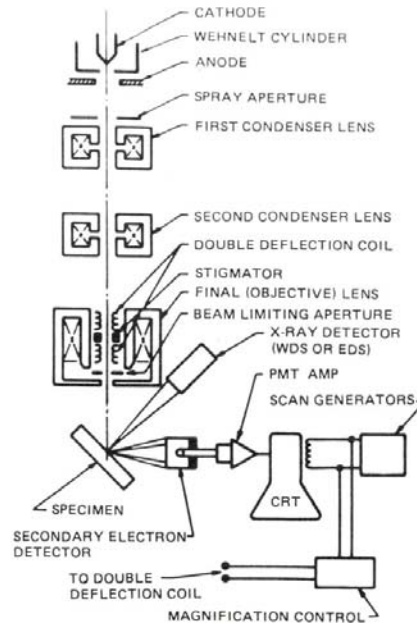


Figure 6.2: Schematic of the scanning electron microscope

Upon hitting the surface, the primary electrons decelerate and, in losing energy, transfer it inelastically to other atomic electrons and to the lattice. A multitude of electrons excite from a teardrop-shaped interaction volume under the surface with an energy spectrum shown schematically in figure 6.3. In addition, target X-rays are emitted and other signals, such as light, heat and specimen current, are produced and the sources of their origin can be imaged with appropriate detectors.

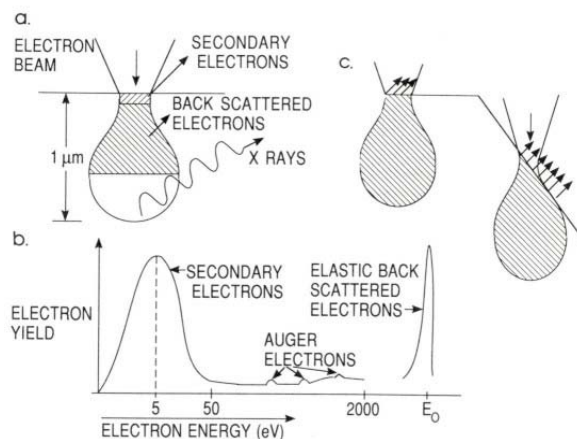


Figure 6.3: (a) Electron and photon signals emanating from tear-shaped interaction volume during electron-beam impingement on specimen surface, (b) energy spectrum of electrons emitted from specimen surface and (c) effect of surface topography on electron emission

The most common imaging mode relies on detection of secondary electrons. Their very low energy indicates they originate from a surface depth of no larger than several angstroms. The contrast variation observed on the SEM picture can be understood by analysing figure 6.3 (c). Sloping surfaces produce a greater secondary electron yield, because the portion of interaction volume projected on the emission region is larger than on a flat surface. Similarly, edges will appear even brighter.

6.1.3 EDX

Through excitation by an incident electron or photon on the sample surface, a hole or electron vacancy is created in the K shell (figure 6.4 (b)). In energy-dispersive X-ray analysis (EDX) an electron from an outer shell lowers its energy by filling the hole, and an X-ray is emitted in the process (figure 6.4 (c)). If the electron transition occurs between the L and K shells, $K\alpha$ X-rays are produced. Different X-rays are generated. There are two facts worth remembering about these X-rays [52]:

- 1) The difference in energy between the levels involved in the electron transition is what determines the energy of the emitted X-ray. For example:

$$E_{K\alpha_1} = \frac{hc}{\lambda_{K\alpha_1}} = E_K - E_{L_1} \quad 6.1$$

$E_{K\alpha_1}$ = energy emitted X-ray [Nm]
 h = Planck's constant [Js]
 c = speed of light [m/s]
 $\lambda_{K\alpha_1}$ = wavelength $K\alpha_1$ X-rays [m]
 E_K = energy K-shell electron [Nm]
 E_{L_1} = energy L_1 -shell electron [Nm]

- 2) The emitted X-rays are characteristic of the particular atom undergoing emission. These characteristic X-rays are also known as fluorescent X-rays when excited by incident photons.

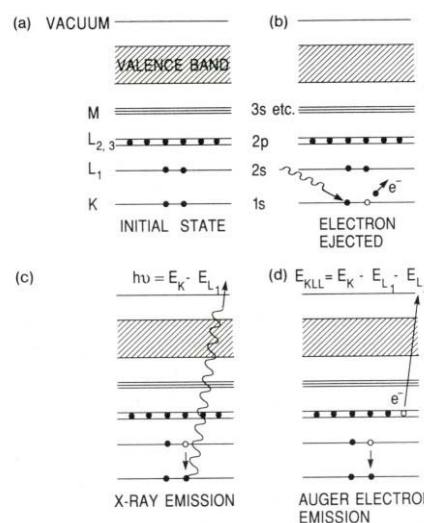


Figure 6.4: Schematic of electron energy transitions (KLL): (a) initial state, (b) incident photon (or electron) ejects K shell electron, (c) X-ray emission when 2s electron fills vacancy and (d) Auger electron emission

Most energy-dispersive X-ray analysis systems are interfaced to SEMs where the electron beam serves to excite characteristic X-rays from the area of the specimen being probed. An incoming X-ray generates a photoelectron that eventually dissipates its energy by creating electron-hole pairs. The incident photon energy is linearly proportional to the number of pairs produced or equivalently proportional to the amplitude of the voltage pulse they generate when separated. The pulses are amplified and then sorted according to voltage amplitude by a multichannel analyser. EDX can therefore detect the separate compounds of a material and plot them according to their amount.

6.1.4 TEM

As the name implies, the Transmission Electron Microscope is used to obtain structural information from samples that are thin enough to transmit electrons. The two basic modes of TEM operation are visualised in figure 6.5 [52].

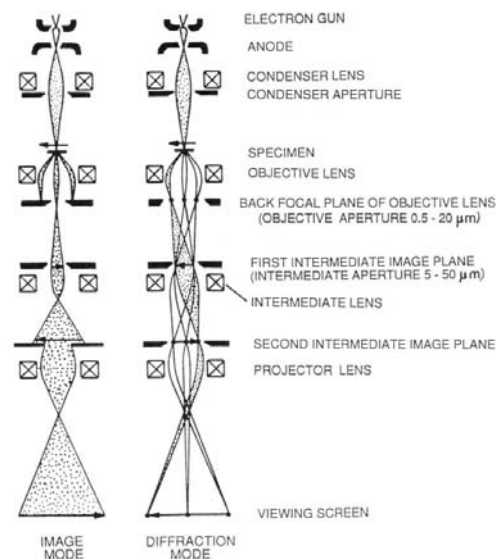


Figure 6.5: Ray paths in the TEM under imaging and diffraction conditions

Electrons thermionically emitted from the gun are accelerated to 100 keV or higher (1 MeV in some microscopes) and first projected onto the specimen by means of a condenser lens system. The scattering processes experienced by the electrons during their passage through the sample determine the kind of information obtained. Elastic scattering (no energy loss when electrons interact with the material) gives diffraction patterns and inelastic interactions between beam matrix electrons at heterogeneities (such as grain boundaries, dislocations, defects) cause absorption and scattering effects (and thus variation in intensities). The primary and diffracted electron beams finally pass a system of lenses before reaching the viewing screen. TEM is a powerful tool to visualize different pore orderings. Figure 6.6, for example, shows the TEM image of a MCM-48 sample [49].

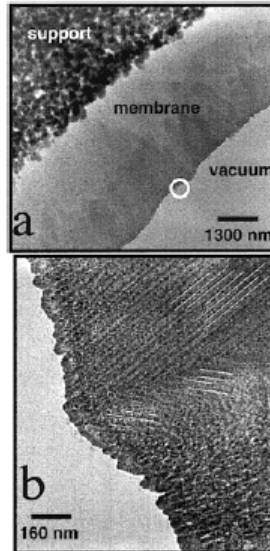


Figure 6.6: (b) TEM picture of pore arrangement in the cross section (white circle in (a)) of a siliceous MCM-48 sample

The high magnification of all TEM methods is a result of the small effective wavelengths (λ) employed, according to the de Broglie relationship (6.2) [52].

$$\lambda = \frac{h}{\sqrt{2mqV}} \quad 6.2$$

m = electron mass [kg]

q = electron charge [As]

V = potential difference [J/As]

Electrons of 100 keV energy have wavelengths of 0.037 Å and are capable of effectively transmitting through about 0.6 μm of Si.

6.1.5 Liquid permeability and retention

When using porous materials in applications with liquid permeation, such as filters and gas distributors, high liquid permeability is usually required for a high filtration rate. Liquid permeability of porous materials provides information about the pore structure, such as tortuosity of pore connections [50]. The liquid permeability of porous materials depends on the degree of open porosity, the pore size, the pore shape and the tortuosity of the pore network.

The liquid permeability of ceramic membranes can be tested using the liquid permeation set-up shown in figure 6.7. After the membrane is placed in the cup (7), the pressure vessel (2) is filled with a liquid and pressurised by nitrogen gas. The flux can be calculated by dividing the amount of liquid passing through the membrane per hour (flow) with the membrane area A perpendicular to the flow. The permeability is defined as the flux per unit pressure drop times the membrane thickness (Darcy's law, equation 6.3).

$$J = \frac{\Phi_{vol}}{A} = -L_p \frac{\Delta P}{\Delta x} \quad 6.3$$

J = flux [l/m^2s]
 Φ_{vol} = volume flow [l/s]
 A = membrane area [m^2]
 L_p = permeability [$l/mPas$]
 ΔP = pressure drop [Pa]
 Δx = membrane thickness [m]

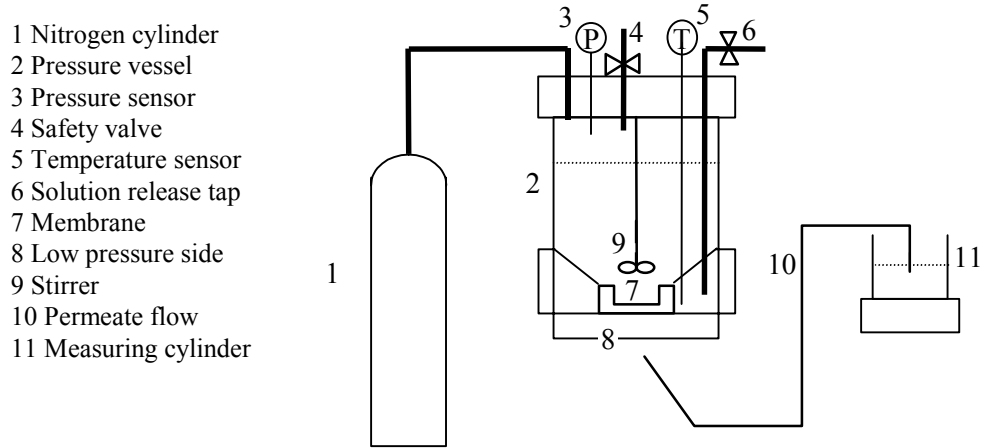


Figure 6.7: Liquid permeation set-up

Retention measurements can also be performed with this set-up. However, when ions or polymer molecules are present, cake build-up or concentration polarization can influence the results. This can be diminished by use of the stirrer at sufficiently high speeds. The retention of a solid is given as equation 6.4.

$$r = 1 - \frac{c_p}{c_f} \quad 6.4$$

r = retention [-]
 c_p = concentration in permeate [mg/kg]
 c_f = concentration in feed [mg/kg]

6.1.6 Gas permeation

The mechanisms by which various components in a gaseous feed stream are transported through the membrane structure determine the separation properties of the membrane. Diffusion is the most commonly recognised gas transport mechanism in a porous material [58]. Different mechanisms are important for different pore sizes. For pores larger than 20 nm in diameter, viscous flow occurs. Knudsen diffusion is important in mesoporous materials like MCM-48 structures ($2 \text{ nm} < d_p < 100 \text{ nm}$) and in micro pores ($d_p < 2 \text{ nm}$) micropore diffusion is present.

Viscous flow occurs when the mutual interactions between molecules in the gas phase occur more frequently than molecule-wall collisions. This happens if the mean free path, λ , of the molecule is smaller than the mean pore diameter ($\lambda \ll d_p$). Knudsen diffusion occurs when the mean free path length of the gas is large with respect to the pore size ($\lambda \gg d_p$). The colli-

sion frequency between gas molecules in this regime is negligible compared to the molecule-wall collision frequency. Pure Knudsen permeance is described by equation 6.5.

$$F = -\frac{2\varepsilon_p r_p}{3\tau l} \sqrt{\frac{8RT}{\pi M}} \quad 6.5$$

F = Knudsen permeance [mol/m²sPa]

ε_p = porosity [-]

1/ τ = tortuosity [-]

l = layer thickness [m]

M = molar mass of the gas [g/mol]

The transport mechanism called micropore diffusion takes place in membranes with pore diameters smaller than 2 nm. The gasses cannot pass freely any more (like with Knudsen diffusion) and differences in permeance are largely determined by differences in sorption characteristics and mobility. If the pore sizes become too small for molecules to enter at all, this is called molecular sieving or size exclusion.

6.2 Experimental

The original goal of this thesis was coating a mesoporous templated silica layer directly on top of α -alumina supports. All synthesis methods were used: the Honma method with CTAB, the Honma method with CTAC, the Kim method with PVA and the McCool method with the refluxed CTAB sol. Also, γ -alumina membranes were prepared and analysed. In order to investigate the influence of the support pre-treatment, two temperatures (800°C and 900°C) were used to sinter the γ -alumina layer. These membranes were also coated with all the CTAB and CTAC sols. The ageing time for the Honma sols was 1 day. For the McCool sols it was 11 or 14 days. An overview of the experimental conditions is given in table 6.1.

The characterisation techniques and their specifications are: permoporometry (home-made equipment, cyclohexane as condensable vapour and oxygen as probe gas), optical microscopy (Nikon Eclipse ME600, enhancement of 5), XRD (PANalytical X'Pert-MPD, CuK α radiation ($\lambda = 1.54 \text{ \AA}$), 40 kV, 50 mA, 2 θ 0 to 10°), SEM (JEOL JSM5800 and LEO 1550 FEG), EDX (Thermo NORAN instruments, Vantage), TEM (Phillips CM30 Twin/STEM), liquid permeation (home-made equipment, different solvents, T = 23°C) and gas permeation (home-made equipment, different gasses, T = 204°C).

6.3 Results

6.3.1 Permporometry

A fast indication of the state of the membrane is obtained from permoporometry. In the case in which the silica layer is only supported by α -alumina (membranes 1-4, table 6.1), all pore radii (Kelvin radius) are in the range of 18-20 nm. The average pore size of α -alumina (AKP-30) is 80 nm. The conclusion from these numbers could be that the membrane either has no layer at all or a cracked silica layer.

As described in paragraph 3.2.2, Kim describes a synthesis route where first the pores of the α -alumina support are filled with PVA and then the silica layer is coated. The sol and procedures used for this are the same as described in the Honma synthesis route. The silica sol is coated on the PVA after which the PVA is burned out in an oven. According to the results measured by permoporometry (membrane 5+6), this procedure is not much better as the one described above. The pore sizes were 19.65 and 22.04 nm.

The McCool sol was also coated directly on top of an α -alumina support (membrane 7+8). Also these results were not satisfying (18.00 and 17.46 nm). Therefore, the decision was made to start coating on γ -alumina, although this would probably be a disadvantage for the liquid permeation results (additional resistance). Comparing the γ -layers sintered at different temperatures (membranes 9+13), one can see that sintering at higher temperatures leads to larger pores in these alumina layers. This is a normal effect for γ -alumina. At higher temperatures different smaller pores agglomerate to one large pore.

There is also a difference in the Kelvin radius for membrane 13 and 14. Membrane 14 has been dipped twice with the γ -alumina solution before heat treatment. The effect could be caused by the measuring error, which is 0.5 nm, but it has been seen more than once (for instance when comparing membrane 15 and 17). The silica layer contains larger pore radii when coated on γ -alumina, which has been coated twice before sintering.

Table 6.1: Synthesis route per membrane and their permoporometry results. All layers are coated on α -alumina.

Membrane	γ -alumina	PVA	Silica synthesis			Kelvin radius \pm error [nm]
			Honma + CTAB	Honma + CTAC	McCool	
1			x			18.31 \pm 0.5
2			x			19.33 \pm 0.5
3				x		19.29 \pm 0.5
4				x		19.14 \pm 0.5
5		x	x			19.65 \pm 0.5
6		x	x			22.04 \pm 0.5
7					x (11 D)	18.00 \pm 0.5
8					x (14 D)	17.46 \pm 0.5
9	x (800°C)					3.13 \pm 0.5
10	x (800°C)		x			< 1
11	x (800°C)			x		2.09 \pm 0.5
12	x (800°C)				x (11D)	1.83 \pm 0.5
13	x (900°C)					4.10 \pm 0.5
14	x (900°C/2x)					4.42 \pm 0.5
15	x (900°C)				x (11D)	1.75 \pm 0.5
16	x (900°C)				x (14D)	1.65 \pm 0.5
17	x (900°C/2x)				x (11D)	2.11 \pm 0.5

From the permoporometry results on membranes 10-12 and 15-17 it can be concluded that for all synthesis routes a layer of silica has formed on top of the γ -alumina. The Kelvin radii seem to be variable with the type of sol and the ageing time of the sol. However, when the measuring error is taken into account all values are comparable. As can be seen from figure 6.8 (a typical pore size distribution) the distribution is quite narrow. All pore size distributions of membranes 9-17 are given in appendix C. Remarkably, the pore size of the silica does not

seem to be negatively influenced by the larger pores of the underlying γ -layer. The pore radius of membrane 10 could not be determined precisely, because the lower detection limit was reached. However, gas still passed through the membrane, which indicates a porous structure.

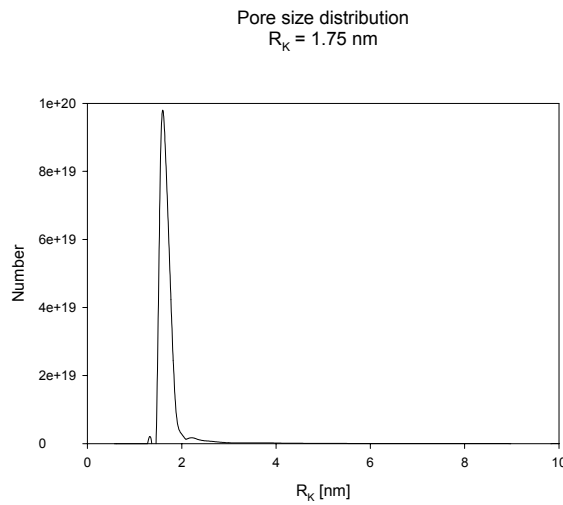


Figure 6.8: Pore size distribution of membrane 15

6.3.2 Optical microscopy

Membranes 1, 2, 5 and 6 have been examined under an optical microscope with a magnification of five. The large pore sized measured by permoporometry measurements indicated a cracked silica layer or even the lack of a layer. The optical microscopy pictures of membranes 1 and 2 (figure 6.9) show a smooth surface without any cracks, but there are some defects visible.

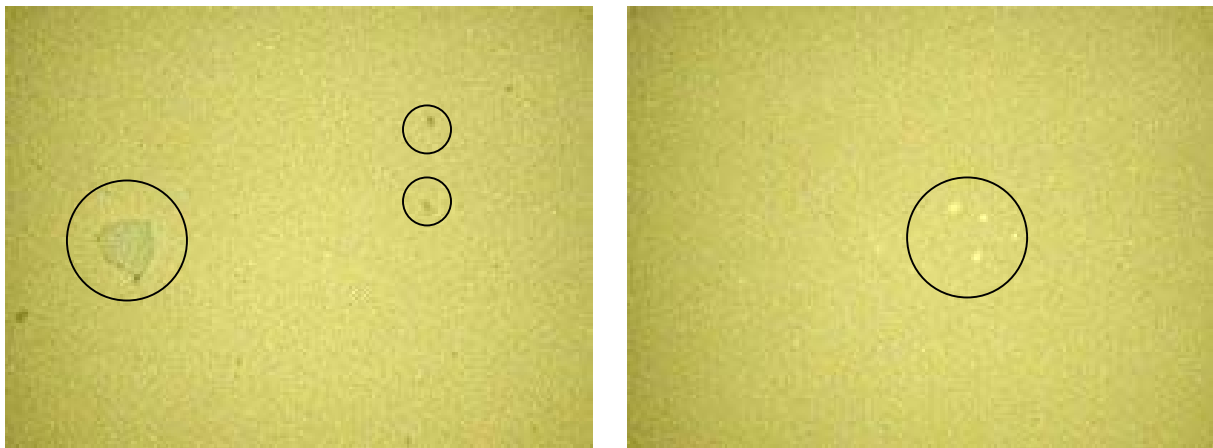


Figure 6.9: Optical microscope pictures; (l) surface of membrane 1; (r) surface of membrane 2

Optical microscopy pictures of membranes 5 and 6 (figure 6.10) show that the silica layer lies on top of the support, but is cracked. It can be scratched off with little effort (figure 6.10, right). Probably, a layer of PVA has formed on top of the membrane during the dip-coating, instead of only filling up the pores. The problems could have been caused by the PVA solution being too viscous or the dip-coating speed not being fast enough. Anyhow, the outcome is that the silica layer does not attach to the alumina support when there is a layer of PVA in between.

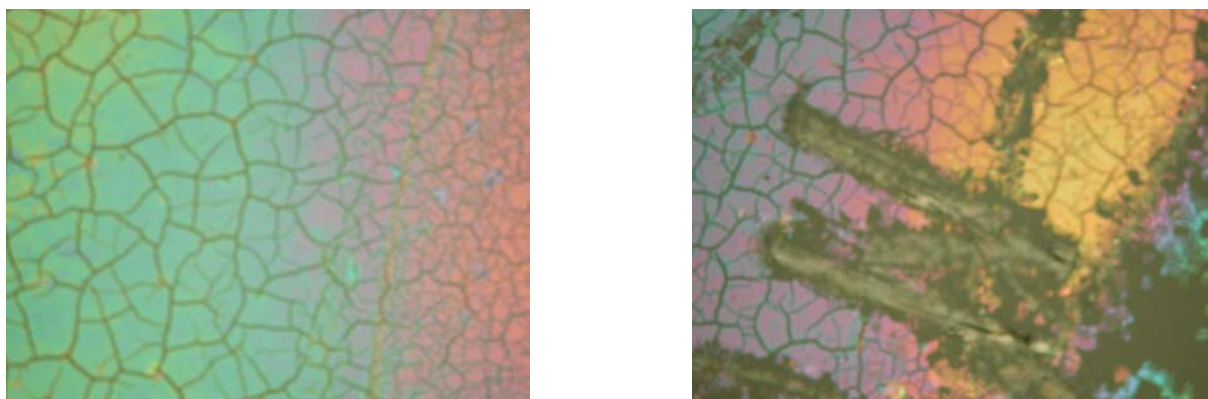


Figure 6.10: Optical microscope pictures; (l) cracked silica surface of membrane 6; (r) scratched-off silica surface of membrane 5

6.3.3 XRD

To get an indication of the structure in the templated silica layer, X-ray diffraction measurements with membranes 10 and 15 were performed. The XRD plots are given as figures B.13 and B.14 in appendix B. Membrane 15 does not show any sign of structure, but it is known to be very hard to see structure on the surface of an alumina membrane. Membrane 10, however, shows signs of the cubic phase. The peaks that seem to appear below an angle of 2° are most likely the result of unstable equipment and should be disregarded. Around 2.5° , however, a clear bump is visible, which has also been enhanced ten times in the same figure. Another peak, but smaller, appears around 3.5° . Unfortunately, because of the low intensities of these peaks no other signs of the cubic structure (like two peaks around 5°) are detected.

6.3.4 SEM and EDX

To verify if the bad permoporometry results of membrane 1 were caused by the defects visualised by the optical microscopy picture (figure 6.9, left) the (LEO) SEM was used. From figure 6.11 can be concluded that the silica has sunk into the α -alumina support. In figure 6.11 (l) a small area of the α -alumina grains is covered with silica. The cross-section (figure 6.11 (r)) is taken in the middle of the support and clearly shows that the silica has settled on some of the alumina grains, but also leaves spaces uncovered. EDX has also been performed on this membrane to verify if most of the surfactant has been eliminated during calcination. The results showed that (unlike in the powders) there is little carbon left after calcining the membrane at 450°C .

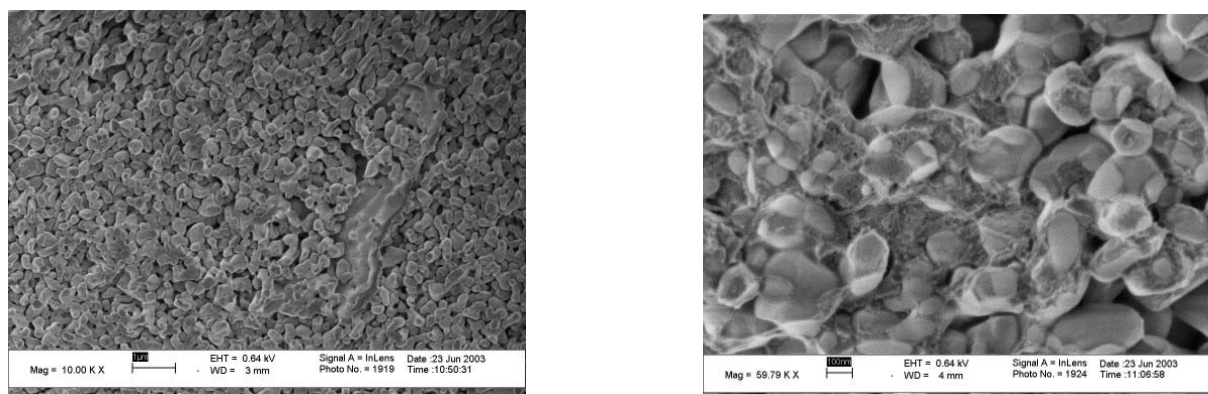


Figure 6.11: SEM picture of (l) the surface of membrane 1 and (r) the cross-section of membrane 1

The McCool sol gives similar results when coated on bare α -alumina. A (JEOL) SEM cross-section of the surface of membrane 7 (figure 6.12) reveals that the silica did not form a layer on the alumina, but also sunk into the support. However, the silica did not sink into the middle of the support, but stayed in the top μm of the α -alumina. This expresses itself in the SEM picture as a region with coarse grains (α -alumina) and a blurry top layer where the silica has covered the alumina grains.

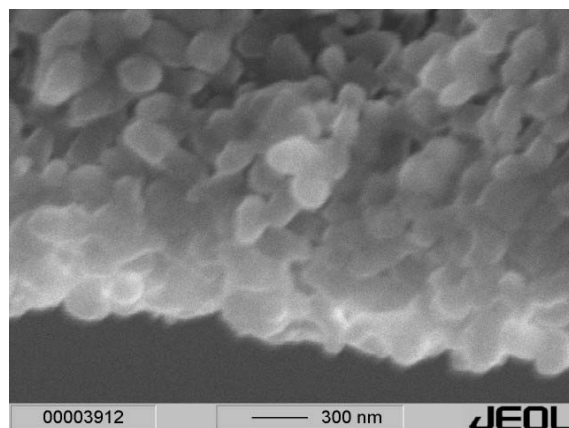


Figure 6.12: SEM picture of the cross-section of membrane 7

Membrane 15 showed good permperometry results. It has also been used to do XRD, liquid permeation and retention measurements with (see paragraphs 6.3.3 and 6.3.6). During the process, also all the organic residues have been burned out. This heat treatment is probably the reason for the cracks in the silica layer on the (JEOL) SEM pictures (figure 6.13). The right picture shows a cracked area with a diameter of approximately $80\ \mu\text{m}$ and the left picture shows that there are many more cracks on the surface. This must have happened after the permperometry measurement was performed. Otherwise, the pore radius for this membrane would have been much larger.

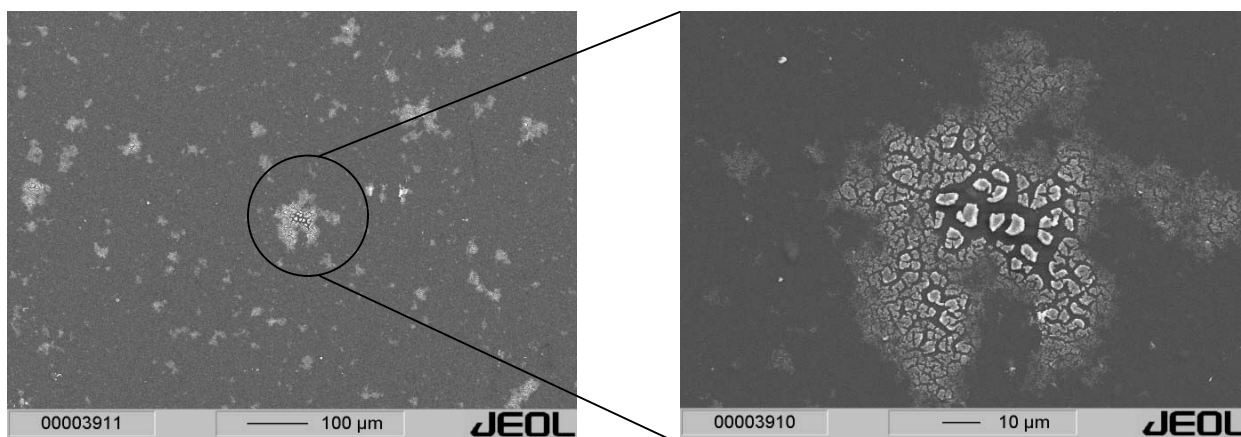


Figure 6.13: SEM pictures of the cracks on the surface of membrane 15; (l) zoomed-out and (r) zoomed-in

6.3.5 TEM

To determine how thick the silica layer is and what the pore structure is, TEM imaging measurements have been done on membrane 10. The cross section of this Honma membrane has

also been viewed with (JEOL) SEM, but only the 1.5 μm thick γ -alumina layer was visible, because the machine was not powerful enough. The top TEM picture in figure 6.14 shows that the double silica layer is approximately 1 μm thick. The zoomed-in figure (6.14, bottom) clearly shows that the silica has a structure like in figure 6.6 from literature. The pore ordering is almost perpendicular to the alumina surface, which is exactly as desired for the cubic structure. Near the surface, there are a few areas where the pores are oriented parallel to the surface. This ‘layer’ is less than 10 nm thick, but could be of influence during permeation measurements. The unordered layer between the γ -alumina and the templated silica (in between the white lines) cannot be accounted for. It might be a silica-alumina phase that has been formed during sintering. This intermediate layer is about 10 nm thick and shows no structure.

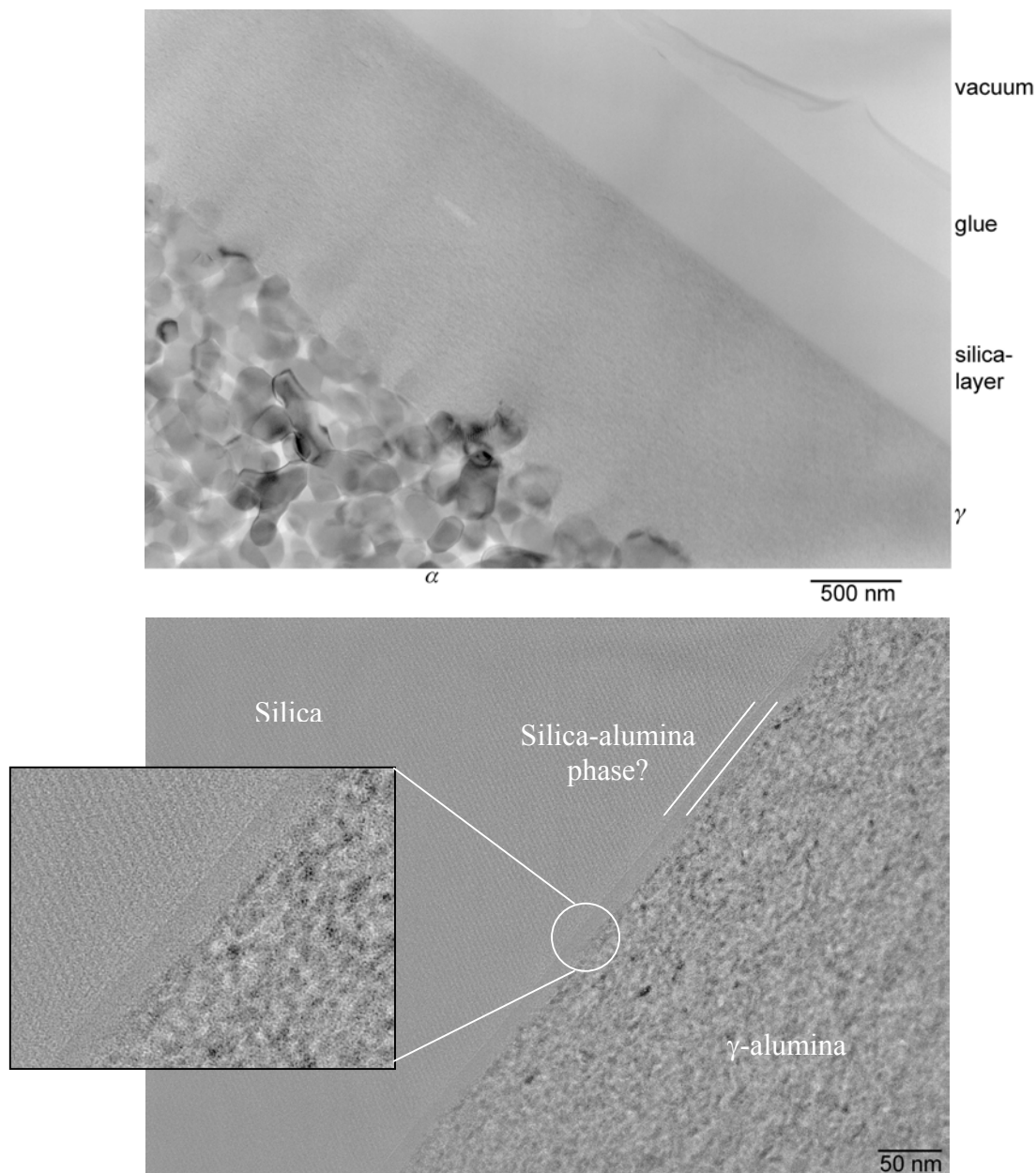


Figure 6.14: TEM pictures of the cross-section of membrane 10; (top) zoomed-out and (bottom) zoomed-in

6.3.6 Liquid permeation and retention

The liquid permeation and retention measurements have been performed with membranes 15, 16 and 17. The permeation of the membranes was measured with hexane, toluene, water and ethanol. The results are summarised up in paragraph D.1 of appendix D. The graphs show the viscosity-normalised fluxes so the flow of different liquids can be compared. A clear separation between the permeation of water / ethanol (top) and the permeation of hexane / toluene is seen in all liquid permeation graphs.

After measuring the liquid permeation of the membrane, the retention of membrane 17 was measured with POM (polyoxomethalate) in water (clear and turbid) and toluene. The clear water solution is purified and contains only POM, but the turbid solution is not purified. Figure D.4 in appendix D is a graph of the flux of the different solutions. These fluxes are not normalised for the viscosity, because the viscosities of the POM solutions are not known. The highest flux belongs to pure toluene, followed by the POM in turbid water, pure water and the POM in clear water. The lowest flux is from the POM in toluene. The fluxes of the toluene solutions are quite far apart. The water fluxes, however, do not differ that much. This is also seen in the analysis results of the permeate. The analysis results of the mother solutions and the permeate solutions at pressures around 9 bar can be found in table 6.2. The zinc content of the permeate solution of POM in toluene (<1 mg/kg) is significantly lower compared to the mother solution (35 mg/kg). The membrane has a retention of more than 97.1% (equation 6.4) and is therefore a good barrier for POM in toluene. The other measurements resulted in a retention of 0%, which might have been caused by a defective silica layer due to a reheating step directly after the toluene measurements.

Table 6.2: Retention results membrane 17

Solution	Zn [mg/kg]
POM/toluene mother	35
POM/toluene P = 9.46	< 1
POM/water clear mother	3220
POM/water clear P = 8.59	3220
POM/water turbid mother	1520
POM/water turbid P = 8.62	1525

6.3.7 Gas permeation

Gas permeation measurements were done to determine the type of flow (i.e. Knudsen or viscous) and whether the mesopores are continuous or connected via micropores. The permeance of nitrogen, hydrogen and helium were measured for membrane 17 at different pressures and a constant temperature of 204°C (figure 6.15 (l)). Hydrogen permeance at 2.45 bar is around $6.7 \cdot 10^{-6}$ m²/s. Helium has a lower permeability ($5.0 \cdot 10^{-6}$ m²/s) and the value for nitrogen is ($1.9 \cdot 10^{-6}$ m²/s). A small slope of 10^{-12} is present in all lines. The sequence of the permeability is expected if the molar mass is taken into account. A linear relationship is found between the three values at one pressure and the molar masses of the gasses (figure 6.15 (r)). In this membrane Knudsen diffusion is therefore the most important type of flow.

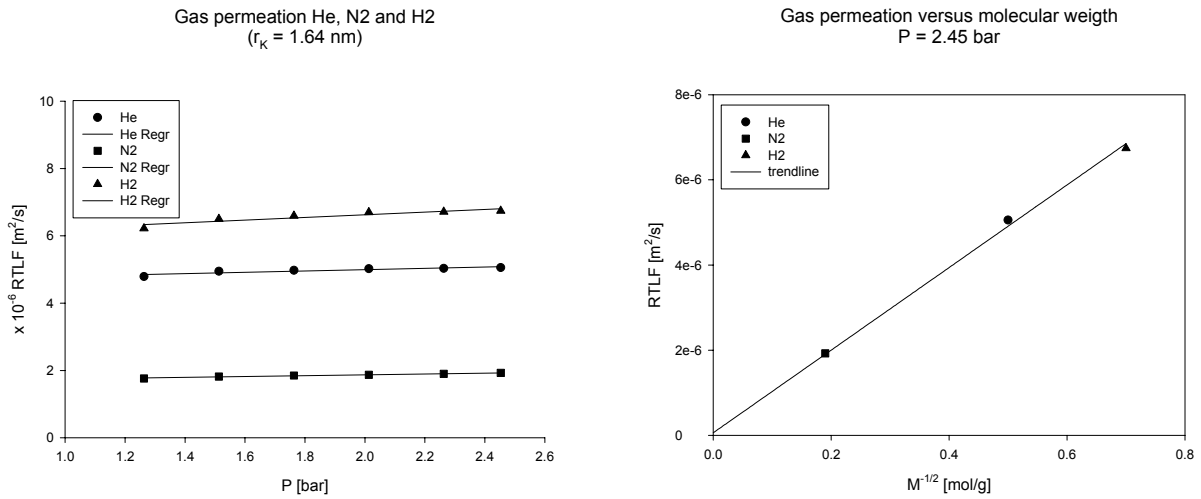


Figure 6.15: Gas permeance through membrane 17; (l) at different pressures, (r) at $P = 2.45$ bar

6.3.8 Rhodamine colouring

Membrane 17, used for permoporometry, liquid permeation, retention and gas permeation measurements, has also been subjected to a destructive colouring test. Where the membrane turns pink, alumina is not covered with silica. Figure 6.16 shows that the membrane turned completely pink during the test. This is a sign that the silica has been harmed by most probably the reheating (as mentioned in paragraph 6.3.6).

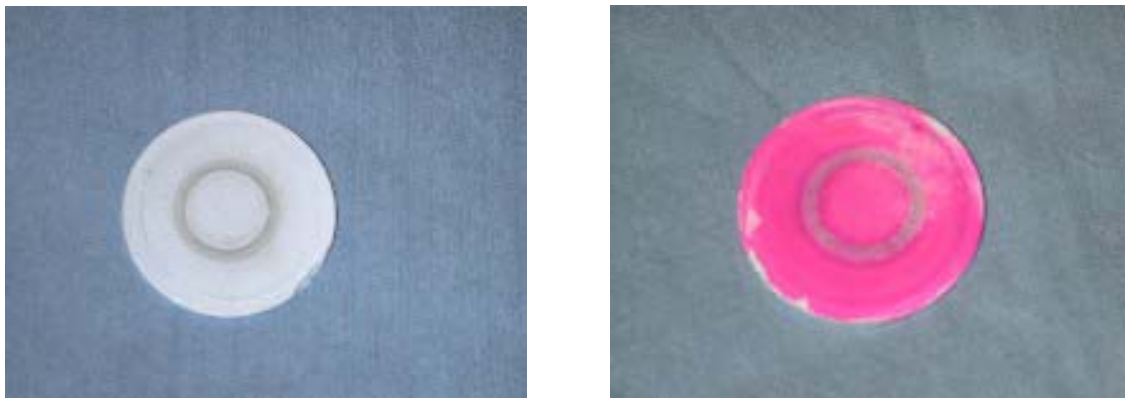


Figure 6.16: (l) before and (r) after rhodamine colouring of membrane 17

7. Discussion

In this chapter, the results obtained from the experimental work on silica powders, wafers and membranes (described in chapters 4 through 6) are discussed. To verify that the produced material is really MCM-48 silica, the characterisation results should clarify that it is mesoporous and that it has a well-defined cubic pore structure. The two sols are discussed separately and in the final remarks a comparison is made.

7.1 *Honma sol*

The first experimental results of the Honma powders and membranes gave negative results. The powders were still brown when calcined at 400°C. Therefore TGA measurements were done to determine at which calcining temperature most of the carbon is removed. Based on the outcome, the temperature was set at 550°C. All Honma powders showed microporous instead of mesoporous adsorption isotherms (paragraph 4.3.1). Also the XRD measurements show no structural ordering at all. The results of the membranes made with the same type of sol (membranes 1 to 4 in table 6.1) were also not as expected. Permporometry results showed large mesopores with radii of 18-20 nm. The pore radius that is expected in a MCM-48 powder is around 1 to 2 nm. The membranes were viewed under an optical microscope, which showed large defects. Also SEM pictures of membrane 1 were taken (figure 6.11 (l)). Apparently the silica sol sunk into the underlying α -alumina layer and did not form a closed separation layer.

Lacking positive results, a few alternative synthesis routes were also explored. These include filling the α -alumina pores with PVA, coating on γ -alumina and using another synthesis route (McCool synthesis discussed in the next paragraph). Filling the pores with PVA and then coating with the silica sol did not result into a better silica layer. The pore sizes were again too big (19-22 nm) and the optical microscope pictures (figure 6.10) showed cracks. The top layer could be easily removed by scratching the surface. The exact reason is not investigated, but two probable situations can be proposed:

1. The PVA filled the pores and left a thin film on top of the alumina, which separated the α -alumina from the silica. Therefore, the silica could not attach to the underlying α -alumina, not even during calcination when the PVA was removed from the membrane.
2. The PVA was removed during calcination via the pores of the silica layer and caused the layer to crack.

The problems with the membranes, however, disappeared when the silica layer was directly dip-coated on silicon wafers or γ -alumina supports. The XRD plots of wafers 1 and 2 are promising. Although not well defined, some peaks of the cubic structure are present on the uncalcined wafer. After calcination the peaks shift to higher angles and the higher angle peaks disappear, which means that the layer loses most of its structure during calcination. Only one membrane, number 10, shows a XRD plot with little structural ordering. The peaks however, have such a low intensity and are partly covered by the incoming beam that no calculations on lattice parameters could be made and that it can only be suggested that it shows a weak cubic MCM-48 structure. The pore size of this membrane is however below the detection limit of the permporometry technique (< 1 nm). Because of the detection of structure by XRD and the uncertain (microporous) pore size, SEM pictures were taken. Unfortunately the JEOL SEM is

not powerful enough to visualise the difference between the γ -alumina and the silica. The XRD measurements were promising enough to try TEM, which can easily distinguish structure. Because of the costs of this technique, only one series of TEM measurements (on membrane 10) have been done. The results are given in figure 6.14. They are the definite proof that an ordered cubic pore structure has been formed. The silica layer contains a well-defined ordering over a distance of at least 400 nm that is organised almost perpendicular to the underlying γ -surface. Near the interface, the pore ordering is parallel to the surface, which might explain the small pore size measured with permoporometry. These conclusions show that TEM is a powerful technique to obtain structural information about these ordered membrane layers.

7.2 McCool sol

For the McCool sol, the results on powder measurements are more promising. The nine powders discussed, all have different ageing times (7-36 days). Most of the adsorption/desorption isotherms show mesoporous curves. The BET surface areas are also quite high (table 4.2) and the pore diameters are as expected. The mesoporous porosity, however, is low. The most remarkable about this series of isotherms is that the 7 and 21-day powders have microporous isotherms. The same results were also seen after duplication of the whole synthesis and drying procedure. It is a fact that the templating mechanism is constantly changing and it is also known that a certain amount of time is needed to form the cubic structure (see chapter 2 and figure 4.4). Why the sol changes from mesoporous into microporous and back again remains however a mystery.

To investigate the structural properties of the McCool powder, XRD measurements were done on some of the powders. All plots (appendix B) show signs of structural organisation, but remarkably enough the plots for the 7, 21 and 28-day old powders resemble the MCM-48 structure (figure 4.3 (top, r)) the most. The 7-day powder has a lattice parameter of 7.82 nm, which is comparable to literature (8.1 nm [42]), and the peaks match with the cubic structure. In the 21 and 28-day powders, not all peaks are very clear, but the [220] shoulder (a characteristic peak of the MCM-48 structure) is visible in all plots. It can therefore be concluded that adsorption/desorption measurements or XRD measurements alone are not enough to determine the properties of a material. Additionally, the conclusions formed based on the results of the powders, cannot directly be translated to the silica layers.

XRD measurements of membrane 15 show no structure at all and XRD plots of wafers 3 and 4 also show unusual structures. The XRD plot of the uncalcined wafer has sharp definite peaks at positions, which indicate a lamellar or horizontal hexagonal structure. The lattice parameter (7.06 nm) could be calculated quite accurately because of the sharpness of the peaks. After calcination a structure is still present. The lamellar structure would have collapsed while removing the surfactant and therefore the lamellar structure is excluded. Another possibility was the parallel ordered hexagonal structure, but the calcined structure remains unknown. Wafer 4, which was calcined directly after coating, shows an unrecognisable spectrum, also after calcination at higher temperatures. The main goal is to synthesise a silica membrane and therefore not much time has been invested into these wafers.

Further structural organisation of the membranes is investigated by SEM and gas permeation. Mesoporosity was investigated by permoporometry. According to the measured pore sizes and the SEM picture taken of the cross section (figure 6.12), direct coating on α -alumina is not possible. The layer sinks into the large pores of the support. The membranes containing a γ -alumina layer, show much better results. The pore radii are approximately 2 nm, which is in the range of desired pore sizes.

Some membranes with good permoporometry results were also subjected to liquid permeation (membranes 15-17), retention (membrane 17) and gas permeation measurements (membrane 17). The liquid permeation measurements were carried out to test the membrane performance and for all three membranes the results are summarised in appendix D. A clear separation between the permeation of water / ethanol (top) and the permeation of hexane / toluene is seen in all graphs. Therefore, it is stated that the more hydrophilic solutions pass through the membrane more easily than the hydrophobic organic solutions. There are however a few remarks to be made. First of all, the largest influence on the results is the sequence of the liquids that are used. In this case, first hexane, toluene, ethanol and then water were measured. When measuring two liquids in a row, the first liquid, which is still in the pores from earlier measurements, influences the permeation of the second liquid. If the sequence is changed, the permeation is influenced differently and the results will be quite different. Recommendations will follow in chapter 8.

The retention of POM has only been measured for one membrane (number 17) due to lack of time. The Zn concentration for the toluene mixture is clearly lower in the permeate solution at high pressures compared to the mother solution. The retention of POM in toluene is more than 97.1% and therefore excellent. The water mixtures show no retention at all. These results are probably due to degradation of the separating silica layer as was detected by SEM for membrane 15 (figure 6.13), which has also been used in liquid permeation experiments. One of the most probable causes is the heating step in between measurements to burn out unwanted components. Doyle and Hodnett [59] however claim that the MCM-48 structure degrades in neutral solutions in 90 minutes at 350°C. In acid conditions (pH < 5.4) the structure remains. As the solution of POM in toluene is acid (pH = 4) and the water-based solutions are neutral (pH 6.5 and 7), this would also be a good explanation for the lack of retention. However, the permeation measurements as described in paragraph 6.3.6 have been performed at room temperature, which would certainly slow down the degradation. Besides the temperature factor, the membrane was also exposed to neutral solutions before the toluene-based measurements were done and for the POM in toluene a good retention was measured. Maybe this could have an effect over a longer period of time, but the exact reason for this lack of retention is not clear yet. A last test with rhodamine colouring was done to determine the damage on membrane 17. The membrane surface turned pink completely, which means that the silica is not intact on most parts of the surface.

Before the destructive rhodamine experiment, gas permeation measurements have been performed on membrane 17 to verify the (connected) mesoporosity of the membrane. The purpose was to determine if the mesopores are connected via micropores or if the micropores exist next to the mesopores. The measurements have, however, been performed after the retention measurements. The silica layer was probably already damaged and therefore the results are not relevant to the silica layer. The gas permeation measurements determined that the flow in the pores is of the Knudsen type, which means that it contains a mesoporous layer, but these results are probably from the γ -alumina layer.

7.3 *General remarks*

Finally, a few remarks on the influence of some parameters should be noted. The type of surfactant in the Honma sol has been changed from CTAB to CTAC during this project. The results obtained from the CTAC sol were comparable to those of the CTAB sol. Therefore this change has little influence (as expected). Also the influence of ageing time was determined. For the adsorption/desorption results of the powders the time dependence was visible. The pore size of the membrane did not fluctuate outside of the (quite large) measuring error. Also the calcining temperature of the underlying γ -alumina layer (800 or 900°C) did not show much effect on the silica, although the pore radii of the γ -layer are about 1 nm apart.

To combine and compare all results, the question that should be asked is: which synthesis or surfactant or temperature can be used best to obtain an ordered powder or a well-performing membrane? The answer is not straightforward, because the Honma and McCool synthesis are not that different, but the results of powder and membrane characterisation are quite far apart. The Honma synthesis led to powders with no mesoporosity and no structural ordering at all. Coating the Honma sol on γ -alumina membranes, however, did lead to a well-defined cubic structure with mesoporous pores. This was discovered fairly late in the research when most hope was set on the McCool sol. The characterisation of the powders of that sol namely showed good results, but in the silica layers not much structure could be detected. Nevertheless, the mesoporosity is as expected and the POM retention in toluene is also very good.

8. Conclusions and recommendations

8.1 Conclusions

The objectives of this research project have been reached. Silica membranes with a MCM-48 structured top layer have been synthesised with the Honma sol. The silica could not be coated on α -alumina directly: SEM pictures show that the silica sinks into the pores of the support. The templated silica layer is therefore coated on γ -alumina, which gives excellent results. TEM pictures reveal a well-ordered cubic structure with an orientation perpendicular to the surface. Permporometry measurements show that the membranes are mesoporous with a pore diameter of 2-4.2 nm, which is expected for MCM-48.

Optical microscopy determined that filling the α -alumina pores with PVA and coating the silica on that PVA layer is not a usable technique. The silica layer could easily be removed after calcination.

The McCool synthesis seemed to be very promising at first. The powders have high BET surface areas, mesoporous adsorption/desorption isotherms and the XRD plots show a MCM-48 structure. The characterisation of the silica layers on wafers and membranes, however, did not result in the same conclusions. The permporometry measurements determine that the pore sizes (3.5-4.2 nm) are in the desirable mesoporous range, but there is no MCM-48 structure visible in the XRD plots. Although no structure was seen, the McCool membranes are effective in retention measurements with POM in toluene. The retention of POM was more than 97.1%, which is very good.

The calcining temperature of the wafers and membranes was set at 450°C, which is an adequate temperature according to EDX measurements. For powders initially 400°C was standard, but TGA measurements show that 550°C is the minimum temperature to burn out most of the carbon. There are no significant differences between the silica layers coated on γ -alumina layers that are calcined at 800°C or 900°C. Also the use of the surfactants CTAB and CTAC show comparable results.

The final conclusion is that using the Honma synthesis seems to be the best route to produce templated MCM-48 membranes, whereas the McCool synthesis route should be taken to find out more details about the silica powders.

8.2 Recommendations

According to the characterisation performed on many different powders and membranes, the following recommendations for further research can be made:

- Research on MCM-48 membranes can be continued more structurally with the Honma sol, because permporometry, XRD and TEM proved that a well structured, mesoporous MCM-48 membrane has been synthesised. No retention measurements were done with these membranes, but this is certainly an interesting research topic.

- The retention was measured with the McCool membranes. Although no sign of structure in the membrane was determined by XRD, the retention was high. As TEM is a powerful technique to determine the cubic structure, it is useful to characterise the McCool membranes this way as well.
- The silica should be coated on γ -alumina instead of direct coating on α -alumina. PVA as a filling material resulted into cracked membranes.
- Many articles propose that the good results of the research done on the silica powders will lead to good templated mesoporous silica membranes. The characterisation results of the materials described in this reports show different conclusions: the Honma sol made good membranes, the McCool sol good powders, but not vice versa. More time should therefore be invested in the membrane characterisation, instead of combining powder and membrane results.
- During liquid permeation and retention measurements there is a lot of influence of the sequence of the liquids that are used. When measuring two liquids in a row, the first liquid, which is still in the pores from early measurements, influences the permeation of the second liquid. If the sequence is changed, the results will be quite different. To overcome this problem, each liquid should be measured on a fresh membrane or the liquid should be burned out of membrane after each measurement. Reheating might be harmful for the membrane, but intermediate permporometry experiments should to prove that.

This last comment is the most important recommendation for performing research structurally: to use a large number of fresh, defect-free membranes of the same type to use in different measurements. This is now possible since most of the exploring work for a good membrane synthesis is available in this thesis. Especially the liquid permeation and retention measurements need fresh membranes, but also gas permeation should be clean. Their XRD, SEM and TEM patterns can afterwards be compared with those of the fresh MCM-48 membranes.

9. Literature

- [1] *Introduction to sol-gel processing*, Pierre, A.C., 1998, Kluwer Academic Publishers, Norwell, p. 340, 362-368
- [2] Beck, J.S., Vartuli, J.C., et al., *J. Am. Chem. Soc.*, 1992, **114**, p. 10834-10843
- [3] Kresge, C.T., Leonowicz, M.E., et al., *Nature*, 1992, **359**, p. 710
- [4] Monnier, A., Schuth, F., et al., *Science*, 1993, **261**, p. 1299-1303
- [5] Vartuli, J.C., Schmitt, K.D., et al., *Chem. Mater.*, 1994, **6**, p. 2317-2326
- [6] Huo, Q., Margolese, D.I., Stucky, G.D., *Chem. Mater.*, 1996, **8**, p. 1147-1160
- [7] *Sol-Gel materials: chemistry and applications*, Wright, J.D., Sommerdijk, N.A.J.M., 2001, Taylor & Francis Books Ltd, London, p. 1, 4-5, 15-19, 22-31, 38-39, 72-77
- [8] *Mass-transfer operations*, Treybal, R.E., 1980, 3rd ed., McGraw-Hill Kogakusha, Tokyo, p. 655-686
- [9] <http://www.chemat.com/html/solgel.html>, (January 16, 2004)
- [10] *Template-directed synthesis of mesoporous ceramic membranes*, presentation Roy Chowdhury, S., 2003
- [11] Raman, N.K., Anderson, M.T., Brinker, C.J., *Chem. Mater.*, 1996, **8**, p. 1682-1701
- [12] *Handbook of porous solids volume 3*, Schueth, F., Sing, K.S.W., 2002, Wiley-VHC, Weinheim, p. 1311-1337
- [13] Yang, H., Kuperman, A., et al., *Nature*, 1996, **379**, p. 703-705
- [14] Ogawa, M., *J. Am. Chem. Soc.*, 1994, **116**, p. 7941-7942
- [15] Tolbert, S.H., Firouzi, A., Stucky, G.D., *Science*, 1997, **278**, p.264-268
- [16] Øye, G., Sjöblom, J., Stöcker, M., *Adv. Coll. and Interface Sci.*, 2001, **89-90**, p. 439-466
- [17] Aksay, I., Trau, M., et al., *Science*, 1996, **273**, p. 892
- [18] Yang, H. Coombs, N., et al., *J. Mater. Chem.*, 1997, **7 (9)**, p. 1755-1761
- [19] Yang, H., Coombs, N., et al., *Nature*, 1996, **381**, p. 589
- [20] Ogawa, M., Kikuchi, T., *Adv. Mater.*, 1998, **10**, p. 1077
- [21] Lu, Y., Ganguli, R., et al., *Nature*, 1997, **389**, p. 364-368
- [22] Gimon-Kinsel, M.E., Balkus, K.J., *Stud. Surf. Sci. Catal.*, 1998, **117**, p. 111
- [23] Tolbert, S.H., Schäffer, T.E., et al., *Chem. Mater.*, 1997, **9**, p. 1962-1967
- [24] Peña, M.L., Kan, Q., et al., *Micropor. and Mesopor. Mater.*, 2001, **44-45**, p. 9-16
- [25] Huo, Q., Leon, R., et al., *Science*, 1995, **268**, p. 1324
- [26] Alfredsson, V., Anderson, M.W., *Chem. Mater.*, 1996, **8**, p. 1141-1146
- [27] Anderson, M.W., *Zeolites*, 1997, **19**, p. 220
- [28] Chan, V. Z.-H., Hoffman, J., et al., *Science*, 1995, p. 1716-1719
- [29] Beck, J.S., Vartuli, J.C., et al., *Chem. Mater.*, 1994, **6**, p. 1816-1821
- [30] Beck, J.S., Vartuli, J.C., *Curr. Opinion Solid Mater. Sci.*, 1996, **1**, p. 76-87
- [31] Huo Q., Margolese, D.I., et al., *Nature*, 1994, **368**, p. 317-321
- [32] Huo, Q., Margolese, D.I., et al., *Chem. Mater.*, 1994, **6**, p. 1176-1191
- [33] Firouzi, A., Kumar, D., et al., *Science*, 1995, **267**, p. 1138-1143
- [34] Honma, I., Zhou, H.S., et al., *Adv. Mater.*, 2000, **12 (20)**, p.1529-1533
- [35] Kim, Y.-S., Yang, S.-M., *Adv. Mater.*, 2002, **14 (15)**, p. 1078-1081
- [36] McCool, B.A., Hill, N., et al., *J. Membr. Sci.*, 2003, **218 (1)**, p. 55-67
- [37] Besson, S., Gacoin, T., et al., *J. Mater. Chem.*, 2003, **13 (2)**, p. 404-409
- [38] Xomeritakis, G., Braunbarth, C.M., et al., *Micropor. and Mesopor. Mater.*, 2003, **66**, p. 91-101
- [39] Grosso, D., Babonneau, F., et al., *Chem. Mater.*, 2002, **14**, p. 931-939
- [40] Zhang, J.-L., Li, W., et al., *Micropor. and Mesopor. Mater.*, 2003, **66**, p. 69-76

- [41] Kruk, M., Jaroniec, M., *Chem. Mater.*, 1999, **11**, p. 2568-2572
- [42] Schmidt, R., Stöcker, M., et al., *Micropor. Mater.*, 1995, **5**, p. 1-7
- [43] Ogawa, M., Masukawa, N., *Micropor. and Mesopor. Mater.*, 2000, **38**, p. 35-41
- [44] Zhao, D., Yang, P., et al., *J. Chem. Soc. Chem. Commun.*, 1998, p. 2499-2500
- [45] Palmqvist, A.E.C., *J. Am. Chem. Soc.*, 2001, **123**, p. 1650-1657
- [46] Alberius, P.C.A., Frindell, K.L., et al., *Chem. Mater.*, 2002, **14**, p. 3284-3294
- [47] Zhao, D., Yang, P., *Adv. Mater.*, 1998, **10 (16)**, p. 1380-1385
- [48] Zhao, D., Yang, P., et al., *Chem. Mater.*, 1999, **11**, p. 1174-1178
- [49] Boissière, C., Martines, M.A.U., et al., *Chem. Mater.*, 2003, **15**, p. 460-463
- [50] *Porous materials: process technology and applications*, Ishizaki, K., Komarneni, S., Nanko, M., Kluwer Academic Publishers, Dordrecht, p. 67, 202-210, 212-214
- [51] *Encyclopedia of materials characterization*, Brundle, C.R., Evans, C.A., Wilson, S., 1992, Manning Publications Co., Greenwich, p. 16
- [52] *The materials science of thin films*, Ohring, M., 1992, Academic Press, London, p. 266-268, 269-282, 286-287
- [53] Zhao, W., Quanzhi, L., *Chem. Mater.*, 2003, **15**, p. 4160-4162
- [54] Martin, J.E., Anderson, M.T., et al., *Langmuir*, 1997, **13 (15)**, p. 4133-4141
- [55] Fyfe, C.A., Fu, G., *J. Am. Chem. Soc.*, 1995, **117**, p. 9709-9714
- [56] *Permporometry manual*, Brinkman, H.W., University Twente, IMS, June 27, 1996, (CT96/392/31)
- [57] *Membrane characterization – An overview of possibilities and limits*, Scharnagl, N., Luo, B., et al., Proc. Filtech Europa 2003, p. II-324
- [58] *High-selectivity, high-flux silica membranes for gas separation*, Vos, R.M., 1998, University Press, Enschede, p. 22-25
- [59] Doyle, A., Hodnett, B.K., *Micropor. and Mesopor. Mater.*, 2003, **63**, p. 53-57
- [60] *Microporous sol-gel derived ceramic membranes for gas separation*, Lange, R.S.A. de, 1993, University Press, Enschede, p. 171-172

10. List of symbols

10.1 Latin symbols

a	lattice parameter [m]
A	membrane area [m ²]
c	speed of light [m/s]
c _f	concentration in feed [mg/kg]
c _p	concentration in permeate [mg/kg]
C	e ^{(Q-L)/R} [-]
d	spacing between atomic planes in crystalline phase [m]
E _{Kα1}	energy emitted X-ray [Nm]
E _K	energy K-shell electron [Nm]
E _{L1}	energy L ₁ -shell electron [Nm]
F	Knudsen permeance [mol/m ² sPa]
h	Plank's constant [Js]
h, k, l	Miller indices [-]
J	flux [l/m ² s]
l	layer thickness [m]
L	latent heat of condensation of the gas [J/molK]
L _p	permeability [l/mPas]
m	electron mass [kg]
M	molar mass of the gas [g/mol]
N _{av}	constant of Avogadro [1/mol]
O _m	area of 1 mol N ₂ [m ²]
p ⁰	vapour pressure above a multilayer of adsorbate [Pa]
p/p ⁰	relative pressure [-]
ΔP	pressure drop [Pa]
q	electron charge [As]
Q	heat of adsorption of the first layer [J/molK]
r	retention [-]
r _k	Kelvin radius [m]
r _p	pore radius [m]
R	gas constant [J/molK]
S _{BET}	BET surface area [m ² /kg]
t	t-layer (monolayer of N ₂ adsorbed at very low concentrations) [m]
T ₀	room temperature [K]
v	volume of gas adsorbed [m ³ /g STP]
v _m	volume of gas adsorbed in the monolayer [m ³ /g STP]
V	potential difference [J/As]
V _p	pore volume [cm ³ /g]
Δx	membrane thickness [m]

10.2 Greek symbols

ε	porosity [%]
ε_p	porosity [-]
θ	angle [°]
λ	wavelength [m]
$\lambda_{K\alpha_1}$	wavelength $K\alpha_1$ X-rays [m]
ρ	density solid phase [g/cm^3]
σ	surface tension [N/m]
$1/\tau$	tortuosity [-]
Φ_{vol}	volume flow [l/s]

Appendix A: adsorption/desorption isotherms

A.1 Honma powders

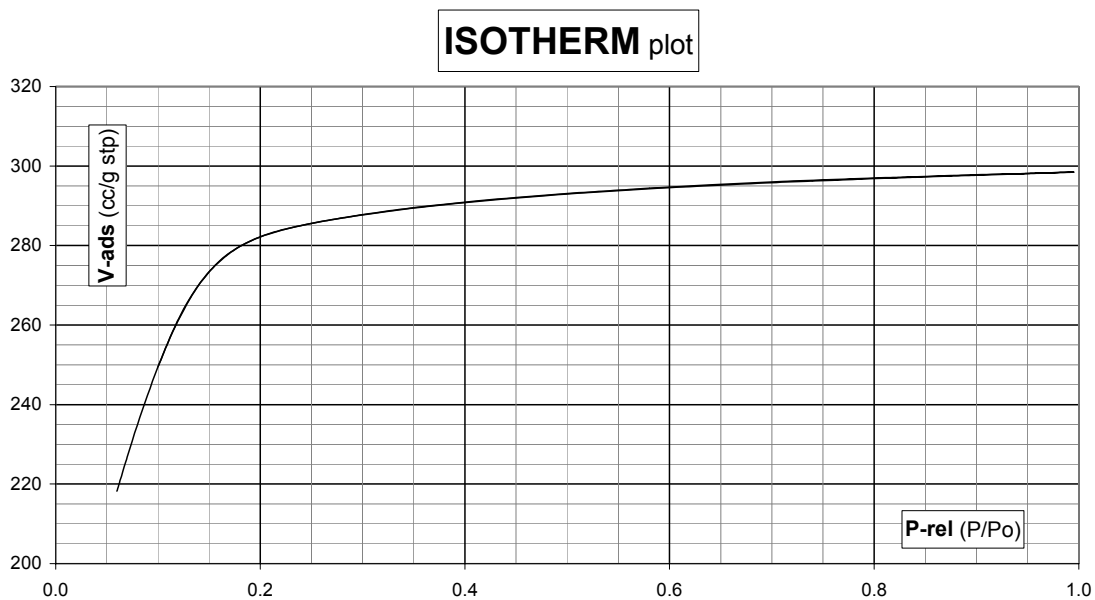


Figure A.1: Isotherm Honma powder; CTAB + ageing 1 day

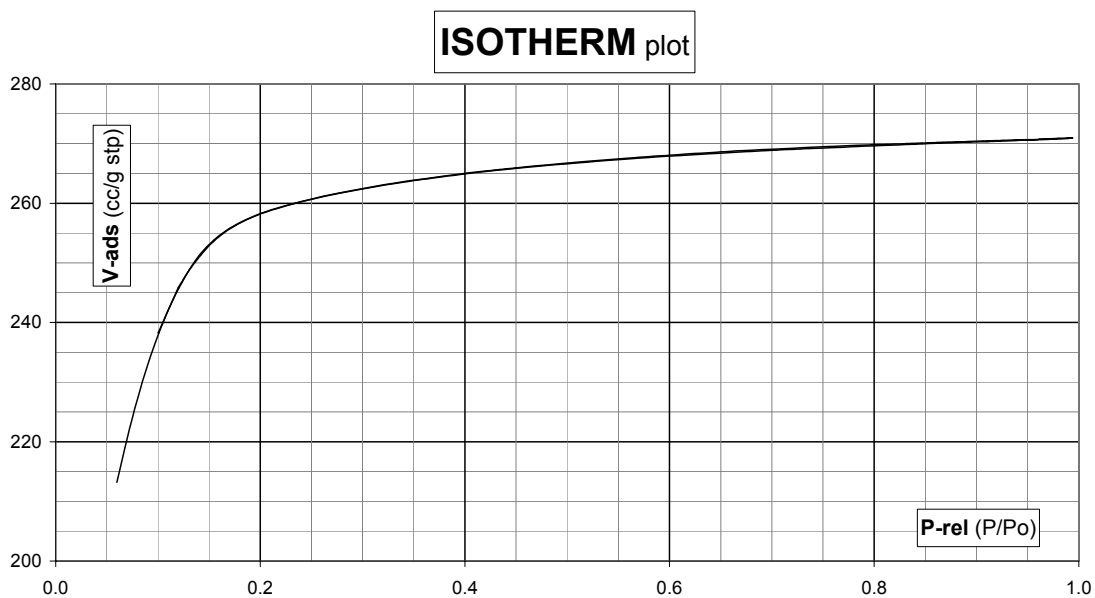


Figure A.2: Isotherm Honma powder; CTAB + ageing 2 days

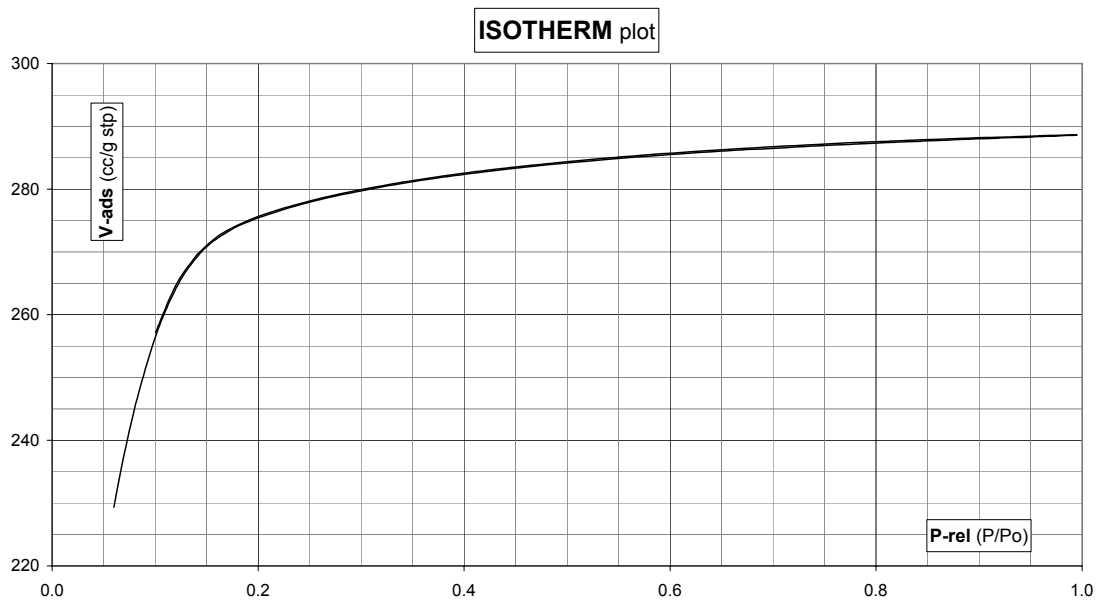


Figure A.3: Isotherm Honma powder; CTAB + ageing 24 days

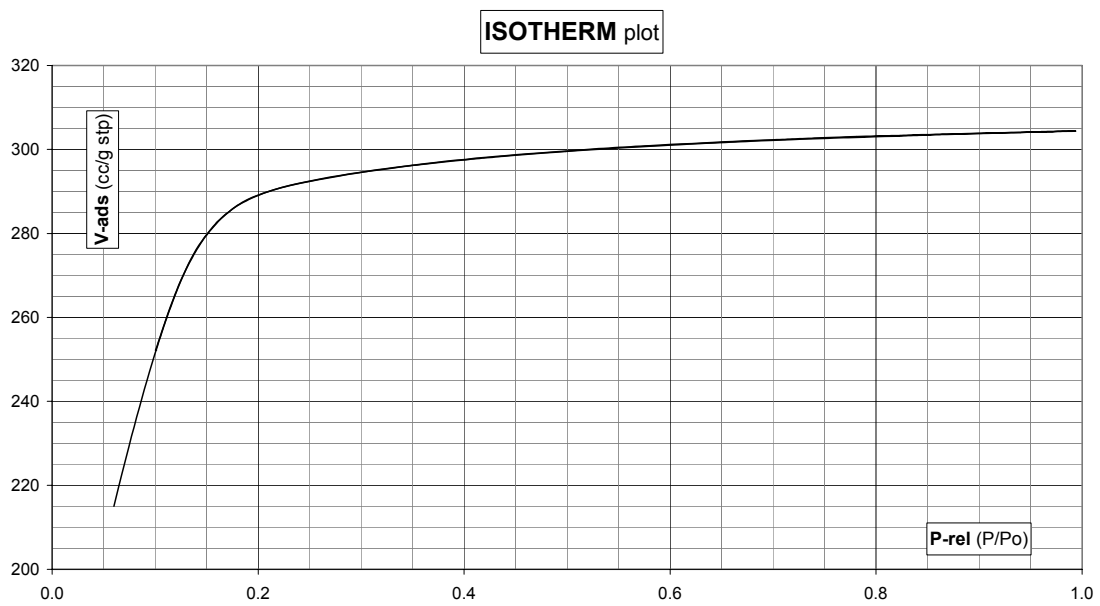


Figure A.4: Isotherm Honma powder; CTAC + ageing 1 day

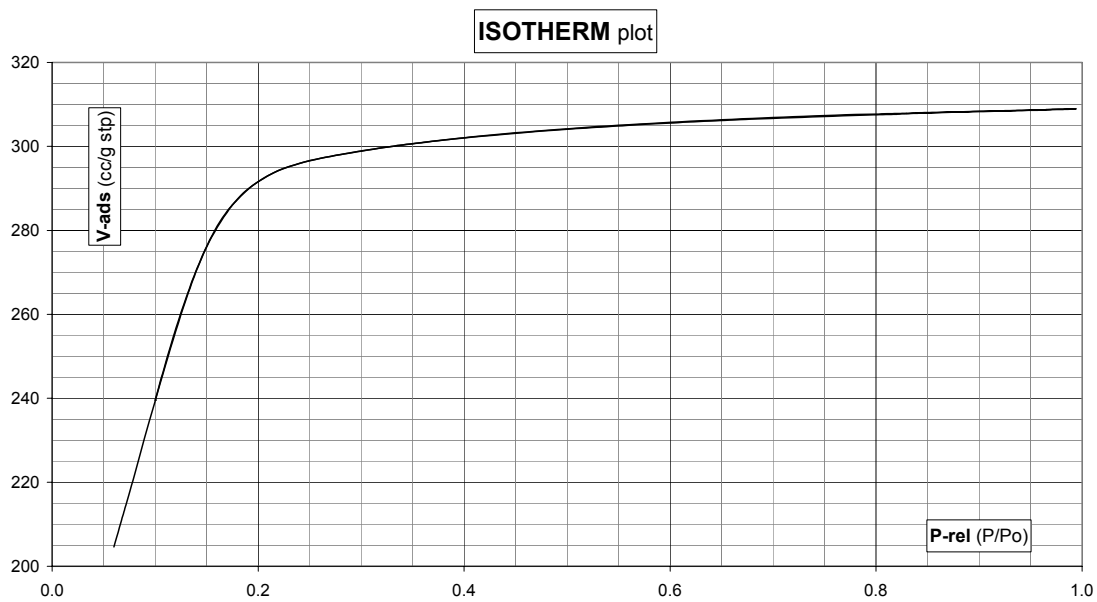


Figure A.5: Isotherm Honma powder; CTAC + ageing 3 days

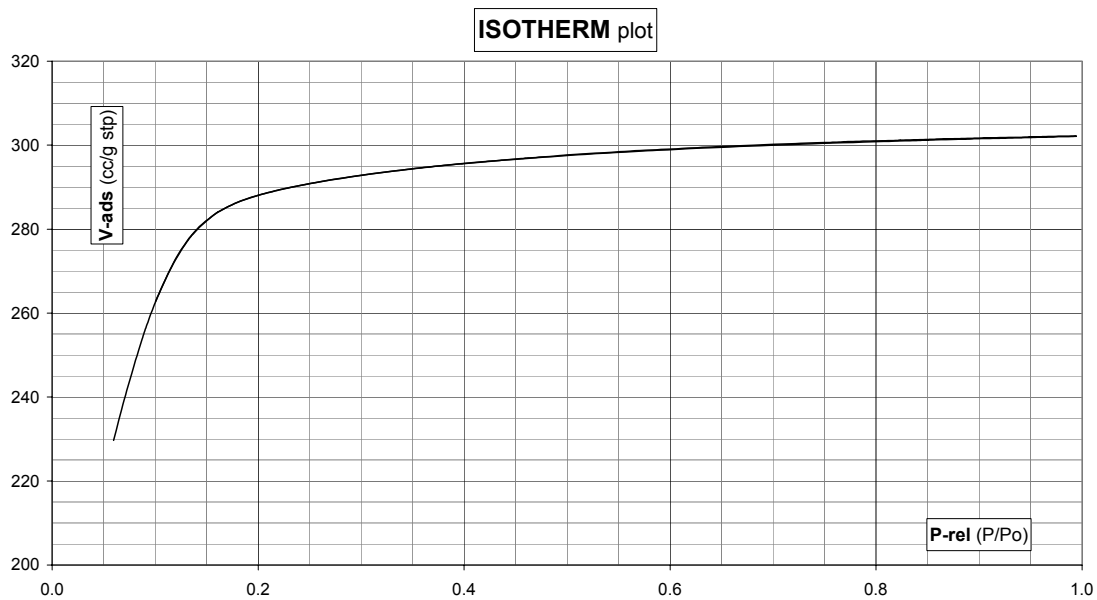


Figure A.6: Isotherm Honma powder; CTAC + ageing 6 days

A.2 McCool powders

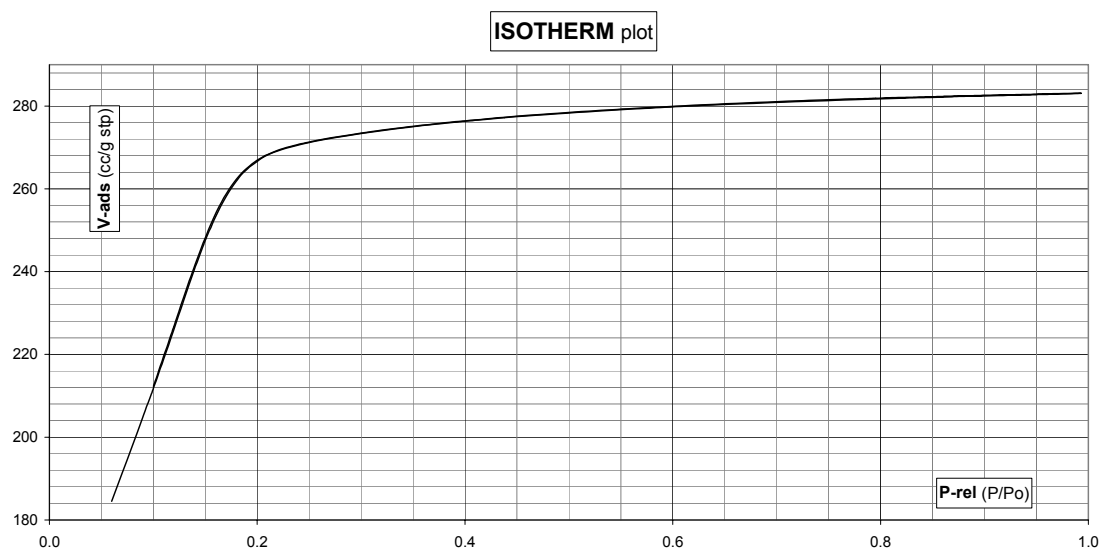


Figure A.7: Isotherm McCool powder; ageing 7 days

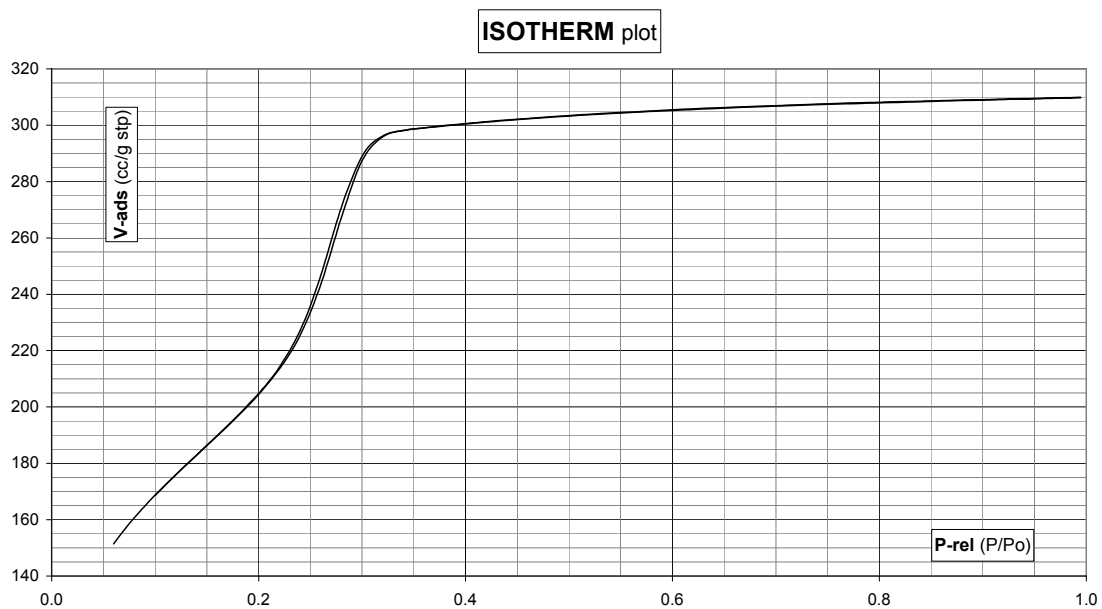


Figure A.8: Isotherm McCool powder; ageing 10 days

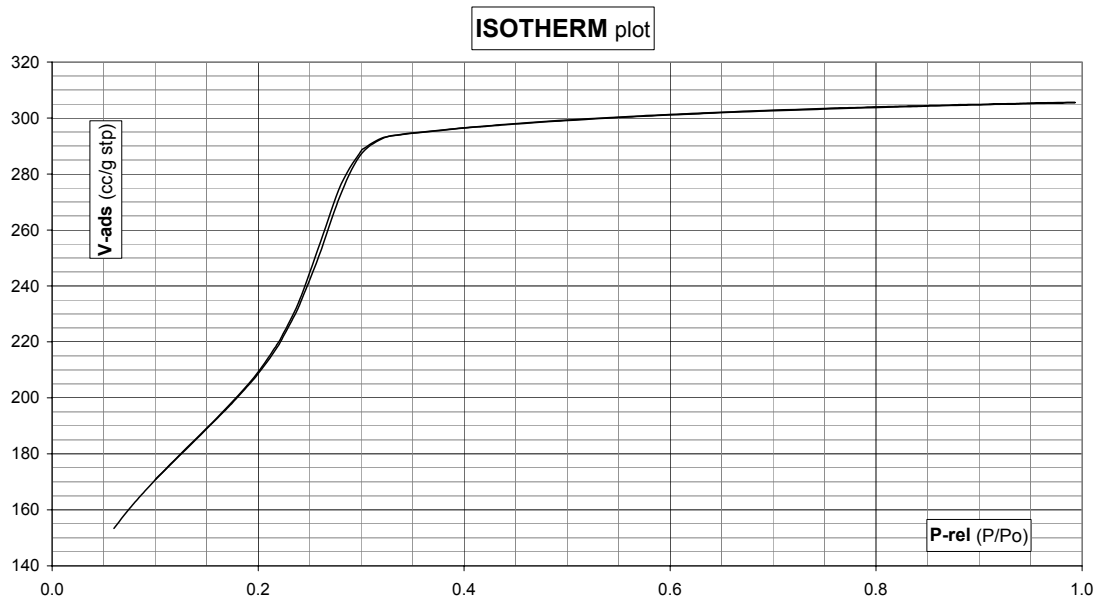


Figure A.9: Isotherm McCool powder; ageing 11 days

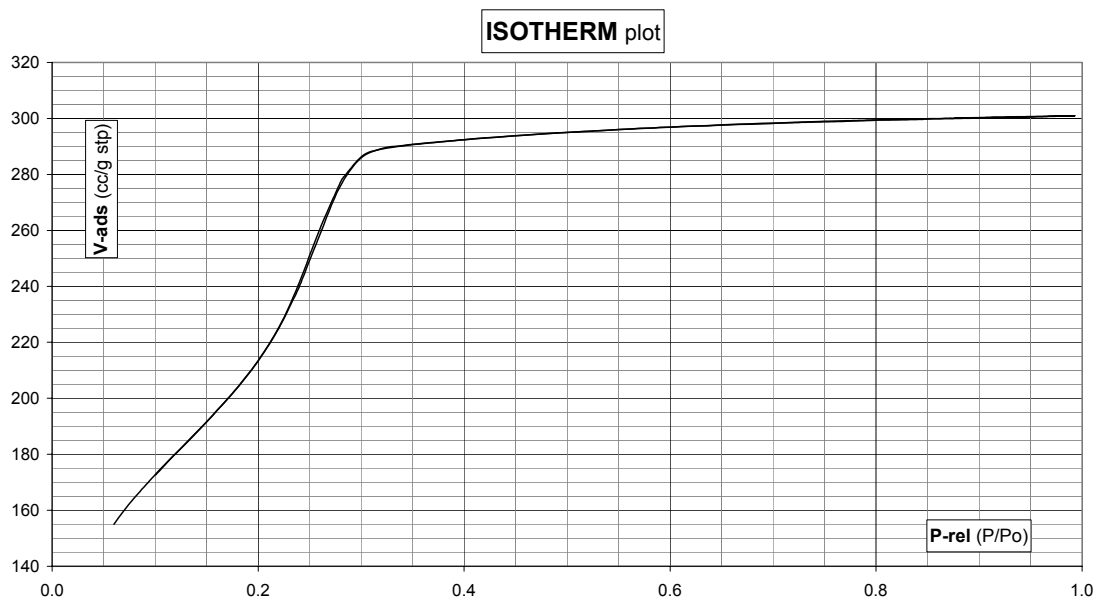


Figure A.10: Isotherm McCool powder; ageing 12 days

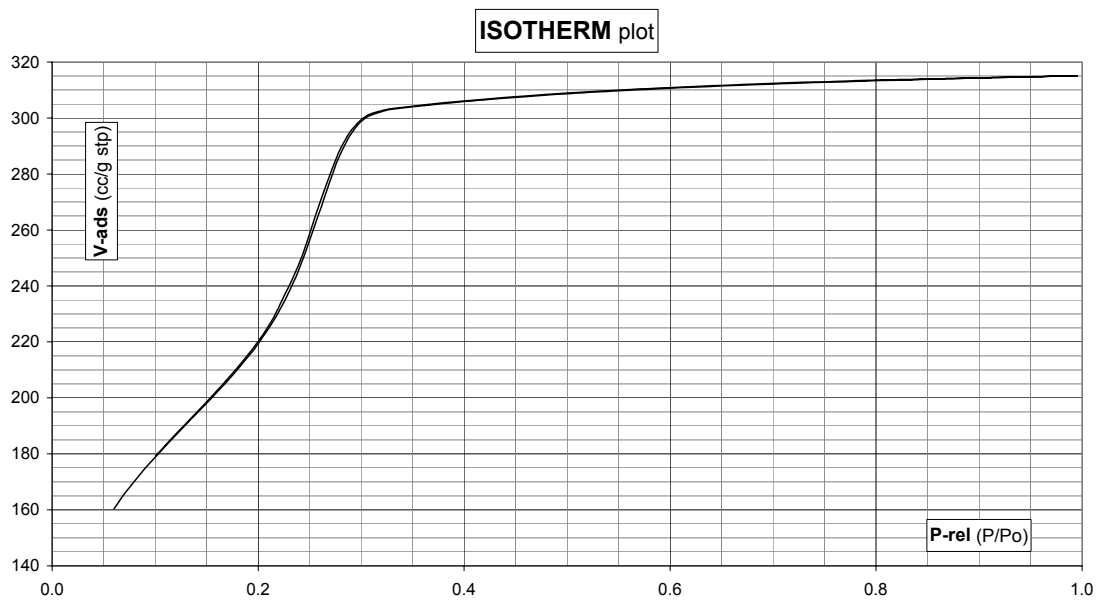


Figure A.11: Isotherm McCool powder; ageing 13 days

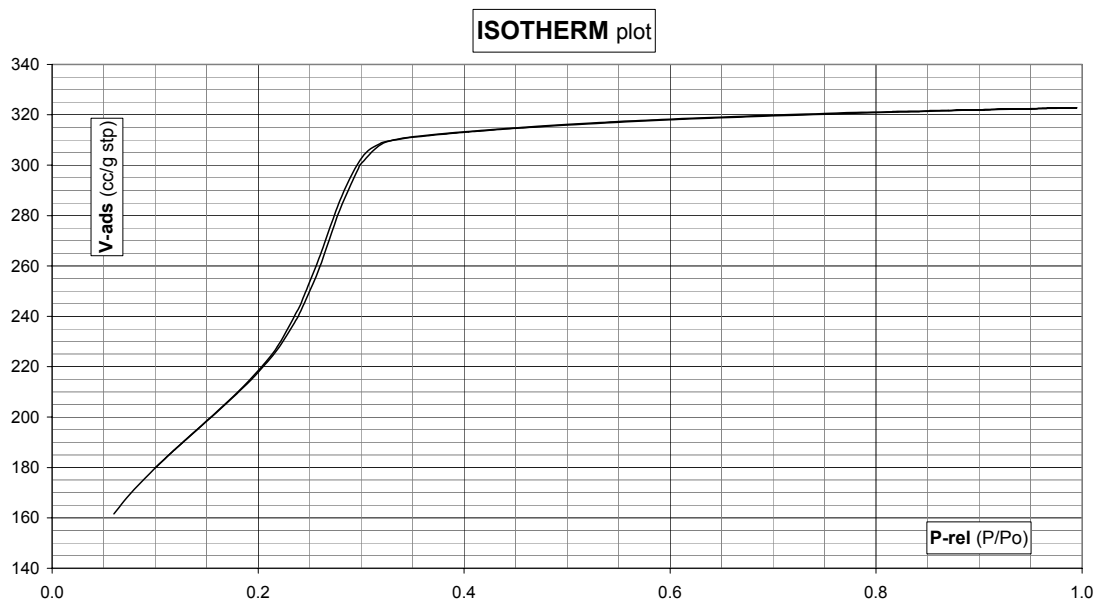


Figure A.12: Isotherm McCool powder; ageing 14 days

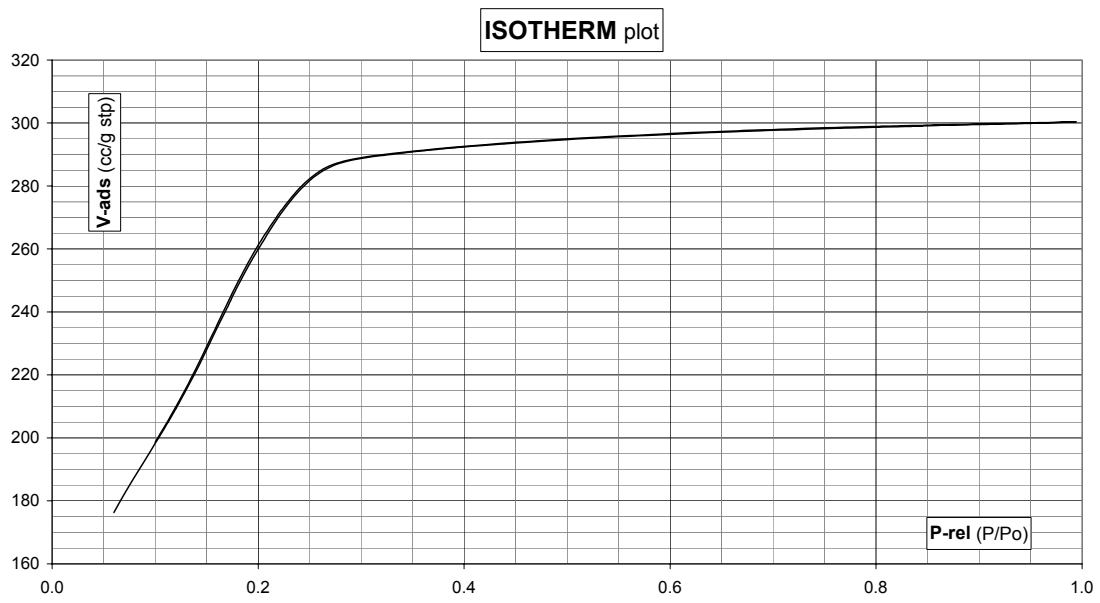


Figure A.13: Isotherm McCool powder; ageing 21 days

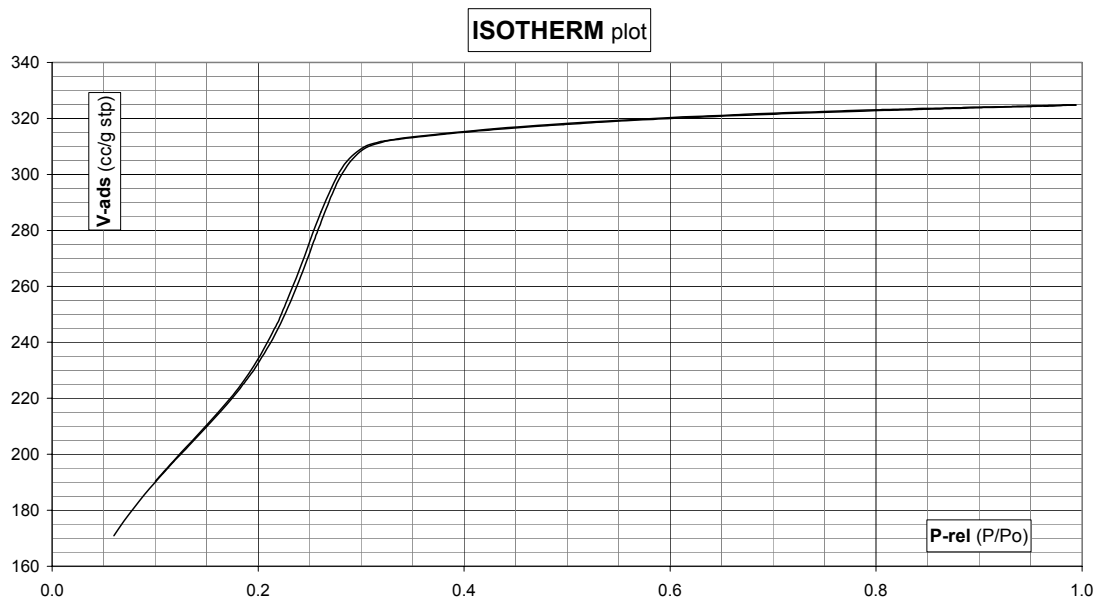


Figure A.14: Isotherm McCool powder; ageing 28 days

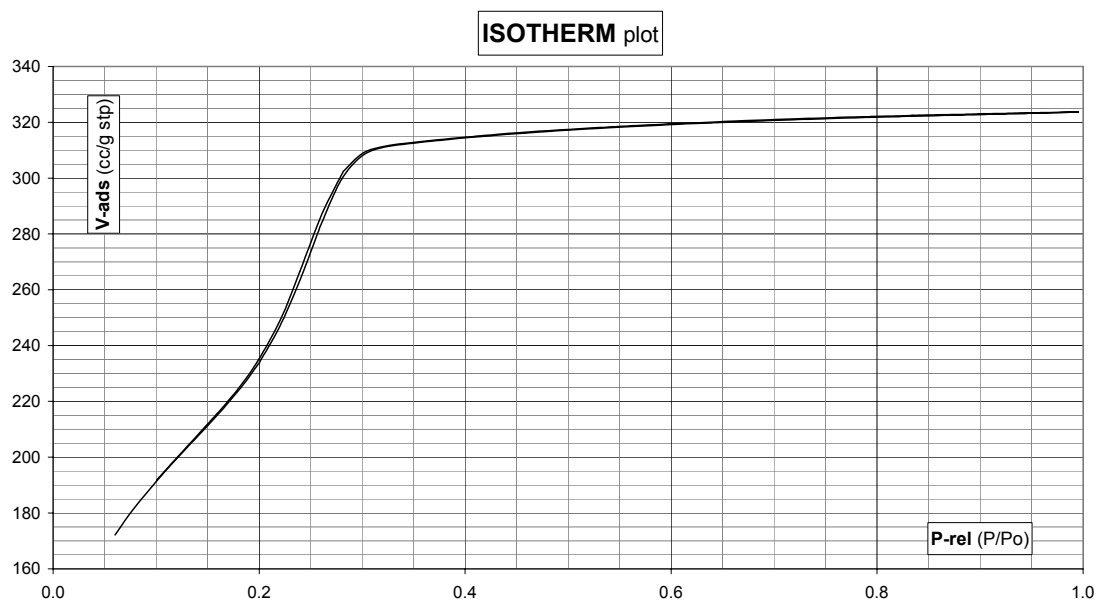


Figure A.15: Isotherm McCool powder; ageing 36 days

Appendix B: X-ray diffraction plots

B.1 Powders

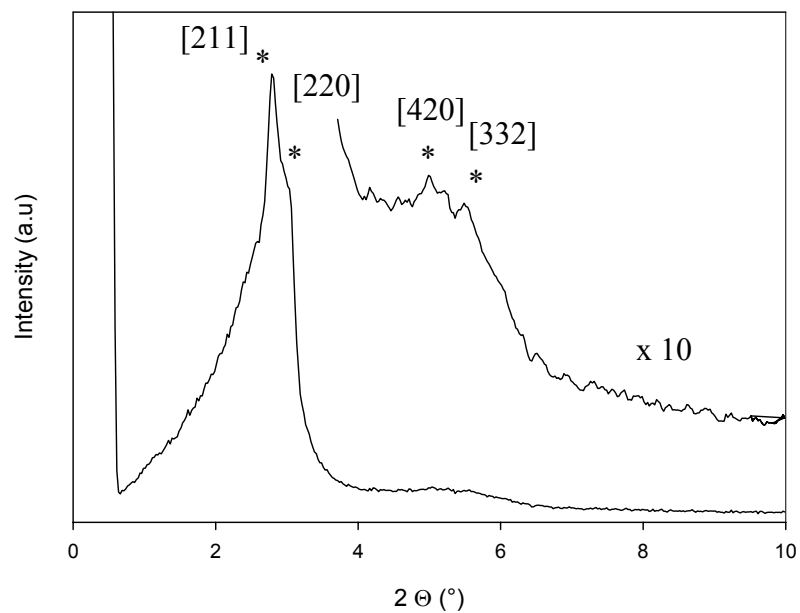


Figure B.1: XRD plot McCool powder with ageing time 7 days

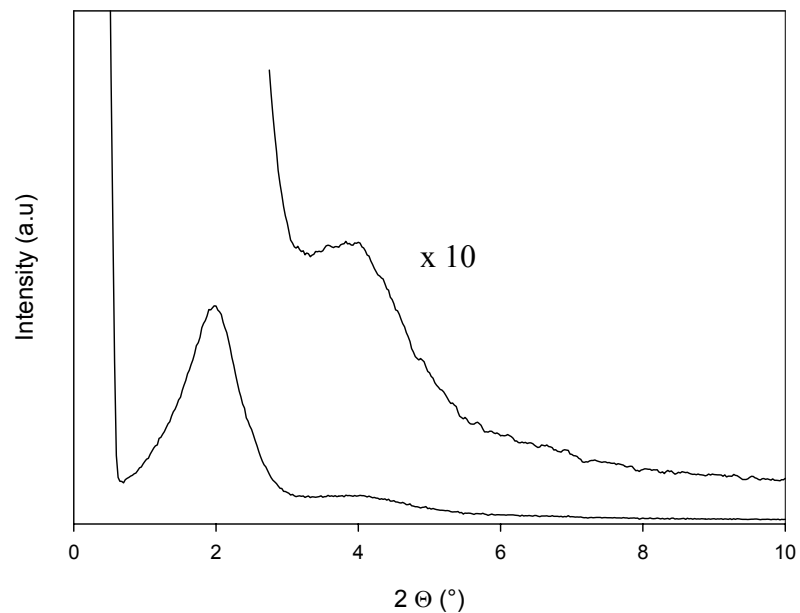


Figure B.2: XRD plot McCool powder with ageing time 10 days

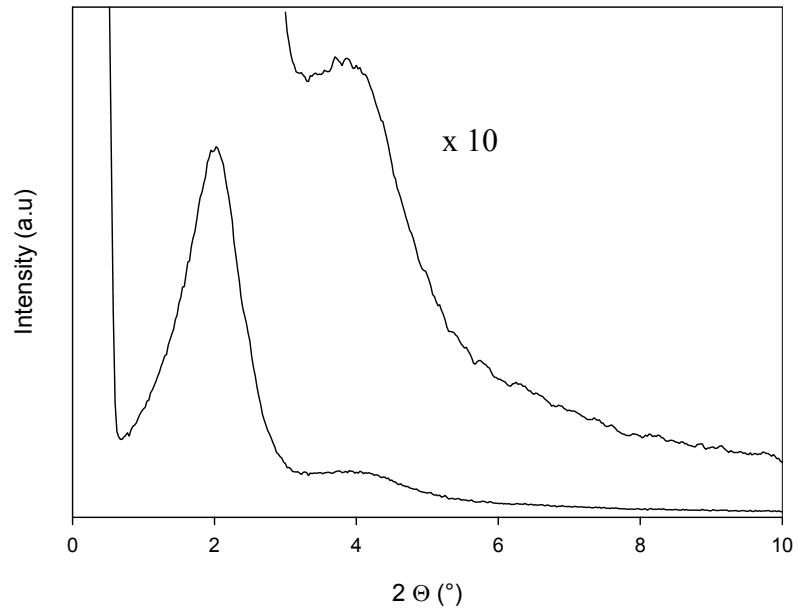


Figure B.3: XRD plot McCool powder with ageing time 14 days

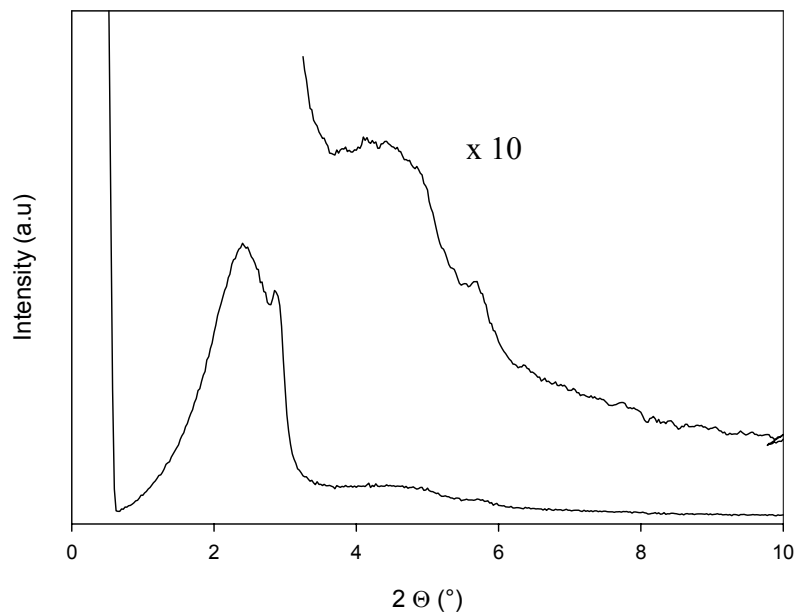


Figure B.4: XRD plot McCool powder with ageing time 21 days

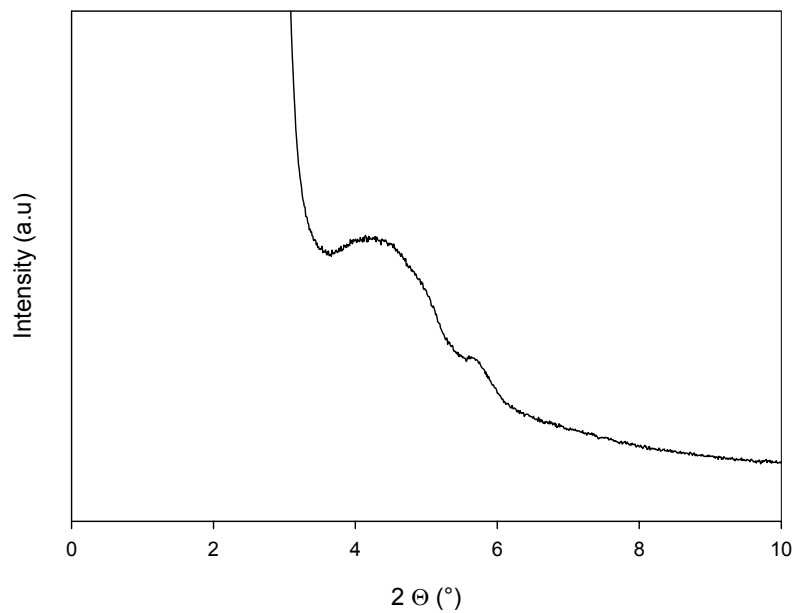


Figure B.5: Slow XRD plot McCool powder with ageing time 21 days

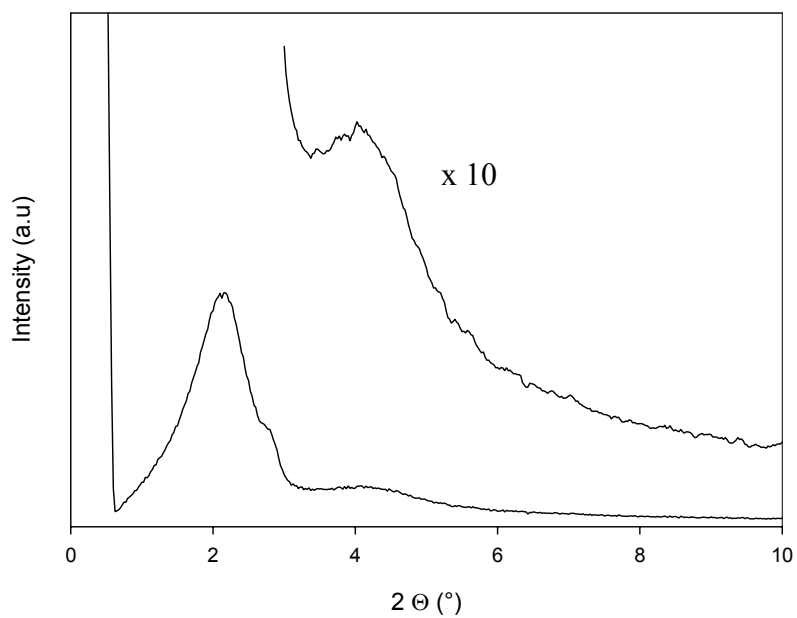


Figure B.6: XRD plot McCool powder with ageing time 28 days

B.2 Wafers

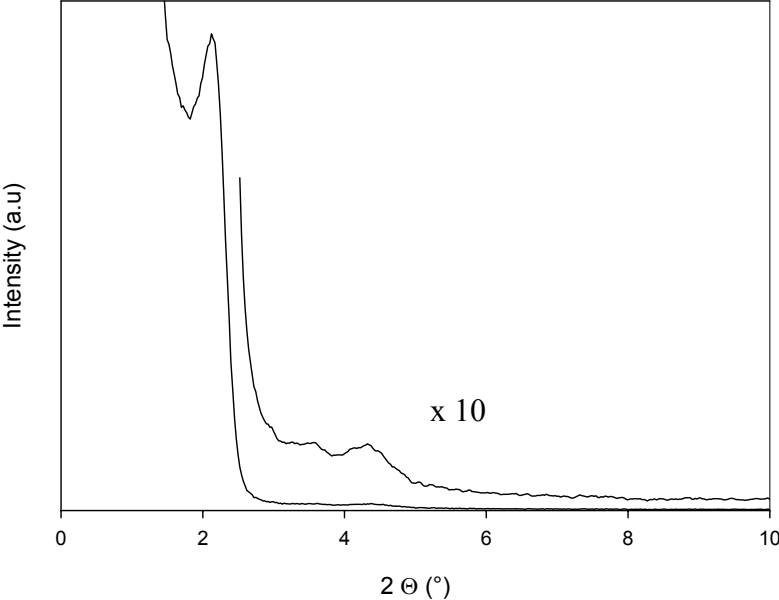


Figure B.7: XRD plot wafer 1 with uncalcined sol from Honma synthesis

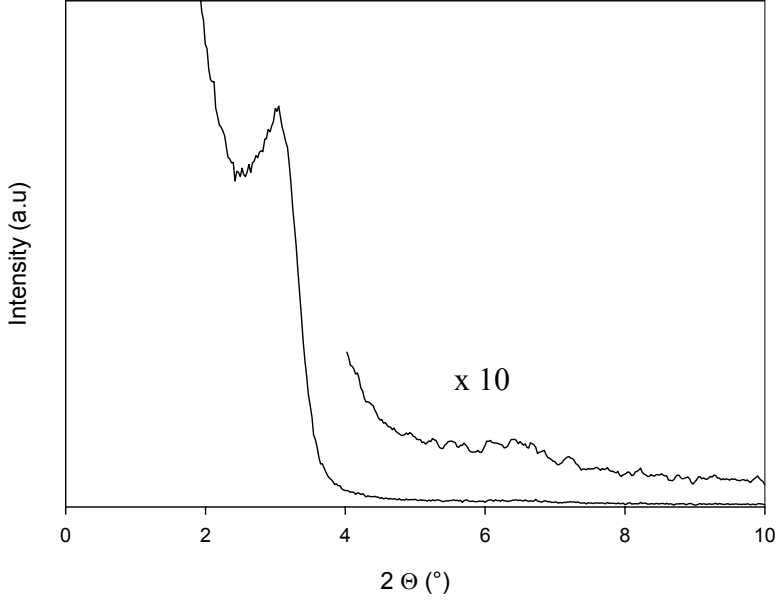


Figure B.8: XRD plot wafer 2 with calcined (450°C) sol from Honma synthesis

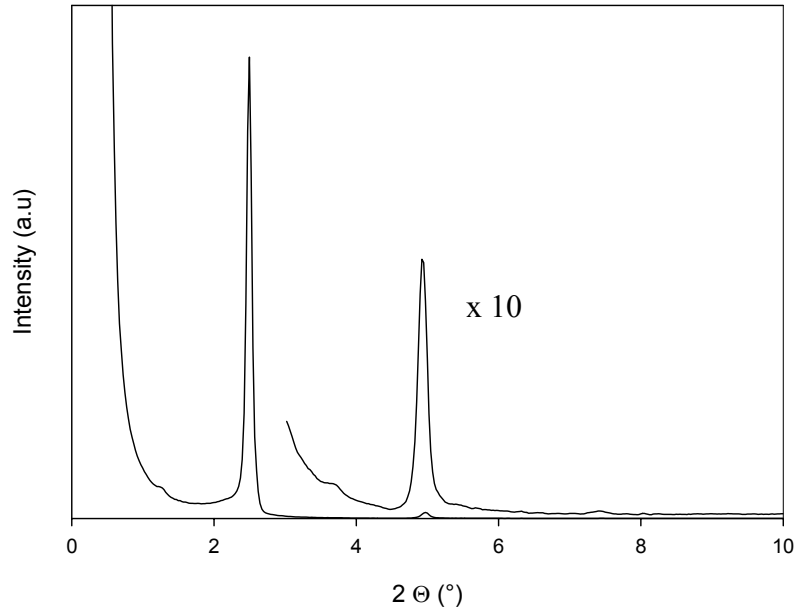


Figure B.9: XRD plot wafer 3 with uncalcined sol from McCool synthesis

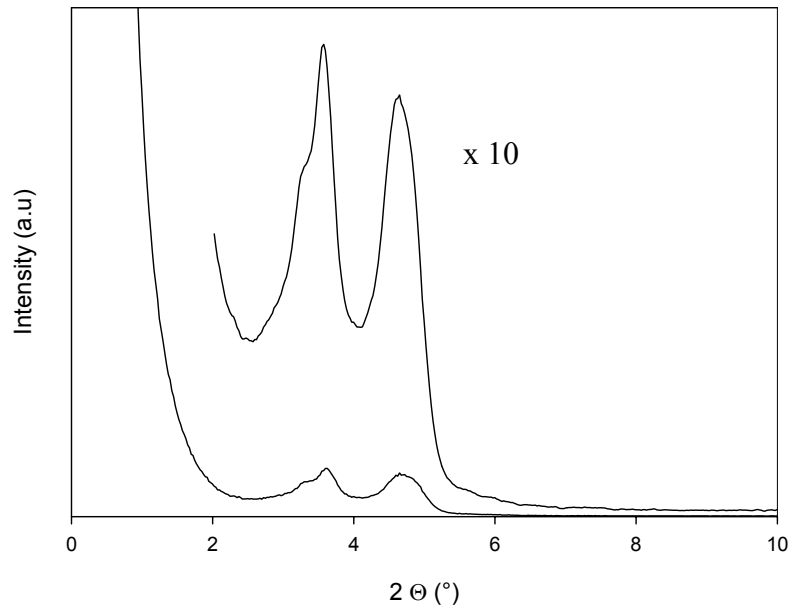


Figure B.10: XRD plot wafer 4 with calcined (450°C) sol from McCool synthesis

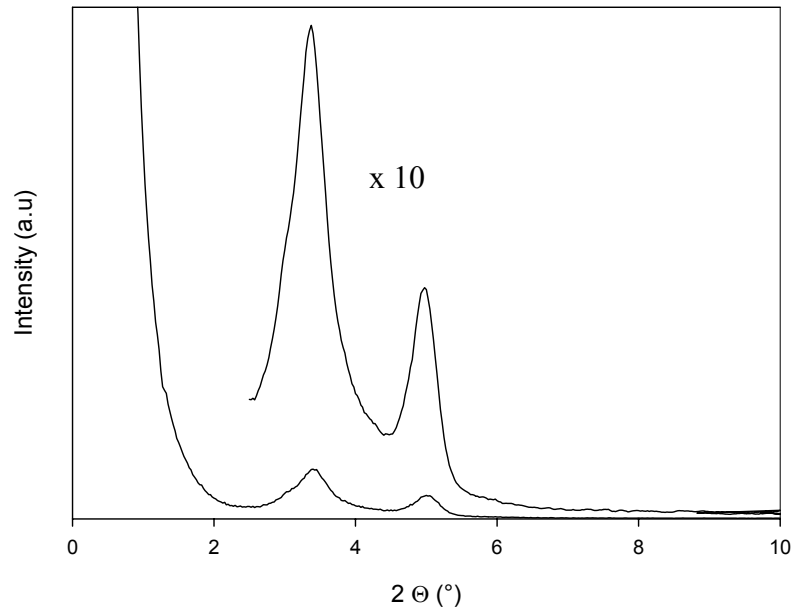


Figure B.11: XRD plot wafer 4+ with calcined (550°C) sol from McCool synthesis

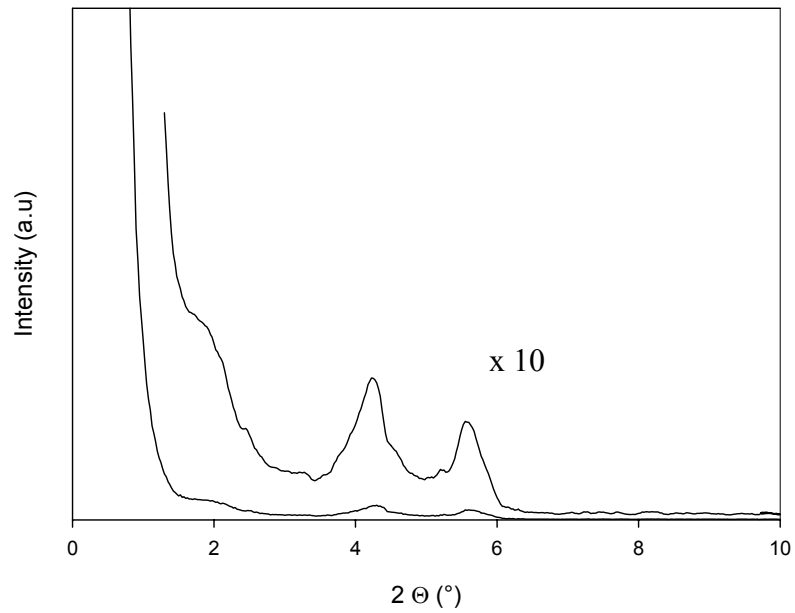


Figure B.12: XRD plot wafer 3+ with uncalcined sol from McCool synthesis, calcined (450°C) after 46 days

B.3 Membranes

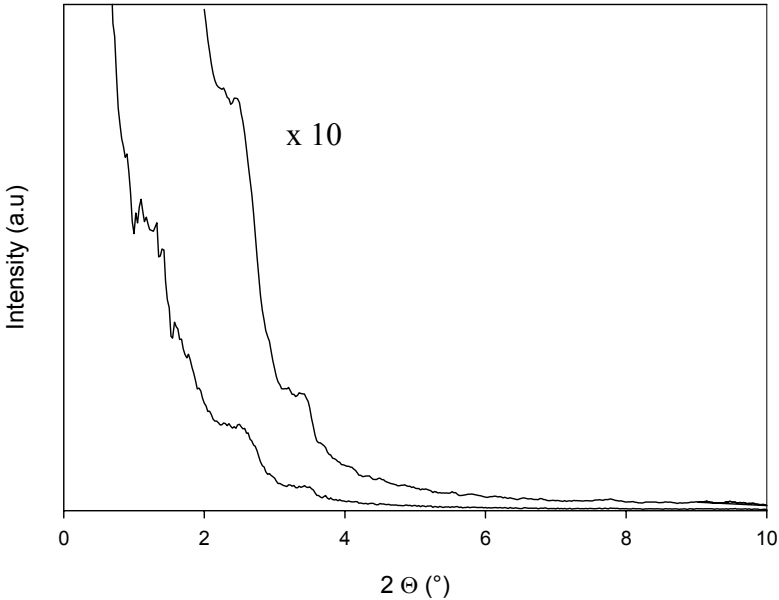


Figure B.13: XRD plot membrane 10

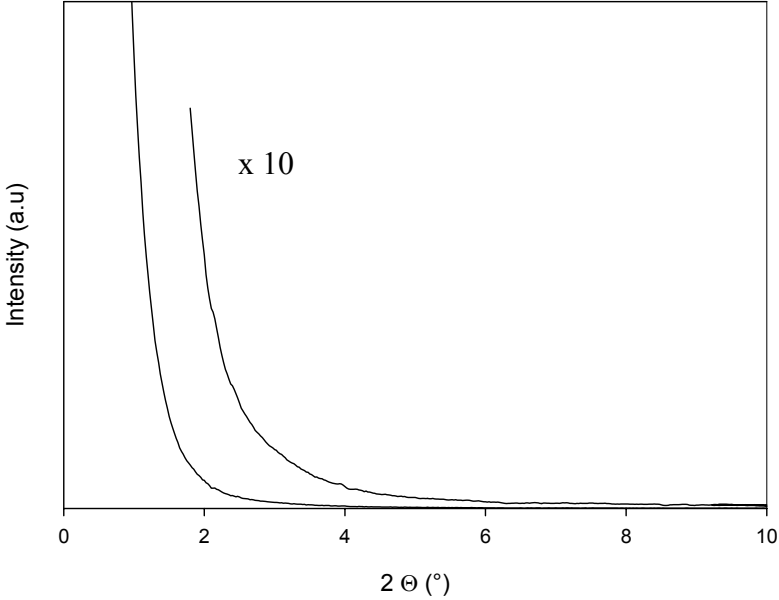


Figure B.14: XRD plot membrane 15

Appendix C: pore size distributions

Pore size distribution
 $R_K = 3.13 \text{ nm}$

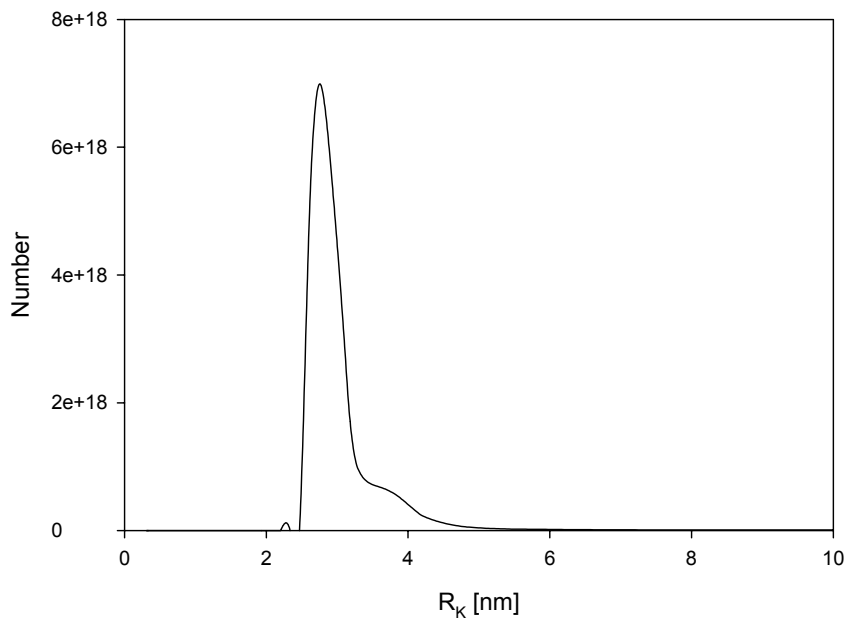


Figure C.1: Permporometry pore size distribution membrane 9

Pore size distribution
 $R_K < 1 \text{ nm}$

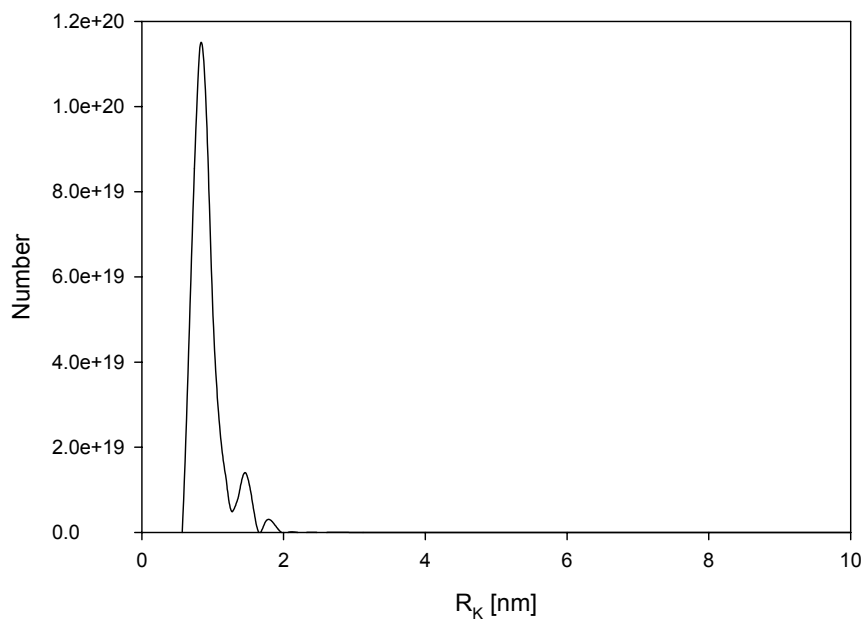


Figure C.2: Permporometry pore size distribution membrane 10

Pore size distribution
 $R_K = 2.09 \text{ nm}$

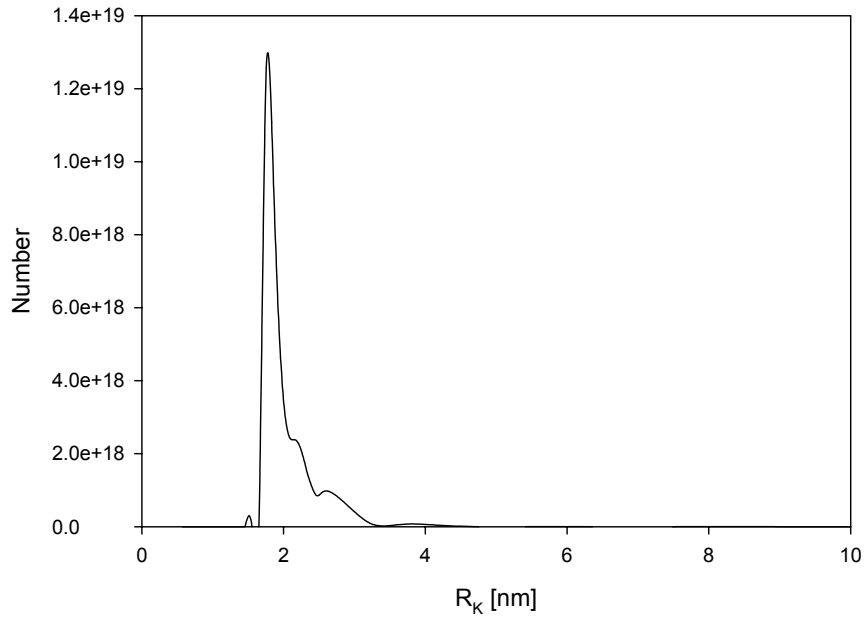


Figure C.3: Permporometry pore size distribution membrane 11

Pore size distribution
 $R_K = 1.83 \text{ nm}$

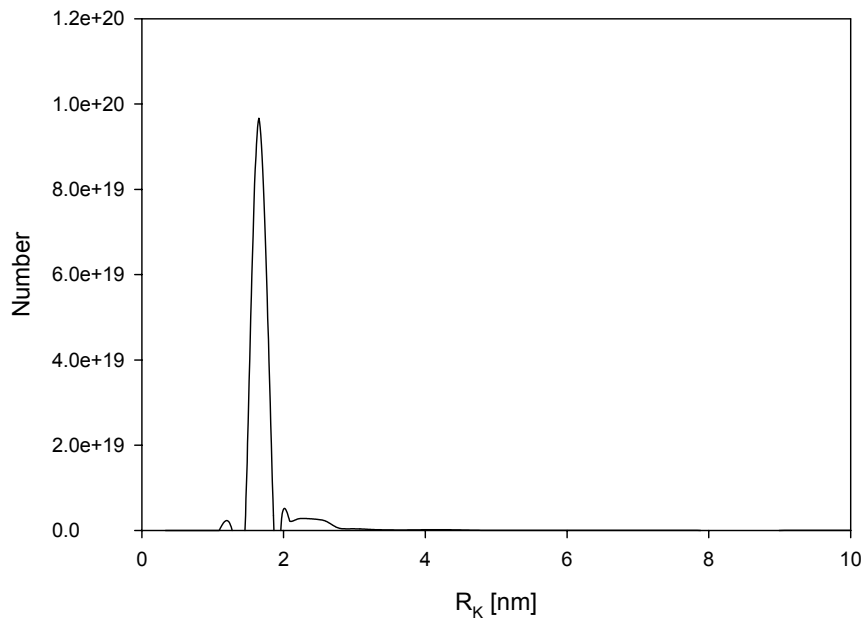


Figure C.4: Permporometry pore size distribution membrane 12

Pore size distribution
 $R_K = 4.10$ nm

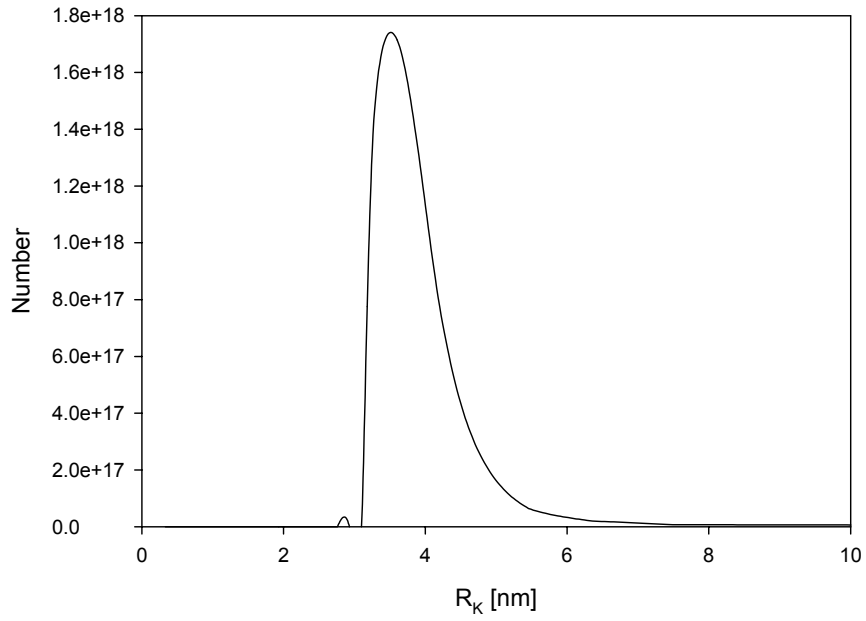


Figure C.5: Permporometry pore size distribution membrane 13

Pore size distribution
 $R_K = 4.42$ nm

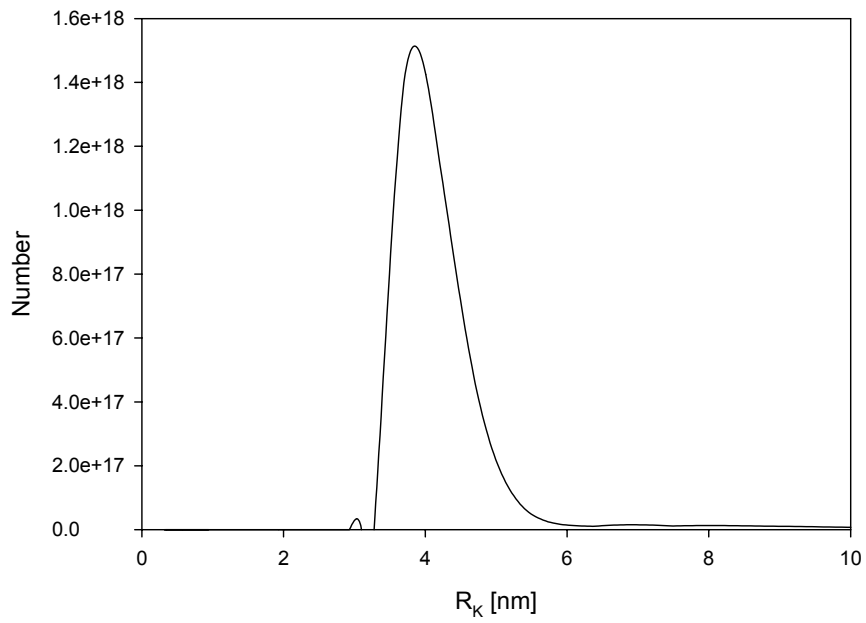


Figure C.6: Permporometry pore size distribution membrane 14

Pore size distribution
 $R_K = 1.75$ nm

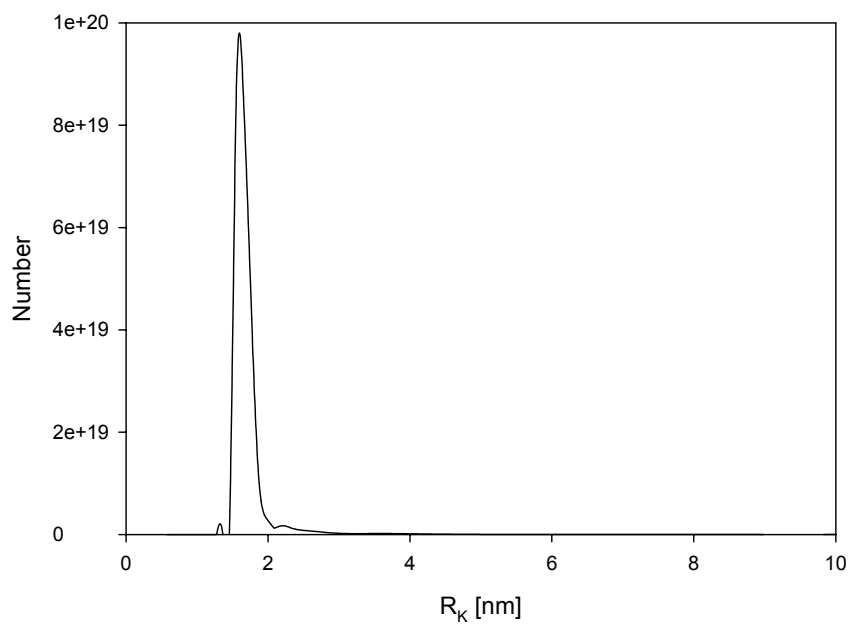


Figure C.7: Permporometry pore size distribution membrane 15

Pore size distribution
 $R_K = 1.65$ nm

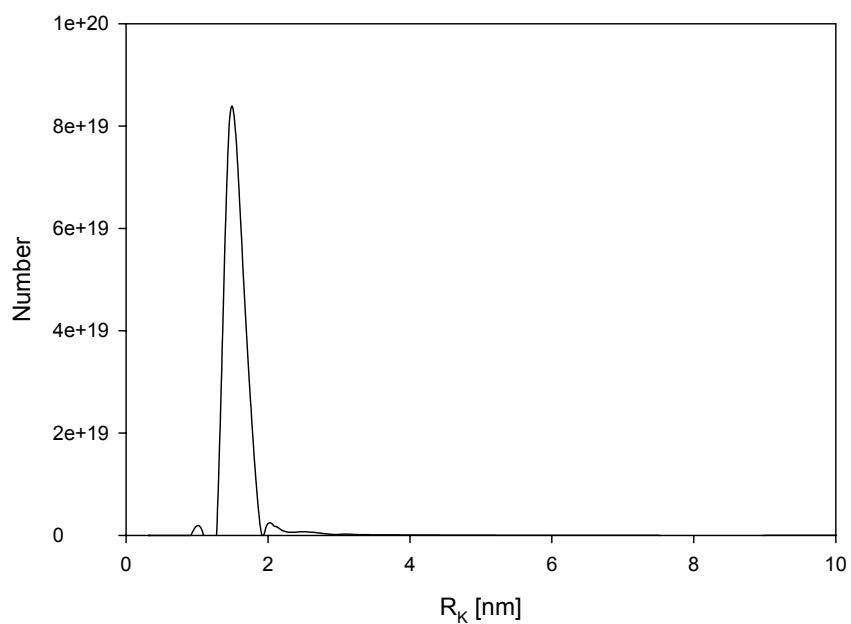


Figure C.8: Permporometry pore size distribution membrane 16

Pore size distribution
 $R_K = 1.65 \text{ nm}$

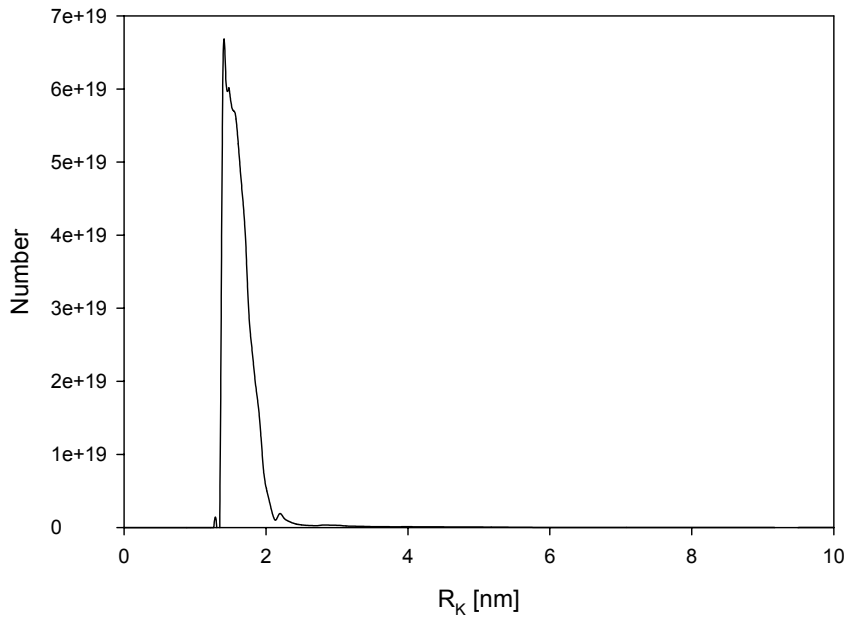


Figure C.9: Permporometry pore size distribution membrane 16, after other measurements

Pore size distribution
 $R_K = 2.11 \text{ nm}$

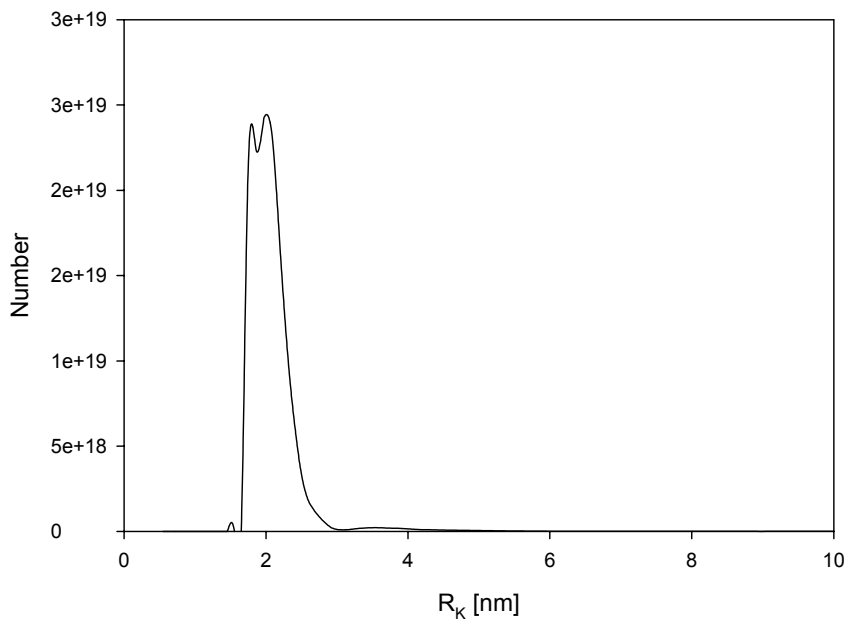


Figure C.10: Permporometry pore size distribution membrane 17

Appendix D: liquid permeation and retention graphs

D.1 Liquid permeation

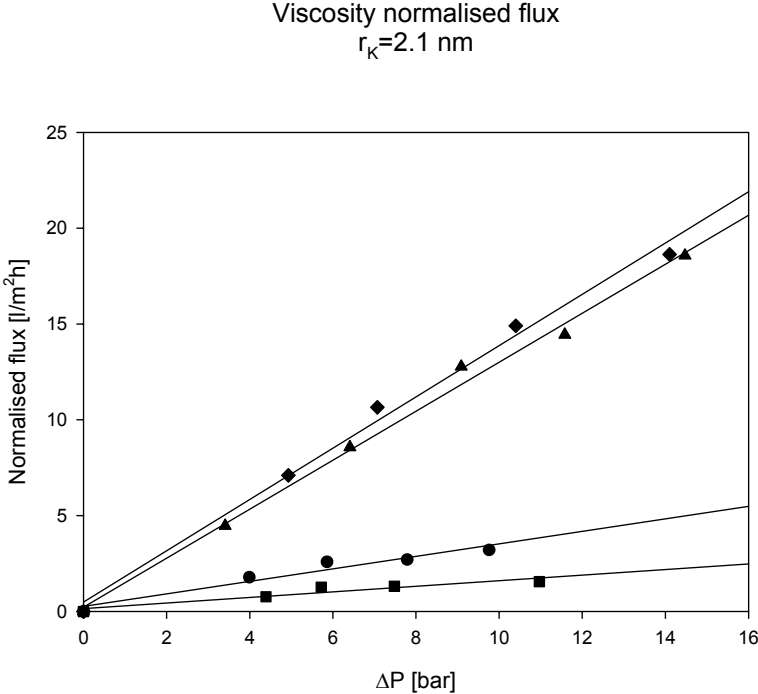


Figure D.1: Normalised liquid permeation membrane 17; \blacklozenge ethanol, \blacktriangle water, \blacksquare toluene, \bullet hexane

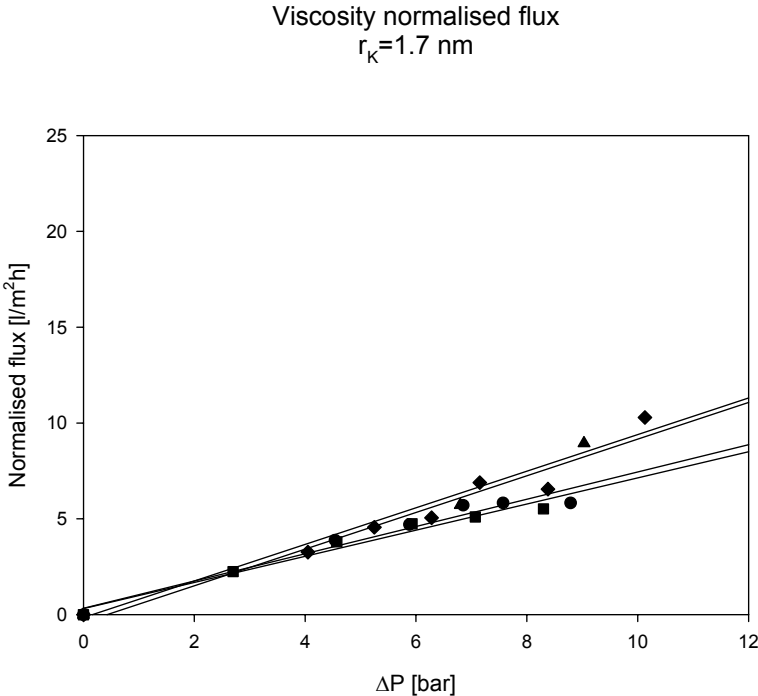


Figure D.2: Normalised liquid permeation membrane 15; \blacklozenge ethanol, \blacktriangle water, \blacksquare toluene, \bullet hexane

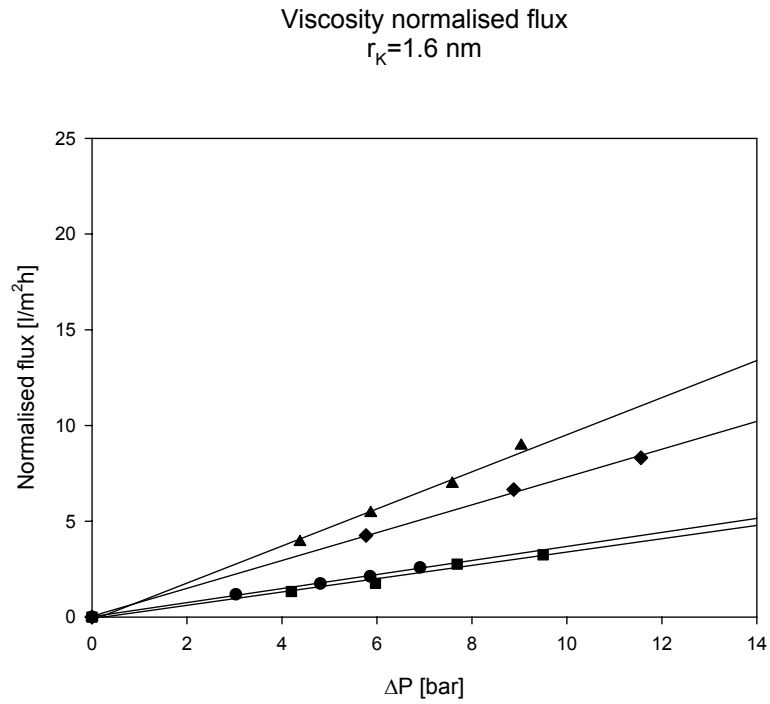


Figure D.3: Normalised liquid permeation membrane 16; \blacklozenge ethanol, \blacktriangle water, \blacksquare toluene, \bullet hexane

D.2 Retention

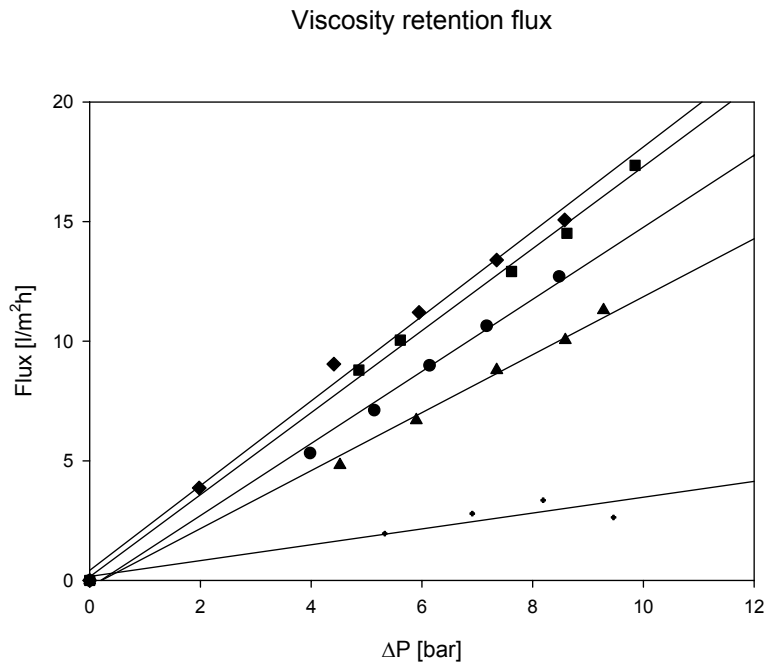


Figure D.4: Retention membrane 17 (not normalised); \blacklozenge toluene, \blacksquare POM/water turbid, \bullet water, \blacktriangle POM/water clear, $+$ POM/toluene